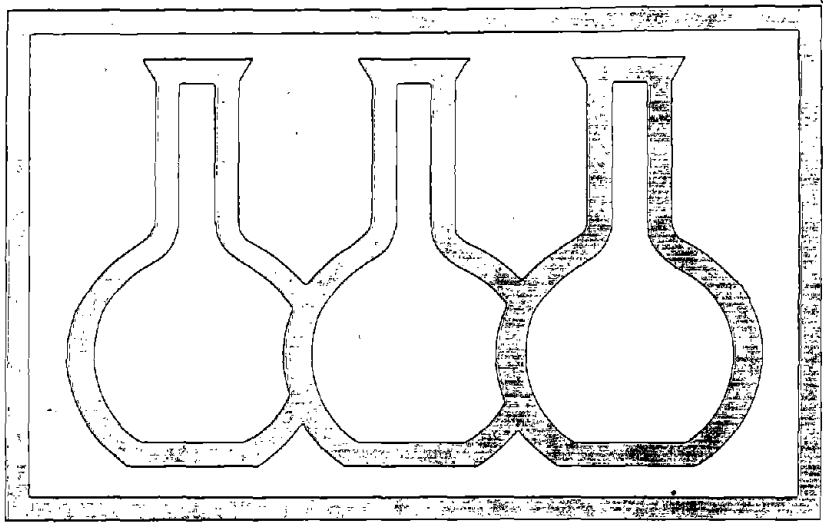

NIOSH RESEARCH REPORT

RF Radiation Absorption Patterns:

HUMAN AND ANIMAL MODELING DATA

U.S. DEPARTMENT OF HEALTH, EDUCATION, AND WELFARE
PUBLIC HEALTH SERVICE / CENTER FOR DISEASE CONTROL
NATIONAL INSTITUTE FOR OCCUPATIONAL SAFETY AND HEALTH

BIBLIOGRAPHIC DATA SHEET	1. Report No. NIOSH-77-183	2.	3. Recipient's Accession No. PB274749
4. Title and Subtitle RF RADIATION ABSORPTION PATTERNS: HUMAN AND ANIMAL MODELING DATA			5. Report Date Sept. 1977 6.
7. Author(s) Arthur W. Guy, Michael D. Webb, and John A. McDougall			8. Performing Organization Rept. No.
9. Performing Organization Name and Address University of Washington School of Medicine Bioelectromagnetics Research Laboratory Seattle, Washington 98195			10. Project/Task/Work Unit No. 11. Contract/Grant No.
12. Sponsoring Organization Name and Address National Institute for Occupational Safety and Health 4676 Columbia Parkway Cincinnati, Ohio, 45226			13. Type of Report & Period Covered 14.

15. Supplementary Notes

Interagency Agreement NIOSH-IA-75-30

16. Abstracts Research performed to obtain the radiofrequency-induced power absorption patterns in models of humans and animal and to extrapolate the results to humans are described. Various models of animals and humans were exposed to radiofrequency fields and power absorption patterns and the rates of power absorption at specific anatomical locations within the models were thermographically recorded under simulated industrial exposure conditions. The results of the modeling research demonstrate the validity of this technique for predicting the magnitude and distribution of radiofrequency power absorption in humans and animals. The utility of the technique for extrapolation to human radiofrequency exposure thresholds from animal data was firmly established.

17. Key Words and Document Analysis. 17a. Descriptors

Industrial hygiene
Electromagnetic radiation
Radiobiology
Radiation protection
Dosimetry
Health physics

17b. Identifiers/Open-Ended Terms

Nonionizing radiation

17c. COSATI Field/Group 06/J

18. Availability Statement	19. Security Class (This Report)	22. Price
Release unlimited	UNCLASSIFIED	A05-A01
	20. Security Class (This Page) UNCLASSIFIED	

RF RADIATION ABSORPTION PATTERNS: HUMAN AND ANIMAL MODELING DATA

Arthur W. Guy
Michael D. Webb
John A. McDougall
University of Washington
School of Medicine
Department of Rehabilitation Medicine RJ-30
Bioelectromagnetics Research Laboratory
Seattle, Washington 98195

Interagency Agreement NIOSH IA-75-30

with

USAF School of Aerospace Medicine
Aerospace Medical Division (AFSC)
Brooks Air Force Base, Texas 78235

U. S. Department of Health, Education, and Welfare
Public Health Service
Center for Disease Control
National Institute for Occupational Safety and Health
Division of Biomedical and Behavioral Science
Cincinnati, Ohio 45226

September 1977

DISCLAIMER

The contents of this report are reproduced herein as received from the contractor, except for changes in the title page, the addition of a disclaimer, a preface, an abstract, contents, and acknowledgments. The opinions, findings, and conclusions expressed are those of the author and not necessarily those of the National Institute for Occupational Safety and Health. Mention of company or product names is not to be considered as an endorsement by the National Institute for Occupational Safety and Health.

NIOSH Project Officer: David L. Conover, Ph.D.

DHEW (NIOSH) Publication No. 77-183

PREFACE

The Occupational Safety and Health Administration (OSHA) Radiofrequency (RF)/Microwave Radiation Personnel Exposure Regulation (29 CFR 1910.97, June 2, 1974) includes electromagnetic (EM) radiation in the frequency range from 10 MHz to 100 GHz. However, from 10 to 300 MHz, instrumentation has not been commercially available for detecting potentially hazardous human exposure levels, and little is known about the biological effects within this frequency range. As a result, there is an acknowledged research gap in the OSHA RF/Microwave Exposure Regulations from 10 to 300 MHz.

To supply OSHA with data to fill this research gap, NIOSH has established an RF radiation research program to obtain biological effects data. These data will be incorporated into a NIOSH RF/Microwave Criteria Document which will serve as one basis for modifying the current OSHA RF/Microwave Exposure Regulations. Determination of human RF biological thresholds is absolutely essential if the modified OSHA RF/Microwave Exposure Regulations are to be valid from 10 to 300 MHz.

The need for human data poses a difficult problem since RF/Microwave bioeffects research must be done with experimental animals. A relatively new modeling technique has recently been utilized to assist in extrapolating from animal exposure thresholds to human thresholds. The modeling technique, perfected by Dr. Arthur W. Guy of the University of Washington, has been accepted by the RF/Microwave research community as a reliable method to determine the extrapolation factors for RF (10-300 MHz) radiation.

Prior to obtaining human RF exposure thresholds from animal data, the relationship between RF-induced power absorption patterns in humans and animals must be reproduced under various exposure conditions. This report describes the research performed to obtain the RF-induced power absorption patterns in models of humans and animals and to extrapolate the results to humans.

ABSTRACT

The OSHA Radiofrequency (RF)/Microwave Radiation Personnel Exposure Regulation includes radiations in the frequency range from 10 MHz to 100 GHz. However, little is known about RF biological effects from 10 to 300 MHz. (The vast majority of industrial sources operate within this frequency range.) As a result, an acknowledged RF research gap exists in this regulation from 10 to 300 MHz. Thus, NIOSH has initiated a program to determine human RF exposure thresholds from 10 to 300 MHz.

Since animals are used in RF/Microwave bioeffects research, extrapolations from animal to human exposure thresholds are necessary. To perform this extrapolation, the relationship between RF-induced power absorption patterns in humans and animals must be ascertained under various exposure conditions.

Various models of animals and humans were exposed to RF fields produced by differing sources. Power absorption patterns and the rate of power absorption at specific anatomical locations within the models were thermographically recorded. These parameters were recorded under simulated RF industrial exposure conditions using a near-field synthesizer. The results of the modeling research demonstrate the validity of this technique for predicting the magnitude and distribution of RF-induced power absorption in humans and animals. The utility of the technique for extrapolation to human RF exposure thresholds from animal data was firmly established. This report was submitted in fulfillment of Interagency Agreement NIOSH IA-75-30, by the USAF, School of Aerospace Medicine, under the sponsorship of the National Institute for Occupational Safety and Health.

CONTENTS

Preface iii
Abstract iv
Acknowledgments x
Introduction 1
Description of the Work 2
Experimental Results 8
Near-Field Synthesizer 8
Exposure of Spheroidal Models 10
Electric Field 10
Magnetic Field 12
Combined Magnetic and Electric Fields . . 18
Exposure of Large Spheroid Model 22
Exposure of Man Model 22
Electric Field Only 22
Magnetic Field Only 28
Magnetic and Electric Field 28
HF Stripline 35
Exposure of Spheroid Model 35
Exposure of Man Model 35
Anechoic Chamber 35
Spheroids 39
Exposure of Man Model 39
Exposure of Animals and Animal Models 45
Microwave Mouse and Rat Brain Deactivators . . . 45
The University of Texas Systems 45
USAFSAM Microwave Brain Deactivator 57
Conclusions 57
Appendix: Calculator Programs 64

FIGURES

1. USAFSAM Near-Field Synthesizer 4
2. USAFSAM Stripline Exposure System 4
3-a. USAFSAM Anechoic Chamber Exposure System . . 5
3-b. USAFSAM Anechoic Chamber Exposure System . . 5
4-a. University of Texas Brain Deactivator Systems 6
4-b. University of Texas Brain Deactivator Systems 7
5-a. Thermograms and maximum values of SAR obtained from sphere models exposed to electric fields 13
5-b. Thermograms and maximum values of SAR obtained from sphere models exposed to electric fields 13
6-a. Thermograms and maximum values of SAR obtained from prolate spheroid models exposed to electric fields 14

6-b. Thermograms and maximum values of SAR obtained from prolate spheroid models exposed to electric fields 14
6-c. Thermograms and maximum values of SAR obtained from prolate spheroid models exposed to electric fields 15
7-a. Thermograms and maximum values of SAR obtained from sphere models exposed to magnetic fields 17
7-b. Thermograms and maximum values of SAR obtained from sphere models exposed to magnetic fields 17
7-c. Thermograms and maximum values of SAR obtained from sphere models exposed to magnetic fields 19
7-d. Thermograms and maximum values of SAR obtained from sphere models exposed to magnetic fields 19
8-a. Thermograms and maximum values of SAR obtained from spheroid models exposed to magnetic fields 20
8-b. Thermograms and maximum values of SAR obtained from spheroid models exposed to magnetic fields 20
8-c. Thermograms and maximum values of SAR obtained from prolate spheroid models exposed to magnetic fields 21
9-a. Thermograms and maximum values for SAR obtained from sphere models exposed to a parallel combination of both electric and magnetic fields 23
9-b. Thermograms and maximum values for SAR obtained from sphere models exposed to a parallel combination of both electric and magnetic fields 23
9-c. Thermograms and maximum values of SAR obtained from sphere models exposed to a parallel combination of both electric and magnetic fields 24
9-d. Thermograms and maximum values of SAR obtained from sphere models exposed to a parallel combination of both electric and magnetic fields 24
10-a. Thermograms and maximum values of SAR obtained from prolate spheroid models exposed to a parallel combination of both electric and magnetic fields 25
10-b. Thermograms and maximum values of SAR obtained from prolate spheroid models exposed to a parallel combination of both electric and magnetic fields 25
11-a. Thermograms and maximum values of SAR obtained for 1.74 m high 70 kg man exposed to electric fields 29
11-b. Thermograms and maximum values of SAR obtained for 1.74 m high 70 kg man exposed to electric fields 29
12-a. Thermograms and maximum values of SAR obtained for 1.74 m high 70 kg man exposed to magnetic fields 32

12-b. Thermograms and maximum values of SAR obtained for 1.74 m high 70 kg man exposed to magnetic fields 32
13-a. Thermograms and maximum values of SAR obtained for 1.74 m high 70 kg man exposed to electric and magnetic fields parallel to the frontal plane and perpendicular to the transverse plane 33
13-b. Thermograms and maximum values of SAR obtained for 1.74 m high 70 kg man exposed to electric and magnetic fields parallel to the frontal plane and perpendicular to the transverse plane 33
14. Thermograms and maximum values of SAR obtained for 1.74 m high 70 kg man exposed to electric and magnetic fields perpendicular to the frontal plane and parallel to the transverse plane 34
15. Thermograms and maximum values of SAR obtained for 1.74 m high 70 kg man exposed to electric and magnetic fields parallel to both transverse and frontal planes 34
16-a. Thermograms obtained from 3.13:1 prolate spheroid exposed in HF stripline 37
16-b. Thermograms obtained from 3.13:1 prolate spheroid exposed in HF stripline 38
17-a. Thermograms and maximum values of SAR obtained for 1.74 m high 70 kg man exposed in HF stripline 40
17-b. Thermograms and maximum values of SAR obtained for 1.74 m high 70 kg man exposed in HF stripline 40
18. Thermograms and maximum values of SAR obtained for 3 cm radius sphere exposed to 1600 MHz plane wave EM fields 43
19. Thermograms and maximum values of SAR obtained for 3.13:1 prolate spheroid exposed to 1600 MHz plane wave EM fields 44
20-a. Thermograms and maximum values of SAR obtained for 58 cm high 2.6 kg man exposed to 1200 MHz plane wave EM fields 46
20-b. Thermograms and maximum values of SAR obtained for 58 cm high 2.6 kg man exposed to 1200 MHz plane wave EM fields 47
21-a. Thermograms and maximum values of SAR obtained for 58 cm high 2.6 kg man exposed to 1200 MHz plane wave EM fields 48
21-b. Thermograms and maximum values of SAR obtained for 58 cm high 2.6 kg man exposed to 1200 MHz plane wave EM fields 48
22-a. Thermograms and maximum values of SAR obtained for 58 cm high 2.6 kg man exposed to 1200 MHz plane wave EM fields 49

22-b. Thermograms and maximum values of SAR obtained for 58 cm high 2.6 kg man exposed to 1200 MHz plane wave EM fields 49
22-c. Thermograms and maximum values of SAR obtained for 58 cm high 2.6 kg man exposed to 1200 MHz plane wave EM fields 50
22-d. Thermograms and maximum values of SAR obtained for 58 cm high 2.6 kg man exposed to 1200 MHz plane wave EM fields 50
23-a. Thermograms and maximum SAR values obtained for 40 g mice and a phantom mouse exposed to 1600 MHz plane wave EM fields 52
23-b. Thermograms and maximum SAR values obtained for 40 g mice and a phantom mouse exposed to 1600 MHz plane wave EM fields 53
24-a. Animal orientation and field configuration of microwave brain deactivations at University of Texas Medical School 56
24-b. Animal orientation and field configuration of microwave brain deactivations at University of Texas Medical School 56
25-a. Thermograms and maximum SAR values obtained for 40 g mice exposed in University of Texas microwave brain deactivator 58
25-b. Thermograms and maximum values of SAR obtained for 40 g mice exposed in University of Texas microwave brain deactivator 59
26. Thermograms and maximum values of SAR obtained for 40 g mice exposed in University of Texas microwave brain deactivator 60
27-a. Thermograms and maximum values of SAR obtained for a 200 g rat exposed in USAFSAM microwave brain deactivator 61
27-b. Thermograms and maximum values of SAR obtained for 40 g mice exposed in USAFSAM microwave brain deactivator 62

TABLES

I Dimensions, Scale Factors, and Simulated Frequencies of Phantom Models 9
II Model Exposure Conditions in USAFSAM Near Field Synthesizer at 19 MHz 11
III Maximum SAR Calculated for Full Scale 70 kg Spheroids 16
IV Maximum SAR Calculated for Full-Scale 70 kg Spheroids 26
V Comparison of Measured SAR for Man Exposed in Near Field Synthesizer and VHF Resonant Cavity 27

VI	Comparison of SAR Ratios for Man Exposed in Near-Field Synthesizer and VHF Resonant Cavity	30
VII	Ratios of SAR of Near-Field Synthesizer Exposure to VHF Resonant Cavity Exposure for a Man	31
VIII	Model Exposure Conditions in USAFSAM Stripline Chamber at 19 MHz	36
IX	Comparison of Measured SAR for Man Exposed in HF Stripline and VHF Resonant Cavity	41
X	Model Exposure Conditions in USAFSAM Anechoic Chamber at 1600 MHz	42
XI	Measured SAR for 0.58 m High 2.6 kg Infant Exposed to 1200 MHz Plane Wave EM Fields . .	51
XII	Exposure Conditions in University of Texas Mouse Deactivators at 2450 MHz	54
XIII	Exposure Conditions in USAFSAM Mouse Deactivator at 2450 MHz	55

ACKNOWLEDGMENTS

We wish to acknowledge the USAF School of Aerospace Medicine (USAFSAM), Aerospace Medical Division (AFSC), Brooks Air Force Base, Texas, for jointly funding this research with NIOSH under Interagency Agreement NIOSH IA-75-30. In addition, we express our gratitude to the USAF Project Officer, Dr. James W. Frazer*, USAFSAM, and to Dr. Arthur W. Guy, University of Washington, for their approval and assistance in publishing this report.

* Present address: Dept. of Diagnosis & Roentgenology
Univ. of Texas, Health Science Center
San Antonio, Texas 78284

I. INTRODUCTION

The interaction of high frequency (HF) electromagnetic fields with objects of various shapes, including figurines representing man (composed of synthetic muscle material), has been studied and reported previously (1)(2). The objects were exposed to very high frequency (VHF) electromagnetic fields in a resonant cavity designed to simulate HF exposure conditions under various field impedance conditions. The frequency of exposure, size, and conductivity of the objects were scaled appropriately to simulate exposure of larger objects to HF electromagnetic fields. Since the cavity operates at a frequency of approximately 144 MHz, models of 1/5 scale or smaller can be used to simulate both near-field and far-field exposure conditions for full scale objects below 30 MHz.

An electromagnetic near-field synthesizer of another type was constructed by the National Bureau of Standards for the United States Air Force School of Aerospace Medicine (USAFSAM) at Brooks Air Force Base, Texas, during the same period (3). The synthesizer provides independent excitation of high level electric and magnetic fields in the frequency range of 10 to 30 MHz. The system was designed to expose various test animals under near-field conditions to assess the biological effects of HF fields.

The purpose of this report is to present a summary of the results of measurements taken by University of Washington, Bioelectromagnetics Research Laboratory (UW BEMRL) personnel while on a field trip to USAFSAM to compare the near-field synthesizer delivery system to that of the VHF resonant cavity system at the University of Washington. Some of the other USAFSAM exposure systems were also used to expose various biological models.

One was a high frequency stripline exposure system designed to provide high level HF electromagnetic fields in the frequency range 5 - 40 MHz for exposure of biological models and animals (4). Another exposure system

---

1. Guy, A.W.; M.D. Webb; A.F. Emery; R.H. Willard; and J.C. Lin, "High frequency electromagnetic fields in phantom models of man and measured electrical properties of tissue materials," BEMRL, Dept. Rehab. Med., Univ. Wash. School of Med., Seattle, Sci. Rpt. No. 3, July 1974. USAFSAM Contract No. F41609-73-C-0002.
2. Guy, A.W.; M.D. Webb; and C.C. Sorensen, "Determination of power absorption in man exposed to high frequency electromagnetic fields by thermographic measurements on scale models," IEEE Trans. Biomed. Eng., September 1976, (in press).
3. Development and Construction of an Electromagnetic Near-Field Synthesizer. NBS Tech. Note 652, May 1974.
4. Mitchell, J.C., "A radiofrequency radiation exposure apparatus," SAM-TR-70-43, USAF School of Aerospace Med., Brooks Air Force Base, Texas.

allows plane wave exposure of actual or phantom biological objects to high level electromagnetic (EM) fields in the frequency range 300-3000 MHz (UHF) to microwaves (5). No comparisons were made of the effectiveness of the latter exposure system, however, since the UW BEMRL did not possess similar facilities at the time of the work.

II. DESCRIPTION OF THE WORK

The comparisons of the measurements at USAFSAM were made from March 17, 1975, to March 28, 1975. Thermographic equipment, model forms, material for constructing biological models, and related equipment used to thermographically obtain the field distribution patterns in models exposed in the UW BEMRL resonant cavity were transported to USAFSAM. The use of the same thermographic equipment and model molds for the exposure work performed at USAFSAM facilitated the comparison of the delivery systems by decreasing the number of variables. Biological model forms used in the experiments at USAFSAM were:

1. 6-cm diameter sphere
2. 8.6-cm diameter sphere
3. 11.1-cm diameter sphere
4. 2:1 prolate spheroid, a = 6.82 cm
5. 5:1 prolate spheroid, a = 12.57 cm
6. 7.73:1 prolate spheroid, a = 16.81 cm
7. 3.13:1 prolate spheroid, a = 19.6 cm
8. 1/4.62th scale human being, h = 37.7 cm

The 8.6-cm and 11.1-cm diameter spheres, the 5:1 prolate spheroid, and the scale model human being were used at the UW BEMRL to evaluate the absorption in man exposed to HF frequencies by exposing the models to VHF frequencies in the resonant cavity. These models are the basis of the verification and comparison of specific absorption rate (SAR) patterns produced by the USAFSAM near-field synthesizer and the UW BEMRL VHF resonant cavity. During the interval between the initial test in the VHF resonant cavity and the verification tests in the near-field synthesizer, a new technique for model sectioning was developed at UW BEMRL. The previous techniques developed by Guy et al., (6)(7) for measuring power deposition patterns in biological

5. Tech. Bull. 31-2, "Eccosorb Anechoic Tapered Chamber Kits," Emerson & Cuming, Inc., Canton, MA.
6. Guy, A.W., "Analyses of electromagnetic fields induced in biological tissues by thermographic studies on equivalent phantom models," IEEE Trans. Microwave Theory Tech., 19:2 205-214, February 1971.
7. Guy, A.W., "Quantitation of induced electromagnetic field patterns in tissue and associated biological effects," Biologic Effects and Health Hazards of Microwave Radiation, Proc. Int'l Symp., Warsaw, October 1973, Polish Medical Publishers, Warsaw, 1974, pp. 203-216.

tissues exposed to EM fields by thermographic measurements using phantom models were limited to symmetrical models exposed to a linearly polarized field. The power absorption patterns in such models could only be measured in the median plane, which was aligned parallel to the incident electric field. This restriction was imposed because the flat surfaces of each half of the model were covered with a thin sheet of plastic to facilitate their separation. The plastic sheet interrupted any induced currents that would normally flow nonparallel to the median plane of separation. This limited the use of the older model to cases where such currents did not exist. The important dosimetry problem, however, of measuring the SAR in a regular shaped body such as man exposed to arbitrary fields requires a more general technique. In order to extend the old technique to handle this new class of problems, the phantom models simulating the biological objects were modified so the proper electrical contact could be maintained between any two sections of the bisected model (8).

The new technique utilizes a silk screen layer in place of the plastic sheet glued over each half-section of the model. After the synthetic tissue gel is poured and set in the two halves of the model, the models are placed together with the silk screen surfaces in contact. Good adhesion and electrical coupling between the two halves are obtained through the gel flowing into and through the silk screen boundary. The models can easily be separated and rejoined repeatedly without loss of adhesion or electrical tontinuity. The new sectioning technique was used almost exclusively during the tests in the USAFSAM exposure systems. Several tests were made using the old model sectioning technique in the near-field synthesizer so comparisons between the two exposure systems could be made.

The near-field synthesizer shown in Fig. 1 has the capability of producing fields of several combinations. Two horizontal plates spaced 75 cm apart produce a uniformly distributed vertical electric field between them. In the center between the plates, the loop inductor provides a magnetic field parallel to the axis of the loop. Since the loop can be rotated over any angle with respect to the plate, the relative orientation between electric and magnetic fields can be varied from parallel to perpendicular. The major comparisons between the near-field synthesizer and the VHF cavity were made using electric fields alone and magnetic fields alone. In addition, tests were made where the models were also exposed in the USAFSAM near-field synthesizer to both electric and magnetic fields with the field vectors aligned parallel.

Although such a configuration is not realistic in terms of simulating most near-field situations, it provides another means of evaluating the system, since the components of electric field induced in the model due to the applied electric and magnetic fields are orthogonal and the SAR contributed by each should add directly. This particular field configuration could not be produced in the VHF resonant cavity, so the results of this exposure were compared only to available theoretical solutions. The models were also

8. Guy, A.W.; M.D. Webb; and J.A. McDougall, "A new technique for measuring power deposition patterns in phantoms exposed to EM fields of arbitrary polarization - example, the microwave oven," IMPI Microwave Power Symp., Univ. Waterloo, Waterloo, Ont., Can., May 1975, pp. 36-47.

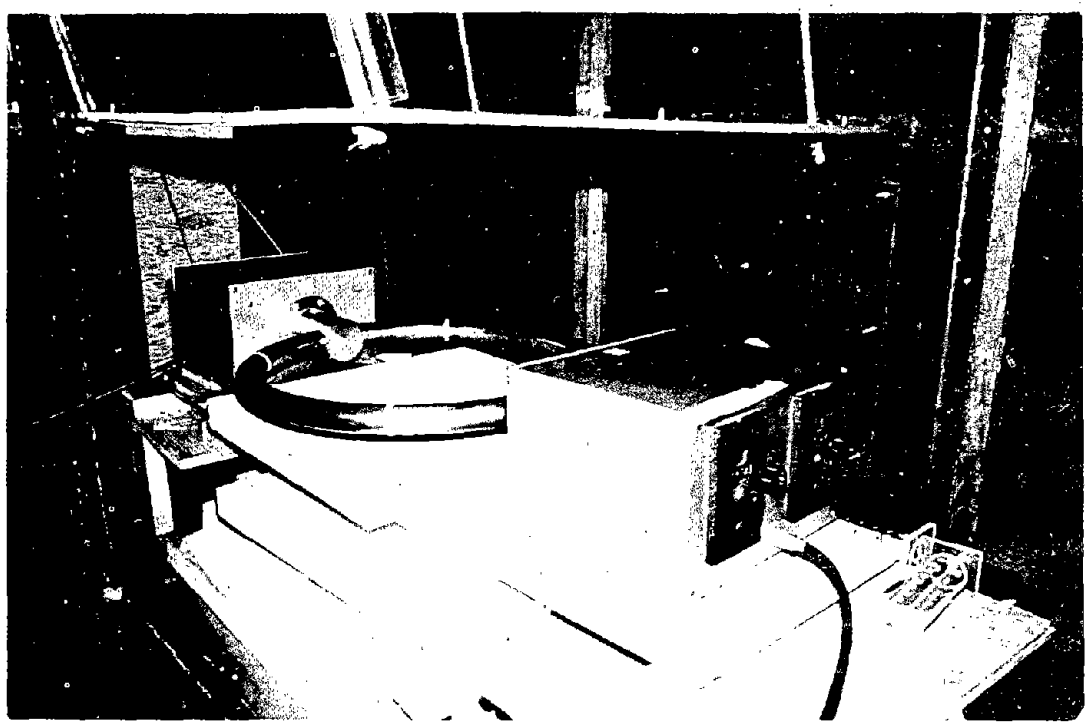

Figure 1. USAFSAM Near-Field Synthesizer

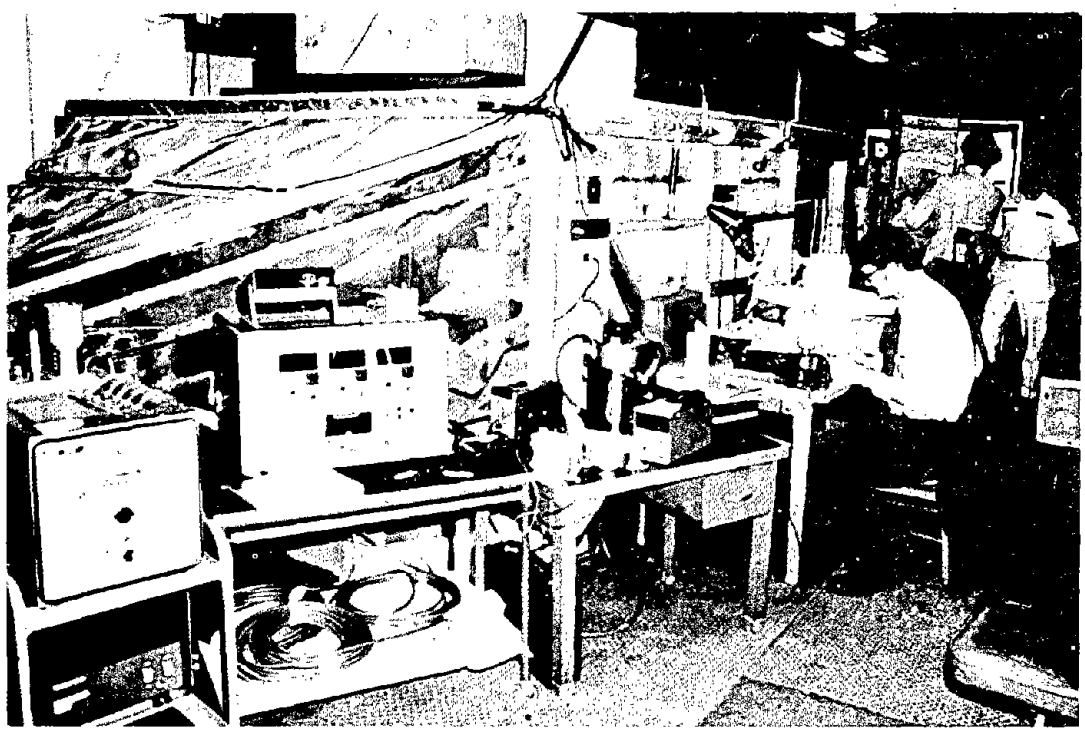

Figure 2. USAFSAM Stripline Exposure System

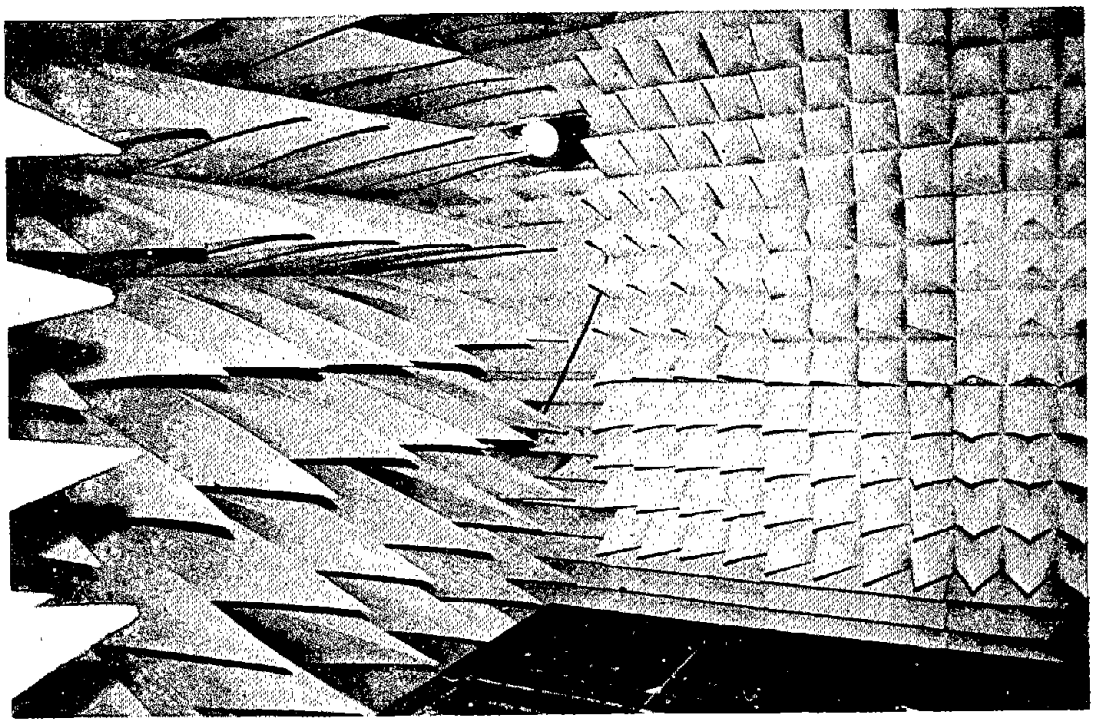

a

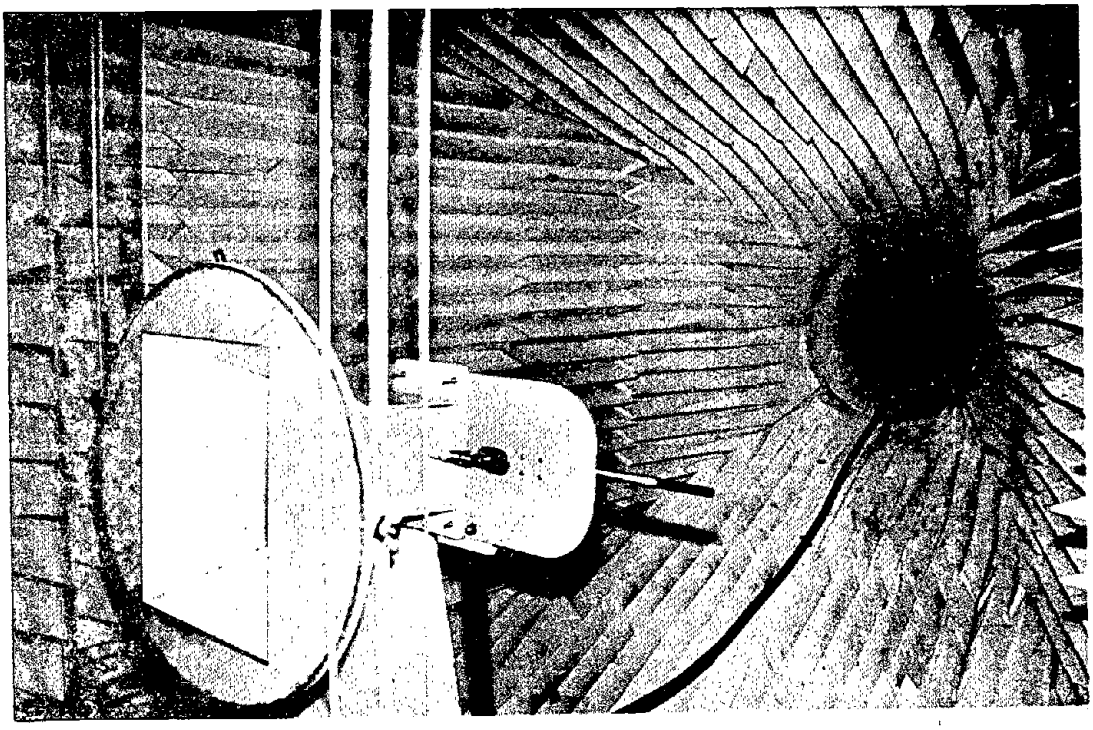

b

Figure 3. USAFSAM Anechoic Chamber Exposure System

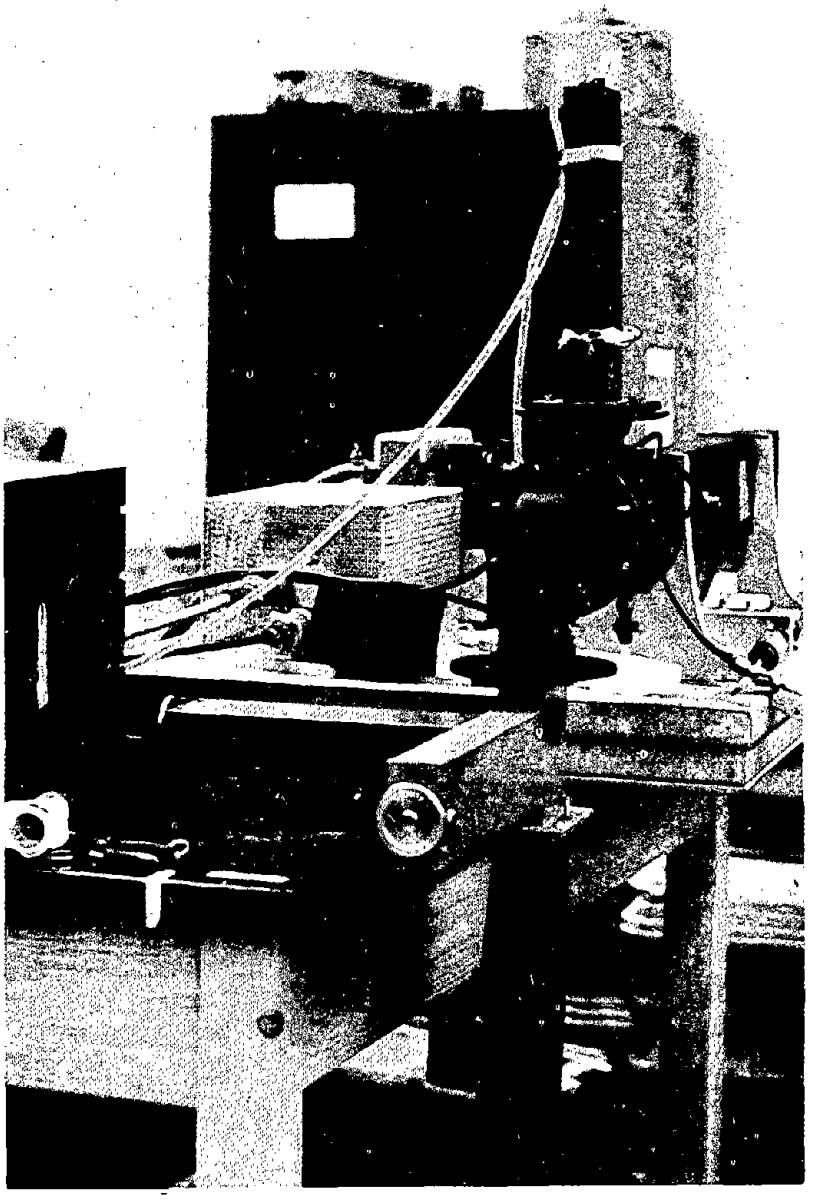

a

Figure 4. University of Texas Brain Deactivator Systems

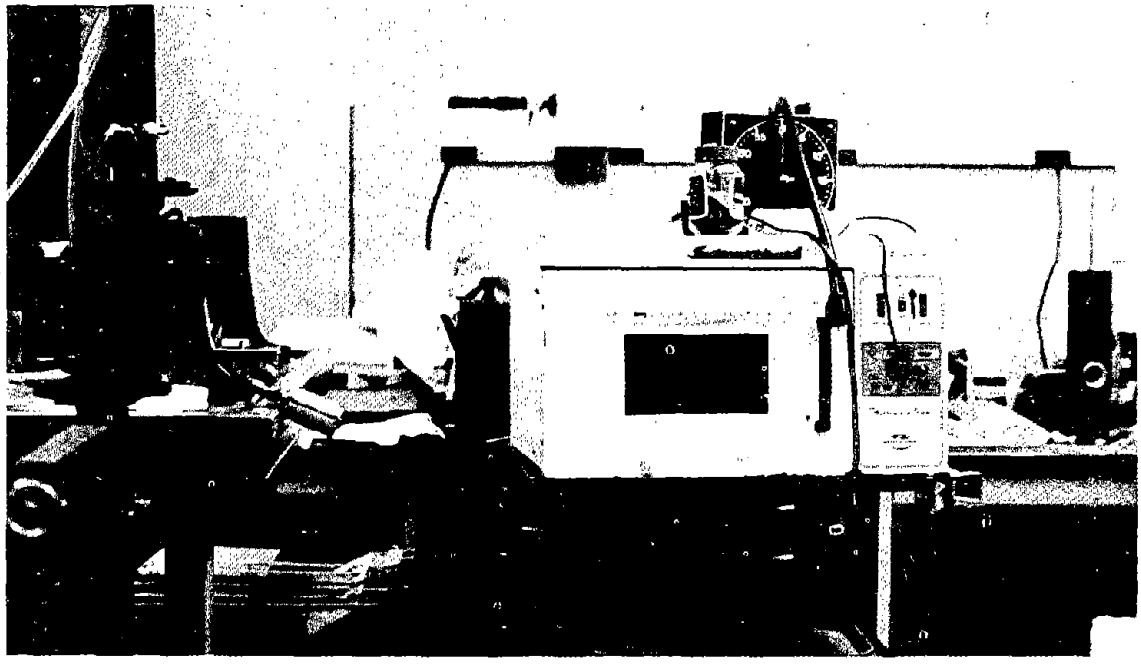

b

Figure 4. University of Texas Brain Deactivator Systems

exposed to 19 MHz HF fields in the USAFSAM stripline exposure apparatus, shown in Figure 2, and to a 1600 MHz plane wave EM field in an anechoic chamber, shown in Figure 3. Thermographic measurements of SAR were also made of 40 gm mice and 200 gm rats exposed to high power microwave brain deactivators used at the University of Texas Medical School, shown in Figure 4, and at USAFSAM.

III. EXPERIMENTAL RESULTS

A. Near-Field Synthesizer

The majority of the phantom models used at USAFSAM were scaled according to the procedures reported in (1). Thus, even though the models were being exposed to 19 MHz electric and magnetic fields in the near-field synthesizer, they were actually simulating full-scale 70 kg objects being exposed to lower frequency electric and magnetic fields. The one exception to this was the full-scale 3.13:1 ellipsoid model used to simulate a full-scale monkey. Table I lists the dimensions and scale factors for these models and the simulated frequencies for an exposed full scale 70 kg model both at the USAFSAM facilities and the UW BEMRL facilities.

It is obvious from the table that direct comparisons cannot be made because the simulated frequencies are not identical for the two exposure systems. However, by assuming that the specific absorption rate is directly proportional to frequency squared (f^2), the measured SAR at USAFSAM may be multiplied by the ratio of the two simulated frequencies and then compared with the measurements in the VHF resonant cavity at UW BEMRL. Thus, for models with a scale factor of 4.62, the SAR frequency scale factor (FSF) equals $(31.0/4.11)^2$, and for those with scale factor of 5.95, FSF = $(24.1/3.19)^2$. Table II illustrates the actual field conditions and measured SAR values as a result of exposing various models in the near-field synthesizer at 19 MHz. The first column lists the size and type of object, the scale factor, and the type of interface between the two halves of the model. The second column illustrates the polarization of various field components at the plane of separation of the model. The third column illustrates the input power to the near-field synthesizer; the fourth column illustrates the electric field strength; the fifth column illustrates the magnetic field strength; the sixth column the exposure time; the seventh column the maximum increase in temperature, measured thermographically as described in the following sections; the eighth column the maximum SAR, as calculated from the temperature rise; and the last column the maximum theoretical SAR where applicable.

In the normal application of the thermographic technique for measuring SAR, the model is first exposed to the particular source of interest, except at a considerably higher power level. The higher than normal power level is needed to heat the phantom model in the shortest possible time. After the short exposure, the model is quickly disassembled and the temperature pattern over the surface of the separation is observed and recorded by means of a thermograph. Exposures are normally applied over a 5-60 sec time interval, depending on the source. After a 3-15 sec delay for separating the two halves of the model, recording is done within 1/16 sec. Since the thermal

TABLE 1

DIMENSIONS, SCALE FACTORS, AND SIMULATED FREQUENCIES OF PHANTOM MODELS

Model	Scale Factor	Simulated Model	Simulated Frequency USAFSAM	Simulated Frequency UW BEMRL
Spheroid				
a/b=1 a=4.3cm	5.95	51.2 cm dia.sphere	3.19 MHz	24.1 MHz
a/b=1 a=5.6cm	4.62	51.2 cm dia.sphere	4.11 MHz	31.0 MHz
a/b=2 a=6.82cm	5.95	2:1 prolate spheroid a=40.6cm	3.19 MHz	24.1 MHz
a/b=5 a=12.57 cm	5.95	5:1 prolate spheroid a=74.8cm	3.19 MHz	24.1 MHz
a/b=7 a=16.81 cm	5.95	7.73:1 prolate spheroid a=100cm	3.19 MHz	24.1 MHz
Human	4.62	70kg h=1.74 in human	4.11 MHz	31.0 MHz

diffusivity of the model is low, the difference in measured temperature distribution before and after heating will closely approximate the heating distribution over the flat surface, except for regions of high temperature gradient, where there may be some error due to heat diffusion. In this investigation, however, due to power limitations, most of the exposure times using the USAFSAM facilities were far in excess of 60 min, as shown in Table II, so we can expect considerable error due to heat diffusion. An analysis by the General Electric Company, appearing in one of our reports (9) indicates that a significant error (for instance, up to 57%), can result in the thermographic recording, from thermal diffusion effects during a 5 min exposure time with the assumption that the heating volume corresponds to a 1" diameter sphere. The error can even be greater if the heating area is smaller or is nonuniform.

The SAR data obtained by the thermographic measurements, which are scaled to full-scale models and normalized to a squared electric field intensity (E^2) for the electric field exposure and magnetic field intensity (H^2) for magnetic field exposure, are tabulated in Table III. The measured values from the USAFSAM exposures were compared to the results obtained from the UW BEMRL exposure system by scaling them up in frequency by the FSF factor described above. In addition, for the case of the spheroids, the measured values were compared to theoretical values based on the analysis by Durney and Johnson (10). Equations were programmed on a Hewlett-Packard 65 hand calculator to facilitate rapid computation. This program and user instructions are given in the Appendix. Detailed discussion of the exposure methods and thermographic results are discussed below.

1. Exposure of Spheroidal Models

a. Electric Field

All of the models exposed to the electric field configuration were oriented with their sectioning plane parallel to the electric field vector between the plates of the near-field synthesizer shown in Figure 1. The spheroids exposed in this configuration were irradiated for 5 min. As discussed previously, this is much longer than the usual exposure time for thermographic measurements, but the long exposure was required to obtain discernible temperature differences. In some cases, this exposure time was insufficient to produce a measurable temperature increase, as was the case for the sphere exposed to the electric field with the results shown in Fig. 5-a for simulating the full-scale exposure to 4.11 MHz, and in Fig. 5-b simulating a full-scale exposure to 3.19 MHz. The upper left photograph of the figures illustrates the intensity scan where brightness is proportional

9. Guy, A.W.; M.D. Webb; and J.A. McDougall, "Assessment of the EM field coupling of 915 MHz oven door leakage to human subjects by thermographic studies on equivalent phantom models," BEMRL, Dept. Rehab. Med., Univ. Wash. School of Med., Seattle, Sci. Rpt. No. 7, March 1976. General Electric Co. Contract No. PO 112-ZA20-224549-P.
10. Durney, C.H.; C.C. Johnson; and H. Massoudi, "Long-wavelength analysis of plane wave irradiation of a prolate spheroid model of man," IEEE Trans. Microwave Theory Tech., 23:2: 246-253, February 1975.

TABLE II

MODEL EXPOSURE CONDITIONS IN USAFSAM NEAR-FIELD SYNTHESIZER AT 19 MHz

OBJECT	ORIENTATION	INPUT POWER (WATTS)	ELECTRIC FIELD STRENGTH (V/m)	MAGNETIC FIELD STRENGTH (A/m)	EXPOSURE TIME (sec)	TEMPERATURE RISE (°C)	MAX SAR MEASURED (W/kg)	MAX SAR THEORY (W/kg)
3.6 cm Dia. sphere Scale Factor = 5.95 Silk Screen Interface	E∥cut	390	8280	----	300	0.2	2.26	9.10
	H⊥cut	400	----	46	120	1.7	40.5	83.2
	H∥cut	390	----	46	120	3.0	90.6	83.2
	E & H∥cut	E 400 H 370	8280	46	120	4.5	136	83.4
	E & H⊥cut	E 370 H 370	8280	46	120	2.4	72.2	83.4
11.2 cm Dia. Sphere Scale Factor = 4.62 Silk Screen Interface	E∥cut	330	8280	----	300	0.6	7.36	9.230
	H⊥cut	390	----	46	120	3.7	94.8	112
	H∥cut	380	----	46	120	2.7	90.7	112
	E & H∥cut	E 370 H 400	8280	46	120	6.2	137	112
	E & H⊥cut	E 370 H 400	8280	46	120	4.0	120	112
2:1 Ellipsoid a = 6.32 cm Scale Factor = 5.95 Plastic Interface	E∥cut	330	8280	----	300	0.4	5.09	6.671
	H⊥cut	380	----	46	120	2.9	86.3	134
5:1 Ellipsoid a = 12.57 cm Scale Factor = 5.95 Plastic Interface	L∥cut	400	8280	----	300	0.9	10.6	6.49
	H⊥cut	400	----	46	120	1.5	41.9	105
7.73:1 Ellipsoid a = 16.31 cm Scale Factor = 5.95 Plastic Interface	E∥cut	400	8280	----	300	0.7	8.49	22.63
	H⊥cut	400	----	46	120	1.1	34.0	82.3
3.13:1 Ellipsoid a = 19.6 cm Scale Factor = 1.00 Silk Screen Interface	E & H∥cut	E 380 H 400	8280	46	120	1.8	50.7	70.6
	E & H⊥cut	E 380 H 400	8280	46	120	3.2	92.1	49.6
Man 1.74 m, two backs Scale factor = 4.62 Plastic Interface	E∥cut ∥ long axis	400	8280	----	60.2	9.3	557	----
	H⊥cut ⊥ long axis	390	----	46	90	3.4	137	----
Man 1.74 m, true shape Scale Factor = 1.62 Silk Screen Interface	E & H∥cut ∥ long axis	E 370 H 400	8280	46	60	5.4	322	----
	E & H∥cut ⊥ long axis	E 380 H 400	8280	46	120	5.0	150	----
	E & H⊥cut ⊥ long axis	E 390 H 400	8280	46	120	5.4	158	----

to temperature and SAR. The upper right photograph of the figures is the profile scan (a vertical array of single line scans where the vertical deflection of each scan is proportional to the temperature or SAR).

Finally, at the bottom of each figure, there is a double exposed line scan, one trace taken before exposure and one trace taken after exposure along the line section marked on the intensity scan. For these cases, the resolution was very poor and resulted in calculated SAR values far in excess of the theoretical values. This was due principally to diffusion of heat from the foam container to the synthetic muscle material contained therein. Since the electric field values are quite high in foam as compared to the muscle as the result of the large ratio in dielectric constants, even a small loss factor in the foam can result in SAR values higher than that in the synthetic muscle. Over the long time period of exposure, this heat diffused into the synthetic muscle material increased its temperature and resulted in calculated SAR values far in excess of theoretical values.

The SAR values are calculated for the position on the line scan indicated by the arrow, usually corresponding to the maximum temperature change. Thermographic results of exposing prolate spheroids to an electric field are shown in Fig. 6-a for a 2:1 axial ratio; 6-b for a 5:1 axial ratio; and 6-c for a 7.73:1 axial ratio. The heating in the ellipsoid with the 2:1 axial ratio was negligible and the calculated SAR values could not be obtained. The heating for the ellipsoids with the larger axial ratios, however, was sufficient to produce calculated SAR values much closer to the theoretical values, since the SAR increases markedly with axial ratio. In these cases, the measured values are somewhat lower than the theoretical values, however, since the thermal diffusion now results in heat flow from the heated synthetic muscle to the foam casing. This is to be expected, considering the long 5 min exposure times based on the analysis reported in (9). The results, when compared in Table III to the UW BEMRL exposure results for the 5:1 axial ratio spheroid, agreed within approximately 40%. Since the UW BEMRL results, which are based on very short exposure times, agreed much more closely with theory than the USAFSAM results based on 5 min exposure times, we would expect the disagreement between results to be due to the thermal diffusion problem.

b. Magnetic Field

Two orientations of the spheroidal models were used when exposing to a magnetic field configuration. One corresponded to the sectioning plane being aligned parallel to the magnetic field vector, and the other aligned perpendicular to the magnetic field vector. In both cases, the model was placed in the center of the loop shown in Fig. 1. Since the magnetic field couples energy much more strongly to the spheroids, the exposure time was decreased to 2 min. Even with the shorter exposure time, however, the period is still much longer than that normally required for accurate results. This exposure condition does eliminate the heating of the foam container, however, since the magnetic heating of such material is negligible. Fig. 7-a illustrates the thermographic results in predicting the SAR patterns for a 70 kg sphere exposed to a 4.11 MHz magnetic field perpendicular to the plane of separation. Note that the measured value, though slightly lower,

SPHERE R=25.6 cm E^2=1 V^2/m^2 sf=4.62 f=4.11 MHz
SECTION PLANE || TO E FIELD

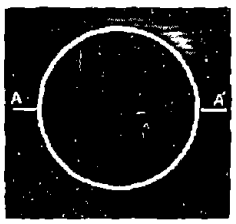

INTENSITY

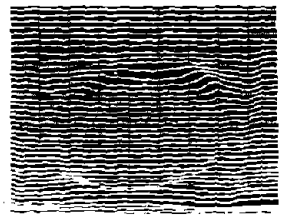

PROFILE

SINGLE LINE

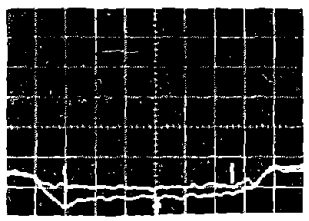

A–A'

MEASURED W=23.2 nW/kg THEORETICAL W=724 pW/kg

a

SPHERE R=25.6 cm E^2=1 V^2/m^2 sf=5.95 f=3.19 MHz
SECTION PLANE || TO E FIELD

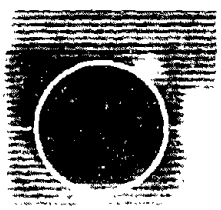

INTENSITY

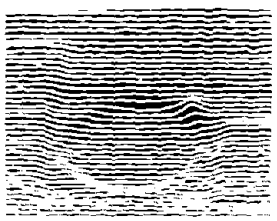

PROFILE

SINGLE LINE

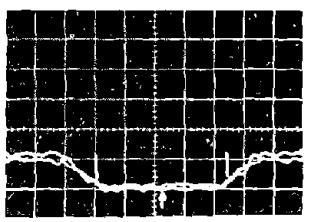

A–A'

MEASURED W=5.55 nW/kg THEORETICAL W=44.7 pW/kg

b

Figure 5. Thermograms and maximum values of SAR obtained from sphere models exposed to electric fields. (All values pertain to full-scale exposure conditions.)

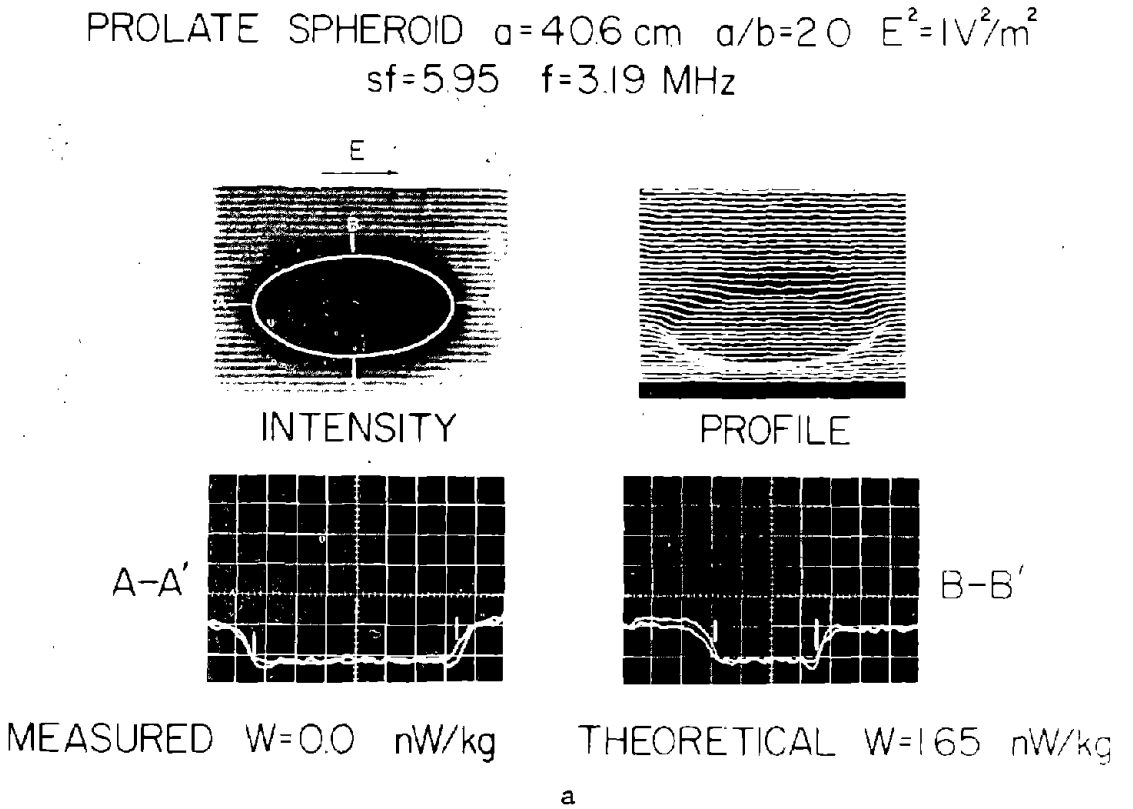

a

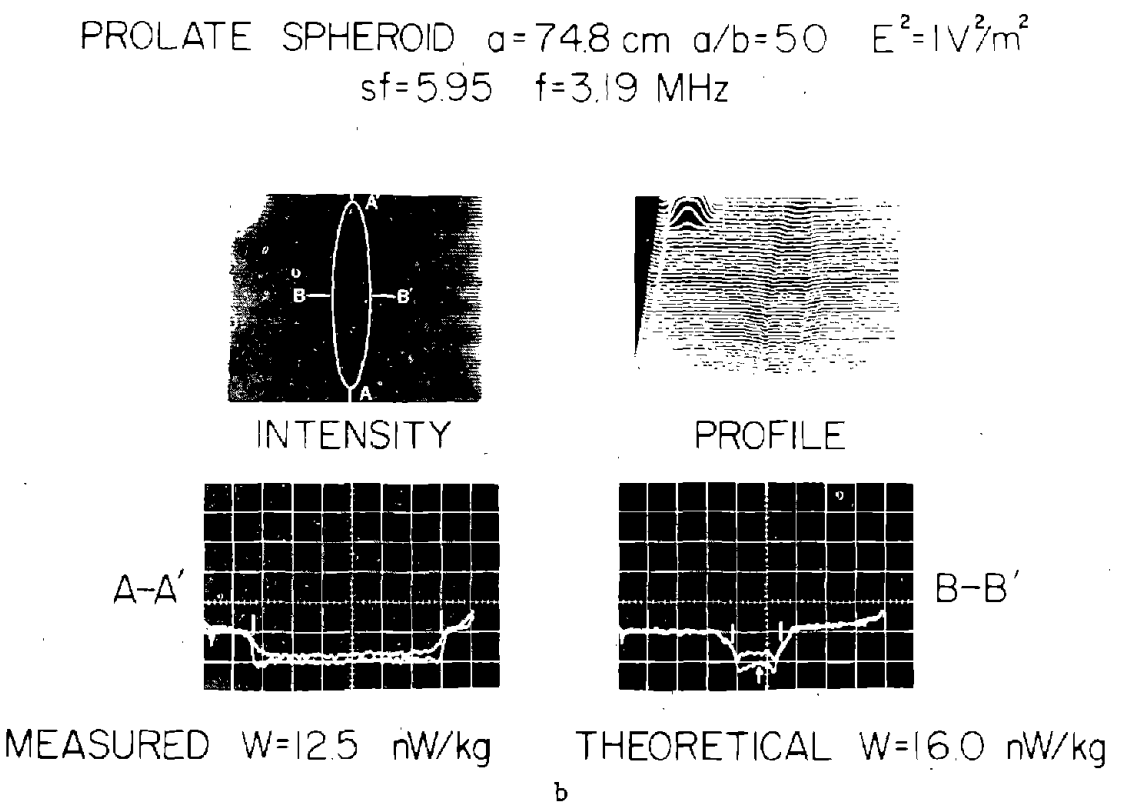

b

Figure 6. Thermograms and maximum values of SAR obtained from prolate spheroid models exposed to electric fields. (All values pertain to full-scale exposure conditions.)

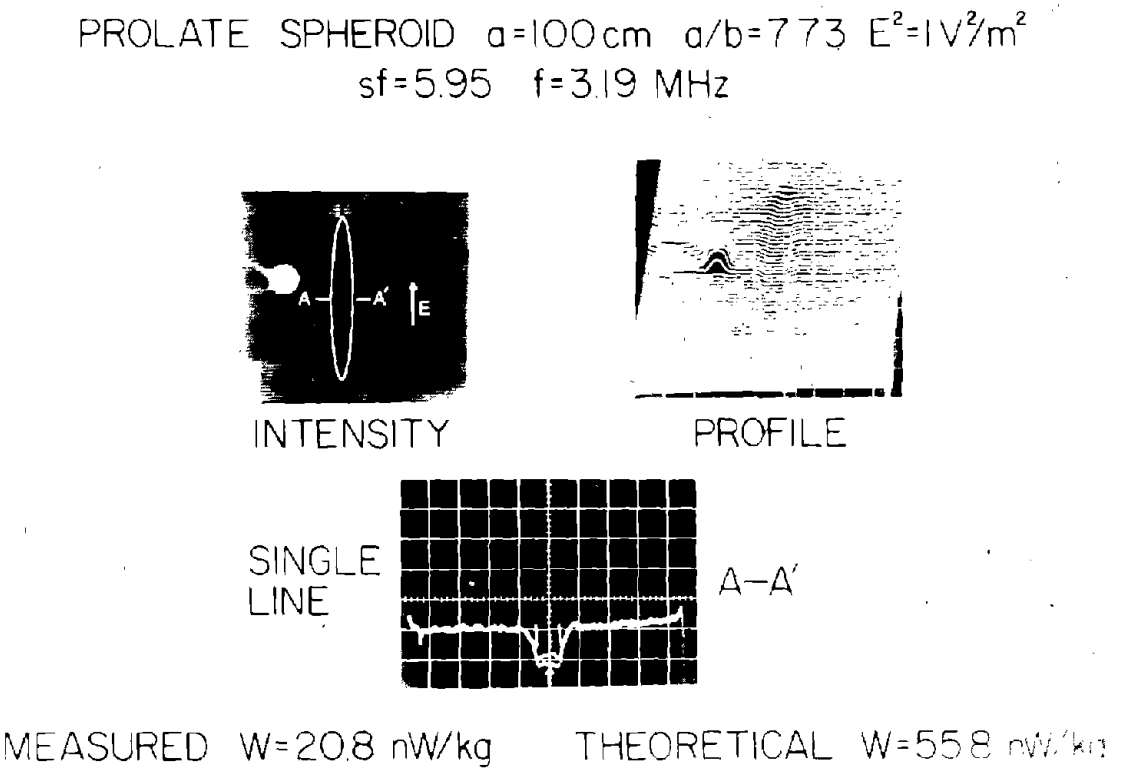

c

Figure 6. Thermograms and maximum values of SAR obtained from prolate spheroid models exposed to electric fields. (All values pertain to full-scale exposure conditions.)

TABLE III

MAXIMUM SAR CALCULATED FOR FULL-SCALE 70 kg SPHEROIDS

ELLIPTICITY	USAFSAM NEAR-FIELD SYNTHESIZER			UW BEARL VHF RESONANT CAVITY	
	MAXIMUM SAR MEASURED W/kg	MAXIMUM SAR THEORETICAL W/kg	FREQUENCY SCALED MAXIMUM SAR MEASURED W/kg	MAXIMUM SAR THEORETICAL W/kg	MAXIMUM SAR MEASURED W/kg
	APPLIED ELECTRIC FIELD PARALLEL TO SECTION PLANE $E^2 = 1\ V^2/m^2$				
	f = 3.2 MHz		Scaled to f=24.1 MHz	f = 24.1 MHz	
a/b = 1	5.55×10^{-9}	0.847×10^{-9}	117×10^{-9}	25.1×10^{-9}	28.0×10^{-9}
a/b = 2	0.0	1.55×10^{-9}	0.0	93.2×10^{-9}	
a/b = 5	12.5×10^{-9}	16.0×10^{-9}	0.212×10^{-6}	0.99×10^{-6}	1.16×10^{-6}
a/b = 7.73	20.8×10^{-9}	25.8×10^{-9}	1.19×10^{-6}	3.16×10^{-6}	
	f = 4.1 MHz		Scaled to 31.0 MHz	f = 31.0 MHz	
a/b = 1	23.2×10^{-9}	0.724×10^{-9}	1.32×10^{-6}	38.9×10^{-9}	43.6×10^{-9}
	APPLIED MAGNETIC FIELD PERPENDICULAR TO SECTION PLANE $H^2 = 1\ A^2/m^2$				
	f = 3.2 MHz		Scaled to f=24.1 MHz	f = 24.1 MHz	
a/b = 1	3.93×10^{-3}	6.61×10^{-3}	0.724	0.359	0.366
a/b = 2	6.86×10^{-3}	10.6×10^{-3}	0.391	0.621	
a/b = 5	1.40×10^{-3}	8.33×10^{-3}	0.599	0.427	0.503
a/b = 7.73	2.70×10^{-3}	6.51×10^{-3}	0.758	0.380	
	f = 4.1 MHz		Scaled to f=31.0 MHz	f = 31.0 MHz	
a/b = 1	9.70×10^{-3}	11.0×10^{-3}	0.552	0.699	0.599
	APPLIED MAGNETIC FIELD PARALLEL TO SECTION PLANE $H^2 = 1\ A^2/m^2$				
	f = 3.2 MHz		Scaled to f=24.1 MHz	f = 24.1 MHz	
a/b = 1	7.19×10^{-3}	6.61×10^{-3}	0.330	0.359	
	f = 4.1 MHz		Scaled to f=31.0 MHz	f = 31.0 MHz	
a/b = 1	8.25×10^{-3}	11.0×10^{-3}	0.469	0.699	

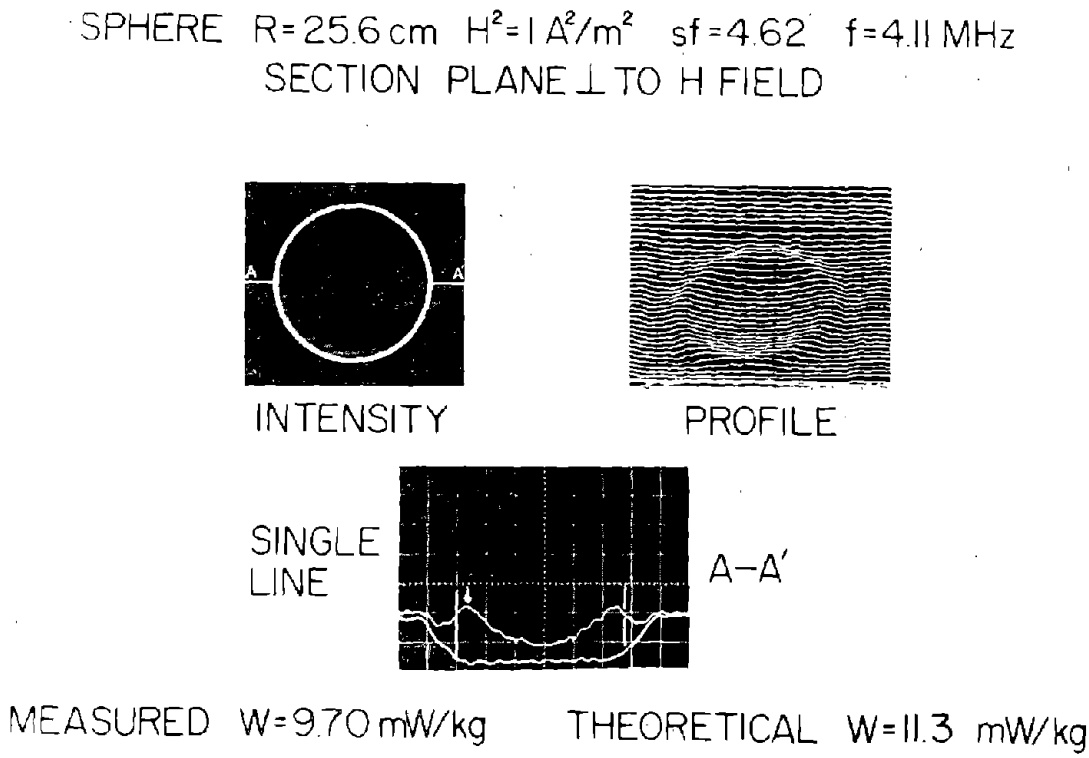

a

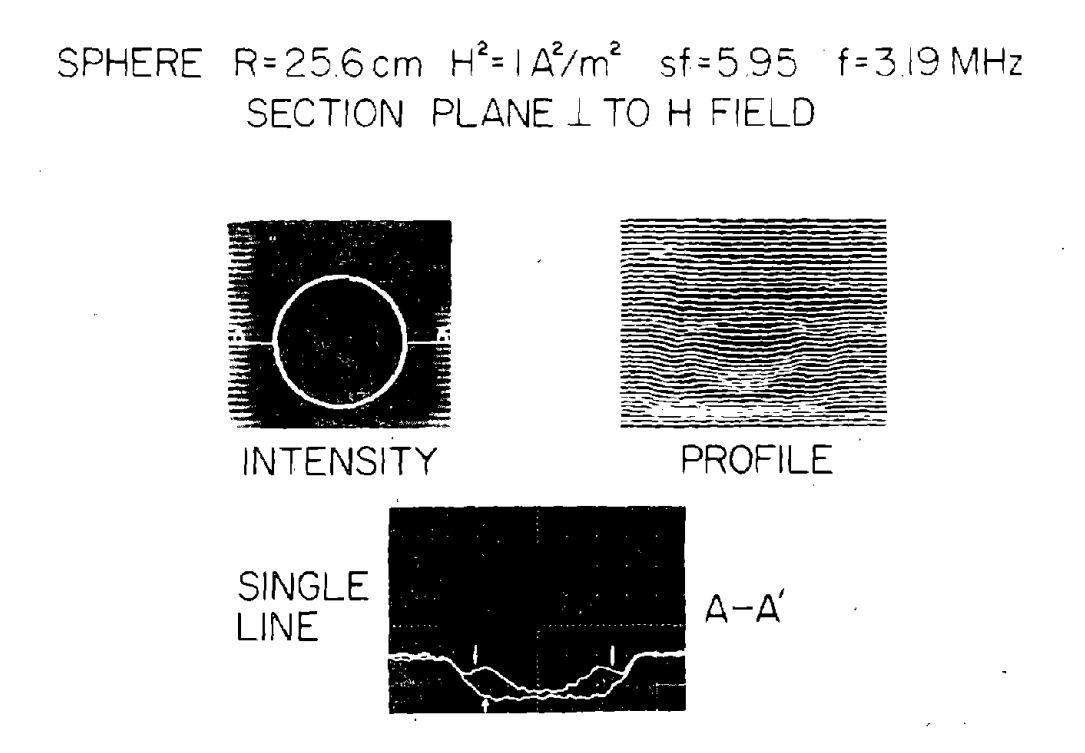

b

Figure 7. Thermograms and maximum values of SAR obtained from sphere models exposed to magnetic fields. (All values pertain to full-scale exposure conditions.)

apparently due to thermal diffusion, is relatively close to the theoretical value.

Fig. 7-b illustrates the thermographic results for 3.19 MHz exposure. In this case, the measured values are somewhat less than the theoretical values. Table III does indicate, however, that the extrapolated values do compare reasonably well with the UW BEMRL exposures. Fig. 7-c and 7-d illustrate the results for the case of the magnetic field applied parallel to the sectioned plane of the model. Again, as shown on Table III, the results compare reasonably well. Fig. 8 illustrates the thermographic results in exposing prolate spheroids to magnetic fields perpendicular to the sectioning plane for axial ratios of 2, 5, and 7.73. In these cases, the measured SAR values differ from the theoretical values by a greater amount than the UW BEMRL results, as seen in Table III. Since the volume of the region heated for these cases is significantly smaller than those for other cases, we would expect the thermal diffusion process to be more serious for these particular configurations, so we attribute the differences to this problem.

c. Combined Magnetic and Electric Fields

Although the near-field synthesizer can produce various electric and magnetic field configurations, during the testing period it was only possible to illuminate the models with electric and magnetic fields parallel to each other, with a field impedance of 180 Ω. This combination was necessary since the loop in the near-field synthesizer had already been oriented and tuned to this particular position, and any rearrangement would have used more time than was available to conduct the experiments. Only the spheres were exposed to this field configuration. The measured specific absorption rate were normalized to the square of the magnetic field (H^2). Theoretical values were obtained by adding the SARs separately for the electric and magnetic fields by means of the calculator, using the programs in the Appendix.

It should be noted that the peak SAR values would be somewhat higher if the electric and magnetic fields were applied perpendicular to each other, since the vector addition of the two parallel electric fields set up in the sphere result in larger net absorbed SAR. Thermographic results and measurements are shown in Fig. 9-a for the smaller diameter simulating a 70 kg sphere exposed to the 3.19 MHz fields polarized parallel to the plane of separation, and Fig. 9-b for the small sphere exposed with the fields applied perpendicular to the plane of separation, Fig. 9-c for the large sphere exposed with the fields parallel to the plane of separation, and in Fig. 9-d for the large sphere exposed with the fields perpendicular to the plane of separation. The SARs calculated for the exposure with the plane of separation parallel to the fields are higher than theoretical. The plane of separation can interrupt the current flow in this case if there is poor contact. This can produce higher field levels at the interface, producing greater heating in that region. This may have been the problem. Extreme care must be exercised to prevent this. Since data reduction did not occur until later, there was no way to confirm this.

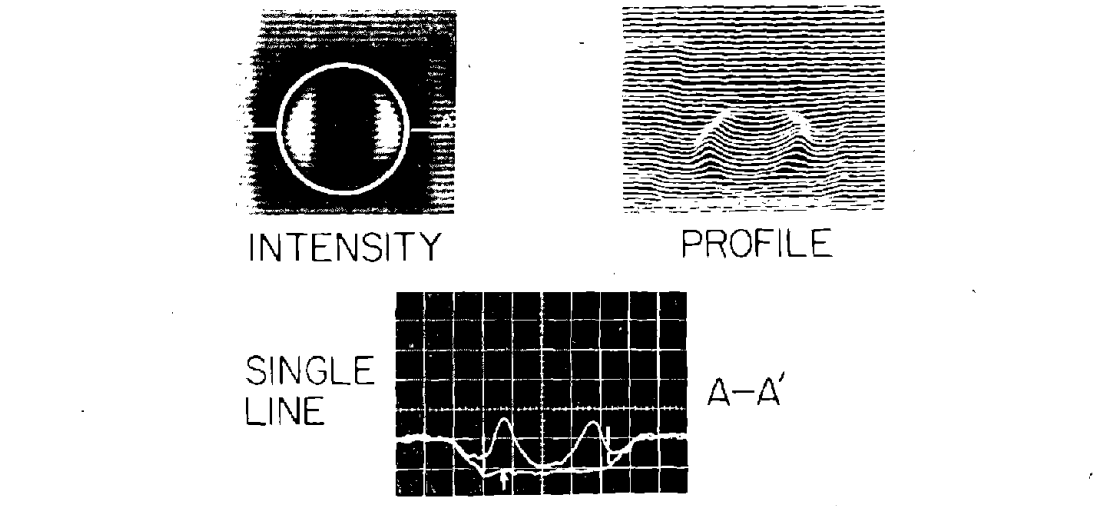

c

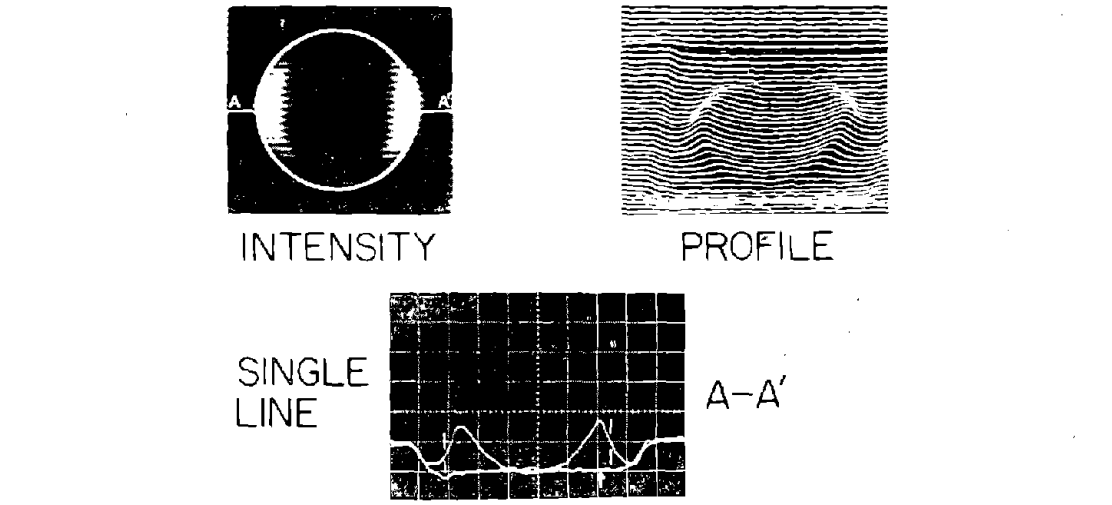

d

Figure 7. Thermograms and maximum values of SAR obtained from sphere models exposed to magnetic fields. (All values pertain to full-scale exposure conditions.)

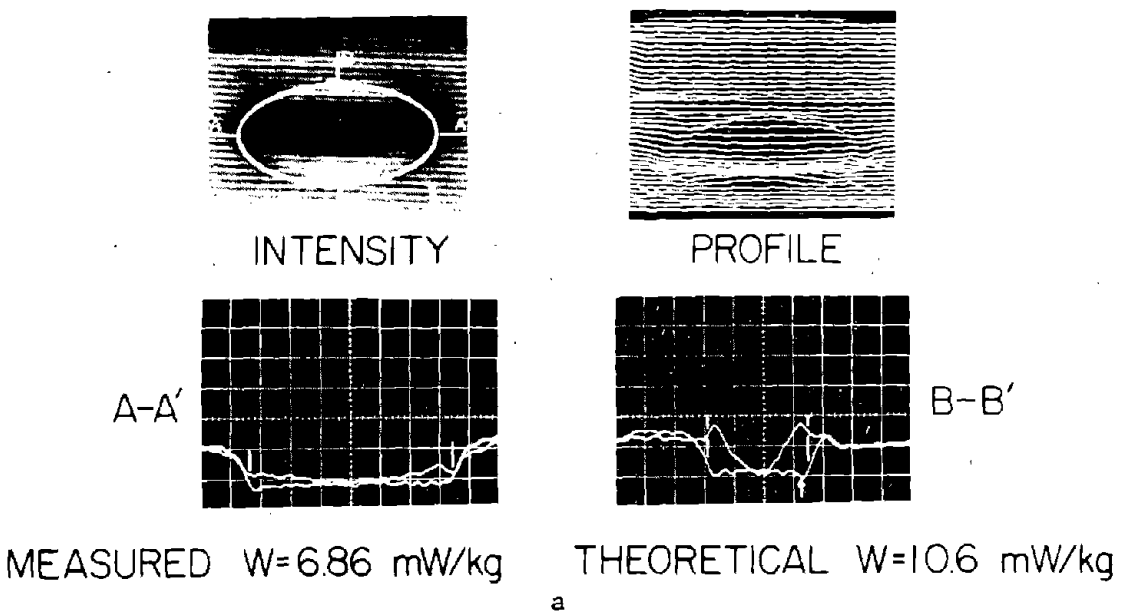

a

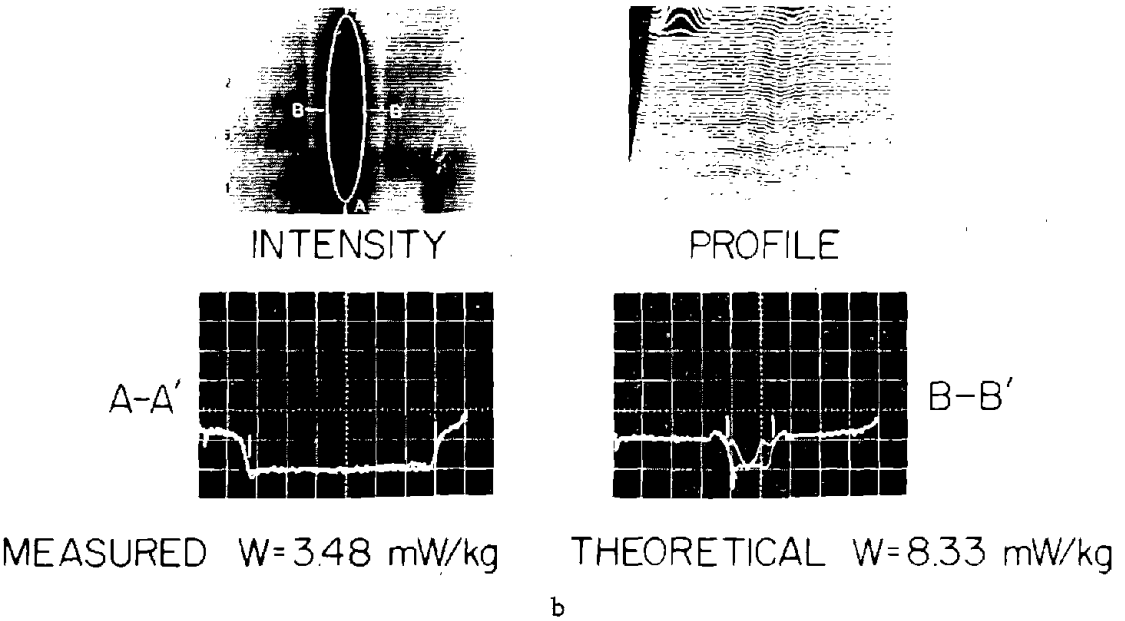

b

Figure 8. Thermograms and maximum values of SAR obtained from prolate spheroid models exposed to magnetic fields. (All values pertain to full-scale exposure conditions.)

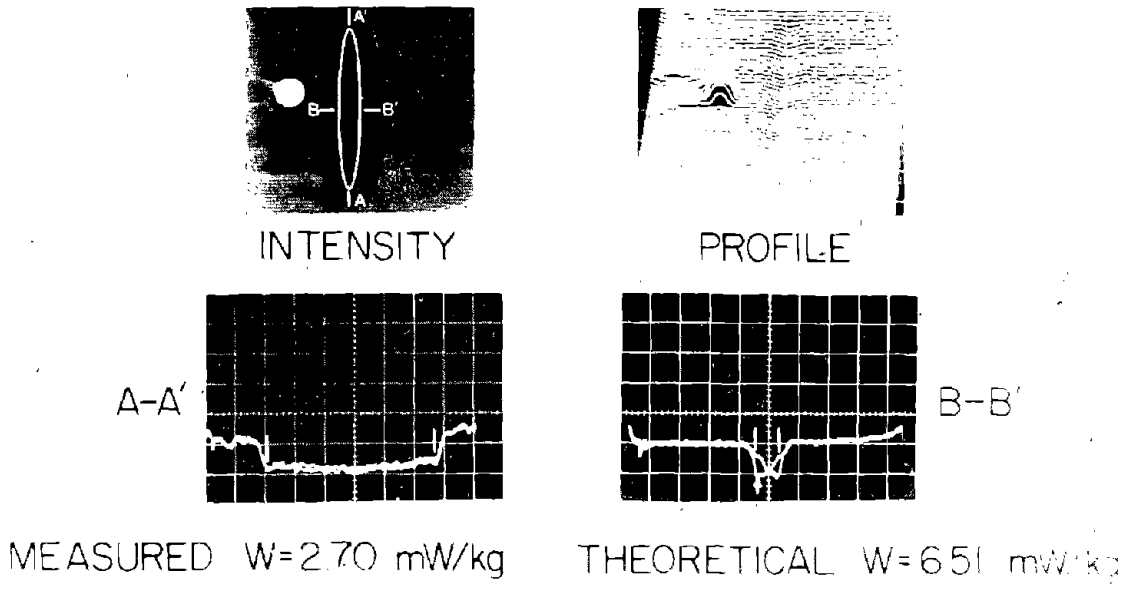

c

Figure 8. Thermograms and maximum values of SAR obtained from prolate spheroid models exposed to magnetic fields. (All values pertain to full-scale exposure conditions.)

2. Exposure of Large Spheroid Model

The prolate spheroid, with a/b = 3.13, a = 19.6 cm, was fabricated by the University of Utah to simulate a 3.5 kg monkey. The synthetic tissue filling the spheroid had electrical properties equivalent to human muscle. This full-scale model spheroid was exposed to the parallel electric and magnetic field configuration in the near-field synthesizer for 2 min. Since the magnetic field provides the major part of the coupling for this field configuration, the measured theoretical SARs were normalized to the square of the magnetic field, with the thermographic results illustrated in Fig. 10 and tabulated in Table IV. The deviations between the theoretical and the experimental values are probably due to a combination of problems. First, an excessively long exposure time led to diffusion which resulted in measured values that are lower than theoretical values, and poor contact between the two halves of the assembled model could lead to measured values higher than the theoretical values.

3. Exposure of Man Model

The 1/4.62th scale model man was exposed to 19 MHz in the near-field synthesizer to simulate a full-scale man exposure at 4.11 MHz. Two configurations of the model were used. One was sectioned using the old technique of covering each half with a thin plastic film or tape, and the other involved the use of the new silk screen technique. In the former technique, since symmetry is necessary on each side of the sectioning plane, two back halves of the man model were used, whereas, in the newer technique, the front and the back were joined at the frontal plane. The old type model was exposed independently to electric and magnetic fields, and the new model was exposed to parallel electric and magnetic field configurations. Since the latter configuration could not be tested in the VHF resonant cavity, and there is no theoretical solution, only experimental results were obtained for the model. The results are illustrated in Table II for the actual values measured in the models, and in the figures discussed below for thermograms and values extrapolated to the full-scale man. The results of exposures of both types of model men in the near-field synthesizer and the VHF resonant cavity are presented in Table V.

a. Electric Field Only

Fig. 11 illustrates the 1/4.62th scale model man exposed to an electric field parallel to the axis of the man. In this case, the model was sectioned according to the old technique along the frontal plane involving two backs. In this case, the exposure time was 60 sec, which was short enough to allow thermal diffusion to be neglected in most areas. There is excessive heating in the foam near the head and feet of the model due to the high concentration of electric fields in this region. Thermograms indicate that some of this heat is transferred to the model from the foam at the head and feet. The absorbed power pattern is very similar to that produced by the VHF resonant cavity, except that the knee and neck heating seems to be somewhat less, as illustrated in Table V. The SAR ratios relative to the value in the knee are shown at the top of Table VI, and the SAR ratios for the same regions for near-field synthesizer exposure compared to the resonant cavity exposure are tabulated at the top of Table VII.

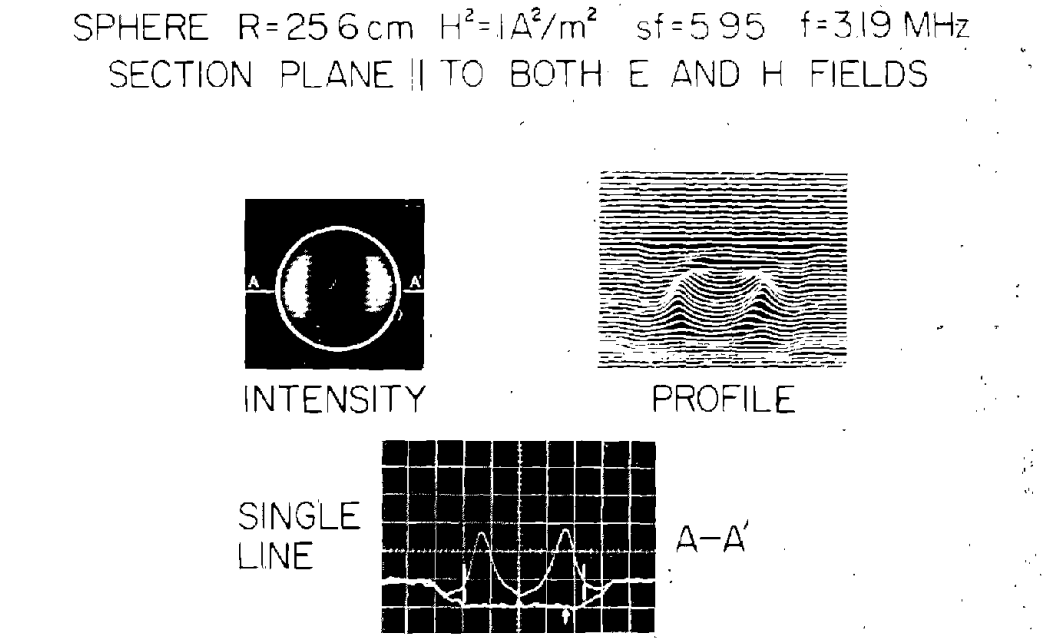

a

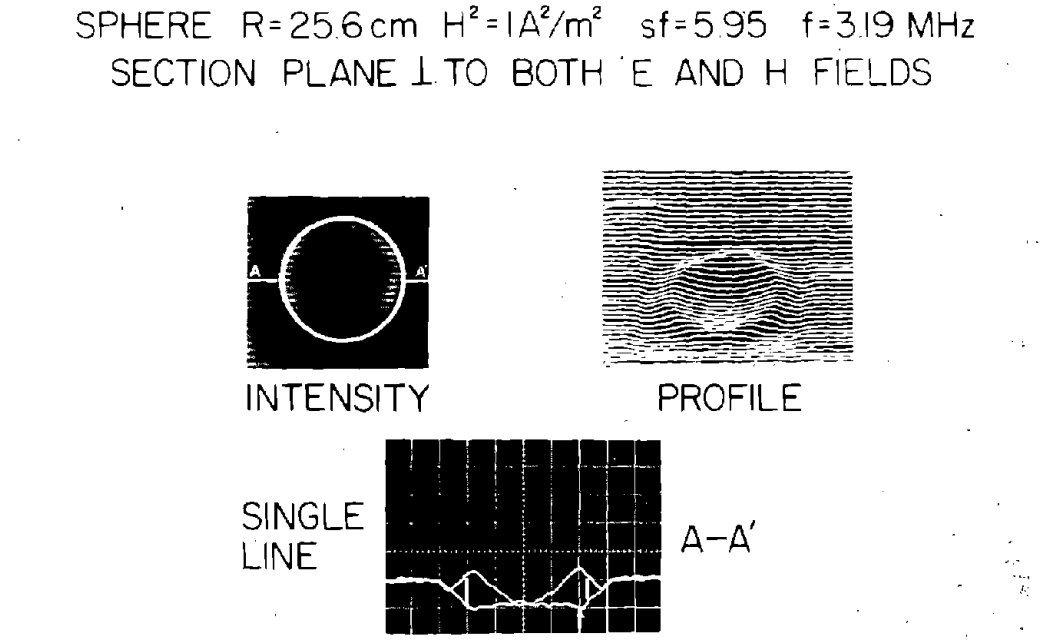

b

Figure 9. Thermograms and maximum values for SAR obtained from sphere models exposed to a parallel combination of both electric and magnetic fields. (All values pertain to full-scale exposure conditions.)

SPHERE R=25.6 cm H^2=1 A^2/m^2 sf=4.62 f=4.11 MHz
SECTION PLANE || TO BOTH E AND H FIELDS

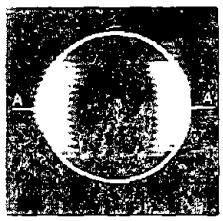

INTENSITY

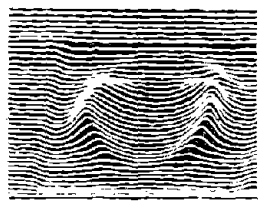

PROFILE

SINGLE LINE

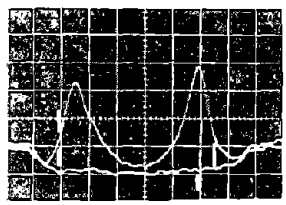

A–A′

MEASURED W=19.1 mW/kg THEORETICAL W=11.46 mW/kg

c

SPHERE R=25.6 cm H^2=1 A^2/m^2 sf=4.62 f=4.11 MHz
SECTION PLANE ⊥ TO BOTH E AND H FIELDS

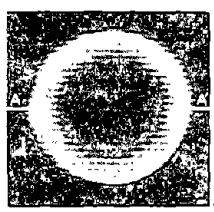

INTENSITY

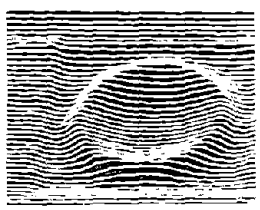

PROFILE

SINGLE LINE

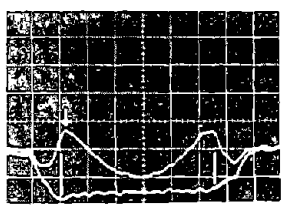

A–A′

MEASURED W=12.3 mW/kg THEORETICAL W=11.46 mW/kg

d

Figure 9. Thermograms and maximum values of SAR obtained from sphere models exposed to a parallel combination of both electric and magnetic fields. (All values pertain to full-scale exposure conditions.)

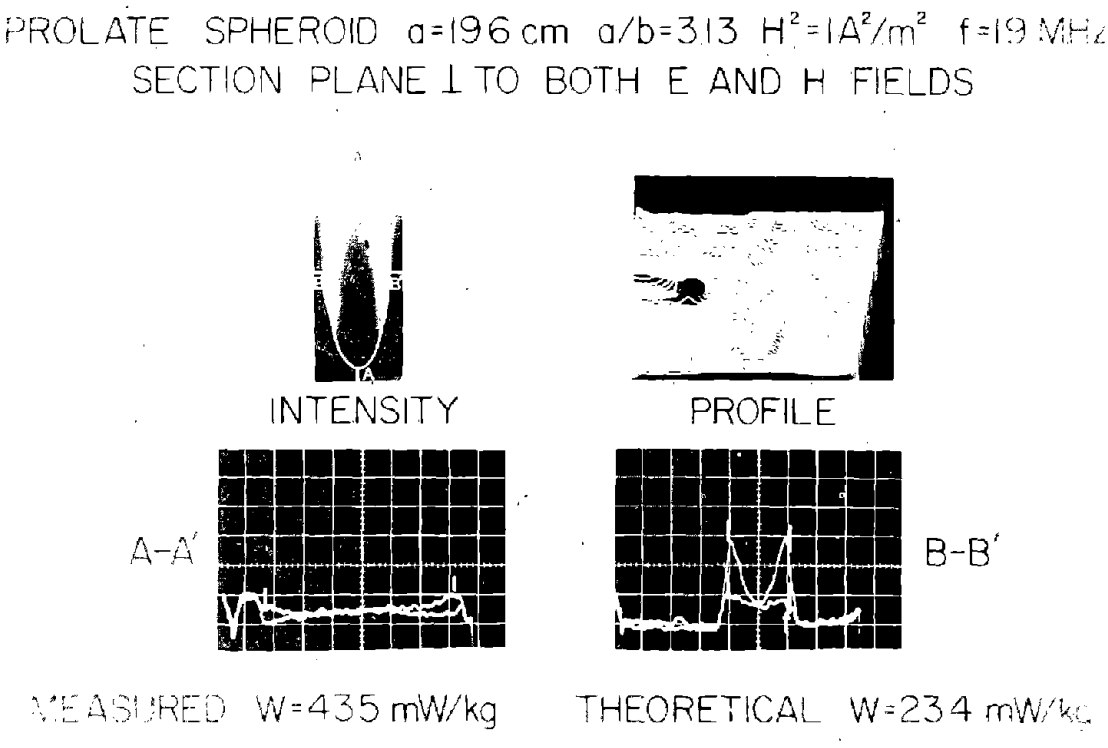

a

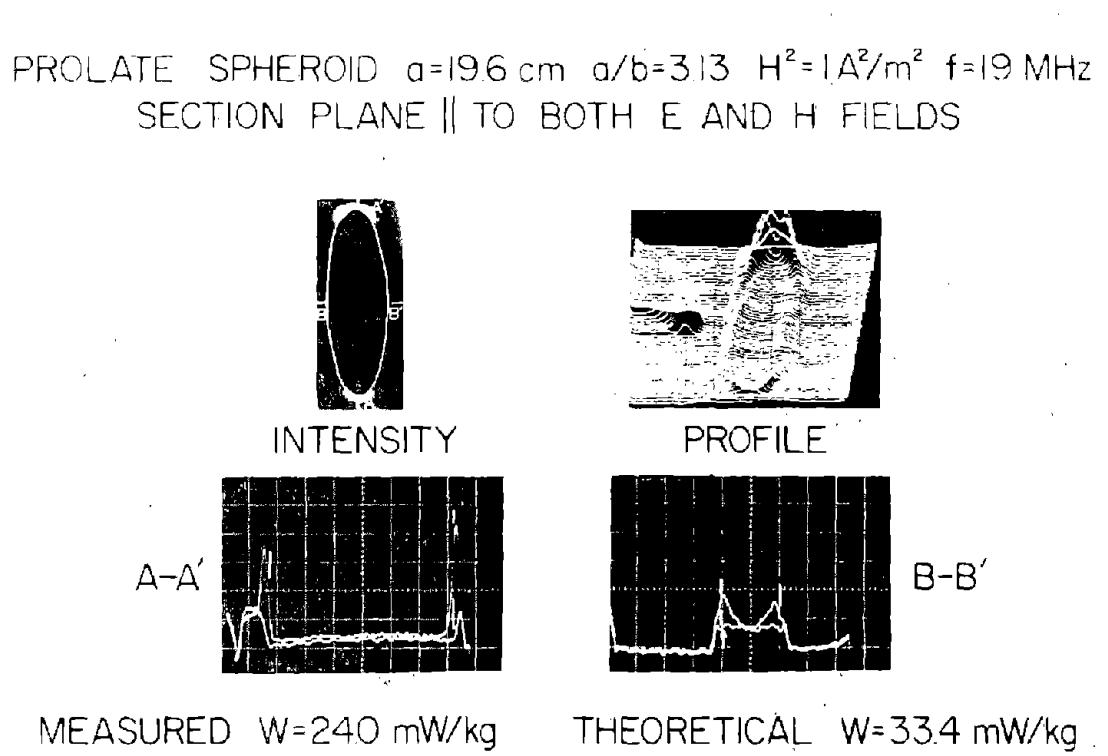

b

Figure 10. Thermograms and maximum values of SAR obtained from prolate spheroid models exposed to a parallel combination of both electric and magnetic fields.

TABLE IV

MAXIMUM SAR CALCULATED FOR FULL-SCALE 70 kg SPHEROIDS

Ellipticity	Frequency MHz	Maximum SAR Measured W/kg	Maximum SAR Theoretical W/kg
Section Plane Parallel to Both Electric and Magnetic Fields $H^2 = 1\ A^2/m^2$			
a/b = 1	3.2	10.8×10^{-3}	6.62×10^{-3}
a/b = 1	4.1	19.1×10^{-3}	11.5×10^{-3}
a/b = 3.13	19	24.0×10^{-3}	33.4×10^{-3}
Section Plane Perpendicular to Electric and Magnetic Fields $H^2 = 1\ A^2/m^2$			
a/b = 1	3.2	5.74×10^{-3}	6.62×10^{-3}
a/b = 1	4.1	12.3×10^{-3}	11.5×10^{-3}
a/b = 3.13	19	43.5×10^{-3}	23.4×10^{-3}

TABLE V

COMPARISON OF MEASURED SAR FOR MAN EXPOSED IN NEAR-FIELD SYNTHESIZER AND VHF RESONANT CAVITY

LOCATION	USAFSAM NEAR-FIELD SYNTHESIZER		UW BRMRL VHF RESONANT CAVITY	USAFSAM NEAR-FIELD SYNTHESIZER	
	MAXIMUM SAR MEASURED W/kg	FREQUENCY SCALED MAXIMUM SAR MEASURED W/kg	MAXIMUM SAR MEASURED W/kg	FREQUENCY SCALED MAXIMUM SAR MEASURED W/kg	MAXIMUM SAR MEASURED W/kg
	f = 4.11 MHz	Scaled to 31.0 MHz	f = 31.0 MHz	Scaled to 31.0 MHz	f = 4.11 MHz
	FRONTAL PLANE ∥ TO E TRANSVERSE PLANE ⊥ TO E $E^2 = 1\ V^2/m^2$			FRONTAL PLANE ∥ TO E & H TRANSVERSE PLANE ⊥ TO E & H $E^2 = 1\ V^2/m^2$	
ANKLE	1.76×10^{-6}	100×10^{-6}	92.5×10^{-6}	57.9×10^{-6}	1.02×10^{-6}
KNEE	0.52×10^{-6}	29.6×10^{-6}	44.9×10^{-6}	13.4×10^{-6}	0.235×10^{-6}
NECK	0.173×10^{-6}	9.85×10^{-6}	18.4×10^{-6}	7.40×10^{-6}	0.130×10^{-6}
ABDOMEN	0.087×10^{-6}	4.93×10^{-6}		3.47×10^{-6}	0.061×10^{-6}
	FRONTAL PLANE ⊥ TO H TRANSVERSE PLANE ∥ TO H $H^2 = 1\ A^2/m^2$			FRONTAL PLANE ⊥ TO E & H TRANSVERSE PLANE ∥ TO E & H $H^2 = 1\ A^2/m^2$	
AXILLA	15.4×10^{-3}	0.876	3.13	0.020	16.2×10^{-3}
PERINEUM	9.95×10^{-3}	0.566	2.57	0.593	10.4×10^{-3}
SHOULDER	10.9×10^{-3}	0.619	0.84	0.705	12.4×10^{-3}
LATERAL THORAX	11.3×10^{-3}	0.641		0.865	15.2×10^{-3}
STERNUM	3.94×10^{-7}	0.224		0.257	4.51×10^{-3}

b. Magnetic Field Only

The thermograms of the same model exposed to the magnetic field are illustrated in Fig. 12. In this case, the exposure time in the near-field synthesizer was 90 sec, therefore, the diffusion effects cannot be completely neglected. Again, the power absorption pattern is similar to that produced by the VHF resonant cavity with maxima appearing in the axilla and the perineum regions. In this case, the magnetic field was perpendicular to the frontal plane and parallel to the transverse plane of the model. The SAR ratios of all areas relative to that of the axilla are shown at the bottom of Table VI. The SAR ratios for the same regions in the two different exposure systems are tabulated at the bottom of Table VII. Both the arm-shoulder area and the lateral thorax areas absorb much more power for exposure in the near-field synthesizer than in the VHF resonant cavity. This could be due to diffusion. Table VII indicates that the SARs produced by the near-field synthesizer are as low as one-quarter of those produced by the VHF resonant cavity. This could be due to the long exposure time resulting in diffusion and also could be due to the fact that the model occupied a large area of the source loop, producing a perturbation which modified the magnetic field pattern.

c. Magnetic and Electric Field

Models sectioned according to the new technique were exposed to the configuration of parallel electric and magnetic fields in the near-field synthesizer. The model was exposed to three orientations relative to this field configuration, and the exposure time of the test was 60 sec. The SAR values were normalized to the square of the electric field for these cases. Fig. 13 illustrates the thermographic results in exposing the model with the E and H fields parallel to the frontal plane and perpendicular to the transverse plane. The SARs were similar to those produced in the electric field exposures, indicating that the electric field coupling is dominant in this case.

In the second orientation, the model was exposed with both the magnetic field and the electric field oriented perpendicular to the frontal plane of the model and parallel to the transverse plane. In this case, it can be seen from the thermograms in Fig. 14 that the SAR patterns are similar to those for man exposed to the magnetic field only, oriented perpendicular to the frontal plane. This indicates that the electric field component couples very little energy to the model, as compared to the magnetic field component.

The final and third orientation, which was not tested in the VHF resonant cavity, involved exposure of the model with the electric and magnetic fields parallel to both the frontal plane and the transverse planes. The thermograms are illustrated in Fig. 15. Note that the specific absorption rates are an order of magnitude lower than those obtained when the man was exposed to the electric field parallel to the frontal plane and perpendicular to the transverse plane. The results indicate a small degree of electrical coupling with the areas absorbing power corresponding to the abdomen, arms, and neck.

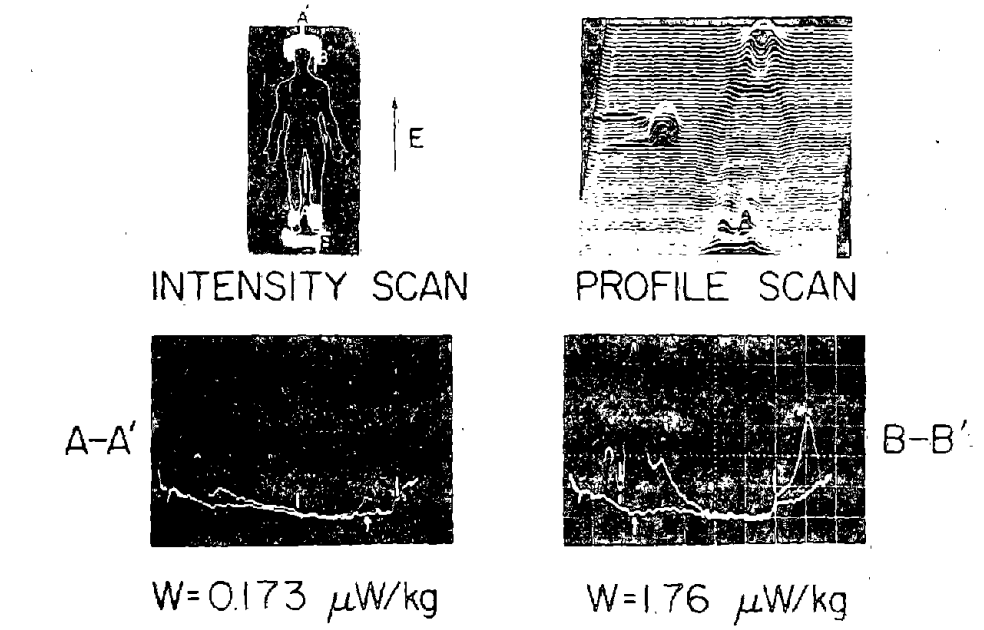

a

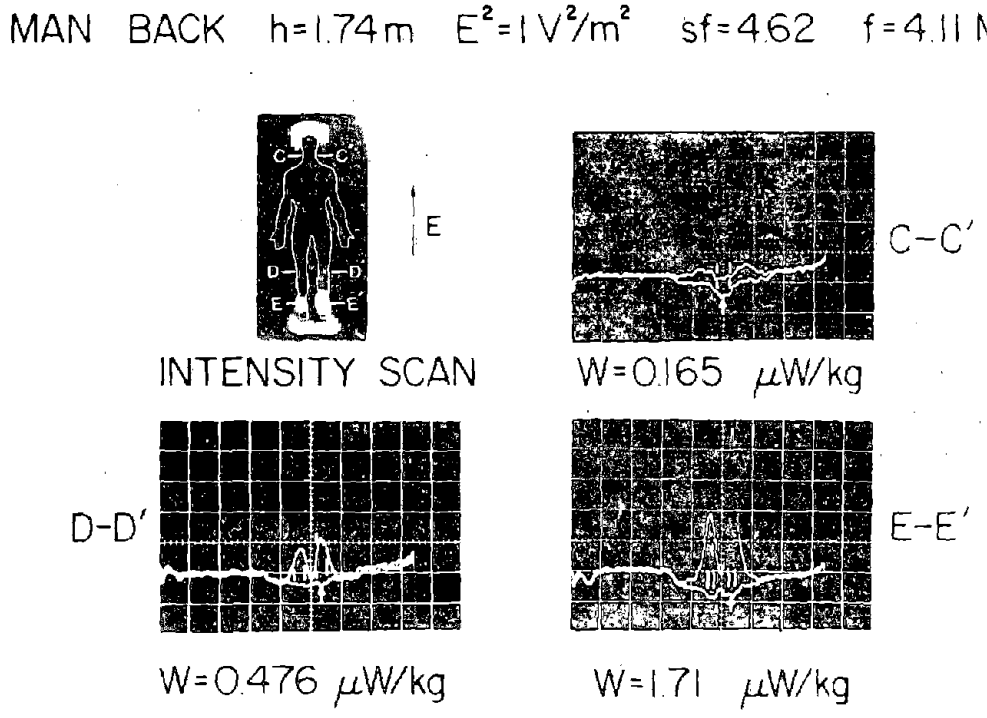

b

Figure 11. Thermograms and maximum values of SAR obtained for 1.74 m high 70 kg man exposed to electric fields. (All values pertain to full-scale exposure conditions.)

TABLE VI

COMPARISON OF SAR RATIOS FOR MAN EXPOSED IN NEAR-FIELD SYNTHESIZER AND VHF RESONANT CAVITY

Location Reference Location	Near-Field Synthesizer Old Model	VHF Resonant Cavity	Near-Field Synthesizer New Model
	Electric Field Only $E^2 = 1\ V^2/m^2$		Parallel Electric and Magnetic Fields $E^2 = 1\ V^2/m^2$
Ankle / Knee	3.38	2.06	4.11
Neck / Knee	0.33	0.41	0.52
Abdomen / Knee	0.17		0.26
	Magnetic Field Only $H^2 = 1\ A^2/m^2$		Parallel Electric and Magnetic Fields $H^2 = 1\ A^2/m^2$
Perineum / Axilla	0.65	0.82	0.64
Shoulder / Axilla	0.71	0.26	0.77
Lateral Thorax / Axilla	0.73		0.95
Sternum / Axilla	0.26		0.28

TABLE VII

RATIOS OF SAR OF NEAR-FIELD SYNTHESIZER EXPOSURE TO VHF RESONANT CAVITY EXPOSURE FOR A MAN

Location	Near-Field Synthesizer / VHF Resonant Cavity	Near-Field Synthesizer / VHF Resonant Cavity
	Electric Field Only $E^2 = 1\ V^2/m^2$	Parallel Electric and Magnetic Fields $E^2 = 1\ V^2/m^2$
Ankle	1.08	0.63
Knee	0.66	0.30
Neck	0.54	0.40
Abdomen		
	Magnetic Field Only $H^2 = 1\ A^2/m^2$	Parallel Electric and Magnetic Fields $H^2 = 1\ A^2/m^2$
Axilla	0.28	0.29
Perineum	0.22	0.23
Shoulder	0.74	0.84

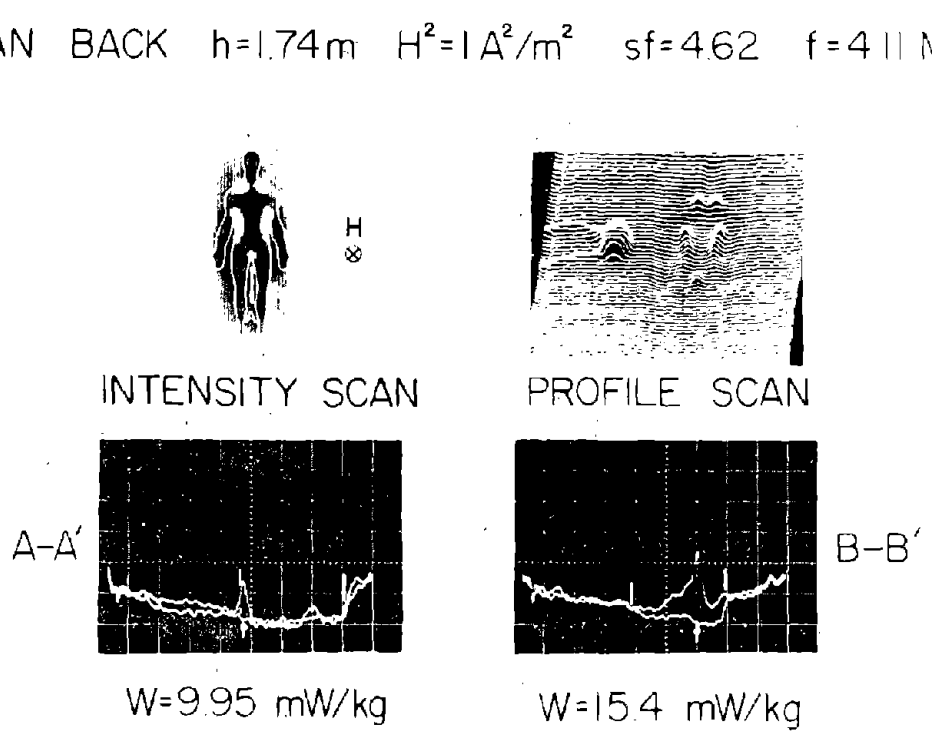

Figure 12. Thermograms and maximum values of SAR obtained for 1.74 m high 70 kg man exposed to magnetic fields. (All values pertain to full-scale exposure conditions.)

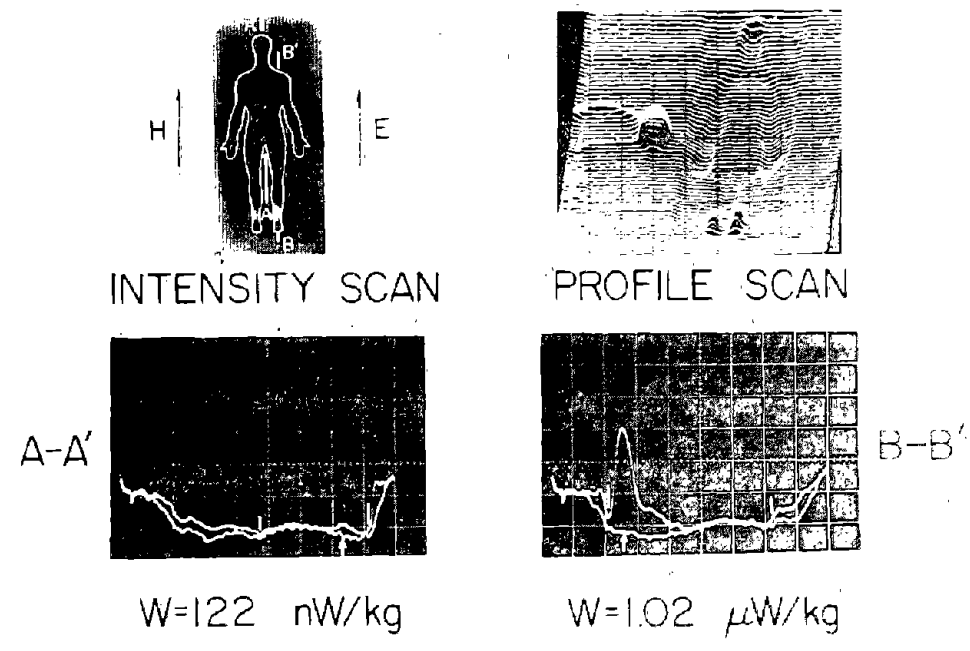

a

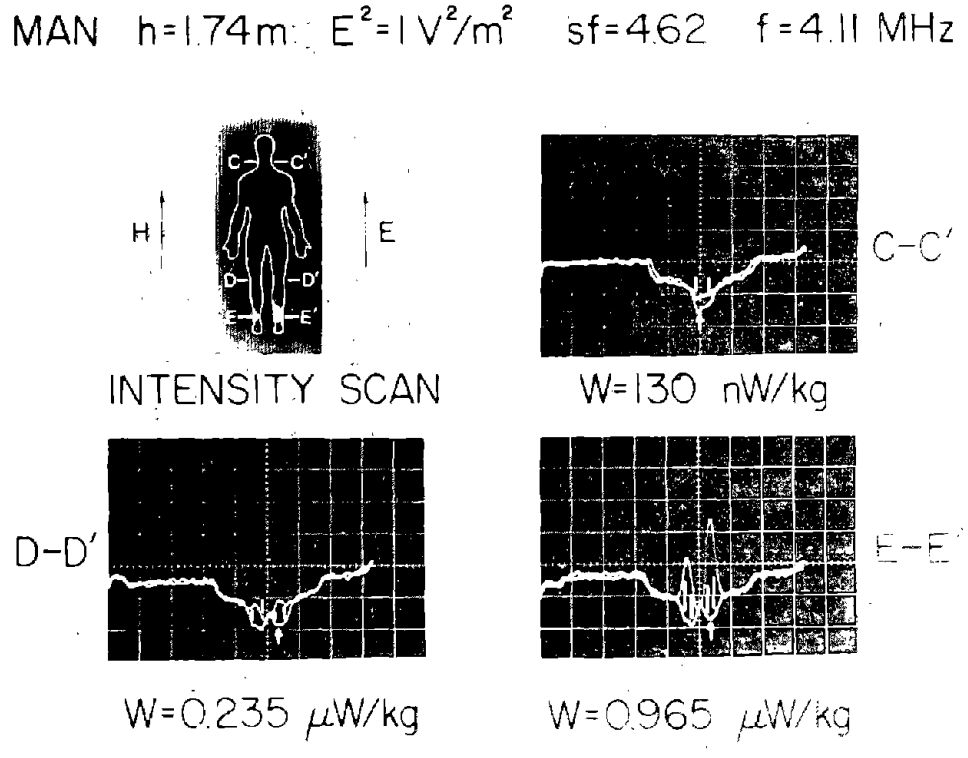

b

Figure 13. Thermograms and maximum values of SAR obtained for 1.74 m high 70 kg man exposed to electric and magnetic fields parallel to the frontal plane and perpendicular to the transverse plane. (All values pertain to full-scale exposure conditions.)

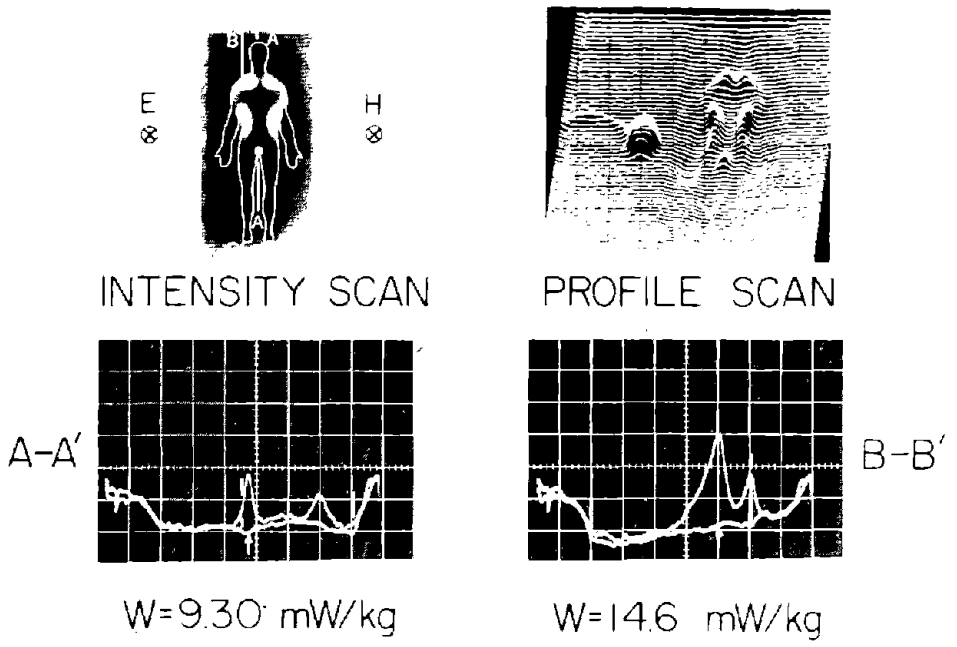

Figure 14. Thermograms and maximum values of SAR obtained for 1.74 m high 70 kg man exposed to electric and magnetic fields perpendicular to the frontal plane and parallel to the transverse plane. (All values pertain to full-scale exposure conditions.)

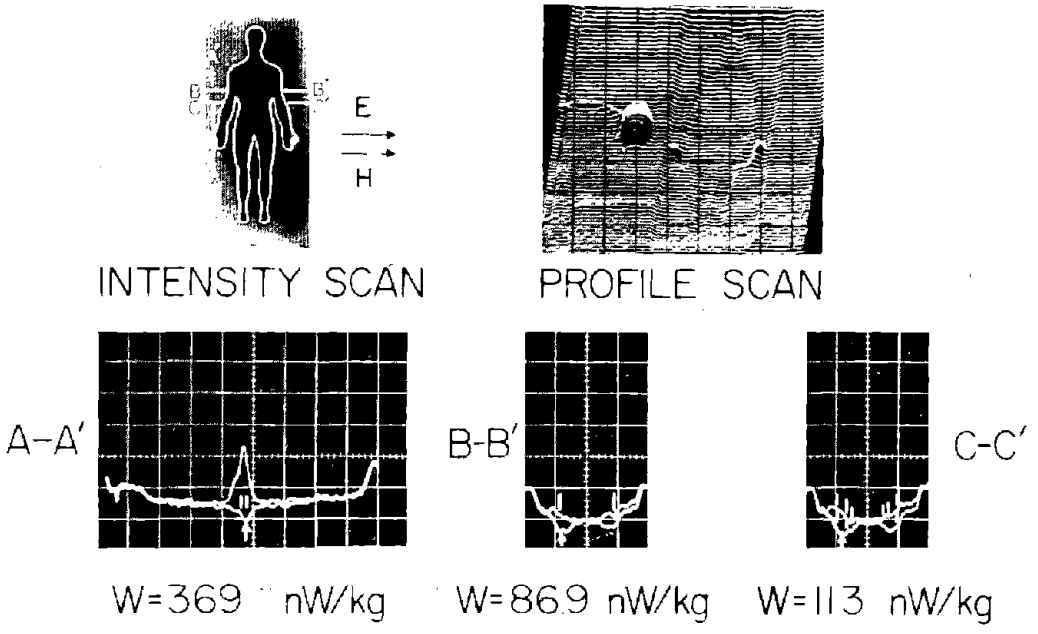

Figure 15. Thermograms and maximum values of SAR obtained for 1.74 m high 70 kg man exposed to electric and magnetic fields parallel to both transverse and frontal planes. (All values pertain to full-scale exposure conditions.)

B. HF Stripline

The HF stripline exposure system at USAFSAM, shown in Fig. 2, is a symmetrical parallel plate structure used for simulating plane wave exposure conditions when the exposed object is small compared to the spacing between the center strip and the surrounding chamber. The tests performed using this exposure system were done at 19 MHz. The 3.5 kg prolate spheroid with an axial ratio of 3.13:1 and the man model used in the previous experiments were irradiated for 5 min. The electric field strength during exposure was 1680 V/m and the field impedance (E/H) was 352 Ω corresponding to an incident power density of 802 mW/cm^2. The experimental results of the actual exposure conditions are tabulated in Table VIII, and the details concerning the thermographic results are discussed below.

1. Exposure of Spheroid Model

The 3.13:1 prolate spheroid was exposed in three different orientations as described in Table VIII, and the thermographic results depicted in Fig. 16. With the exposure time of 5 min, the only discernable temperature rise in the phantom model was that due to diffusion of heat from the foam material. This is not surprising since an absorbed power density of 12 W/kg or more was required to raise the temperature 1^{o} for an exposure time of 5 min, assuming no diffusion effects. It can be shown theoretically, using the calculator program in the Appendix, that the stripline power density was capable of inducing a maximum of only 3.57 W/kg in the prolate ellipsoid used in the experiment.

2. Exposure of Man Model

The 1/4.62th scale man model was irradiated in the two orientations depicted in Table VIII. Thermographic results for 5 min exposures are illustrated in Fig. 17. In the first orientation, the model was exposed with E and H field components simulating plane wave irradiation with the E parallel to the long axis of the man. The coupling should be predominantly by means of the electric field for this orientation. When the electric field is perpendicular to the long axis of the man, the coupling should be predominantly due to the magnetic field. Thus, the results from the USAFSAM HF stripline can be indirectly and roughly compared to the UW BEMRL VHF resonant cavity results, even though the latter were measured for the model exposed to single field components. This comparison is made in Table IX, which illustrates the SAR values for the full-scale man exposed to 4.11 MHz and the results of the frequency scaled to 31 MHz for the full-scale man. The latter results compare favorably to the results obtained in the VHF cavity representing a full-scale man exposed to 31 MHz.

C. Anechoic Chamber

The models were irradiated in an anechoic chamber with power density levels of 176 mW/cm^2 at a frequency of 1600 MHz. Exposure times from 30 sec to 2.5 min were used. The six objects exposed in the chamber were the 3.5 kg prolate spheroid, the model man, the 6 cm diameter sphere, a 200 gm rat, a 40 gm mouse, and a phantom 40 gm mouse. The only model in which the frequency

TABLE VIII

MODEL EXPOSURE CONDITIONS IN
USAFSAM STRIPLINE CHAMBER AT 19 MHz

OBJECT	ORIENTATION	INPUT POWER (KILOWATTS)	INCIDENT POWER DENSITY (mw/cm^2)	EXPOSURE TIME (sec)	TEMPERATURE RISE (^oC)	Max. SAR W' (W/kg)
3.13:1 Ellipsoid a=19.6 cm	Cut $\parallel$E, $\perp$ H E$\parallel$ long axis	50	802	300	0.4	4.79
Scale Factor = 1.00	Cut $\parallel$E, $\parallel$ H E$\parallel$ long axis	50	802	300	0.5	5.32
Silk Screen Interface	Cut $\parallel$ H, $\perp$ E H$\parallel$ long axis	50	802	300	---	----
1.74 m Man True Shape	Cut $\parallel$E & $\parallel$ H E$\parallel$ long axis	50	802	300	3.4	40.7
Scale Factor = 4.62						
Silk Screen Interface	Cut $\perp$E, $\parallel$H H$\parallel$ long axis	50	802	300	0.3	3.9

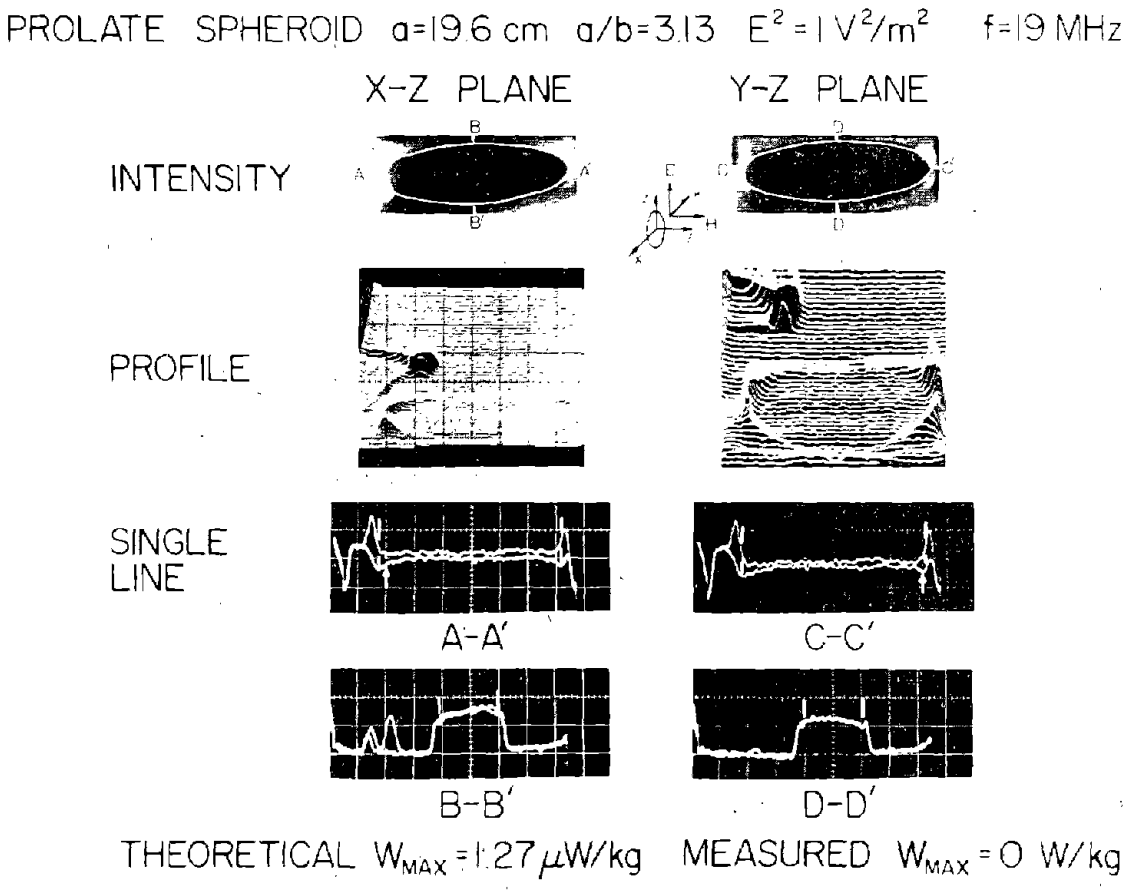

a

Figure 16. Thermograms obtained from 3.13:1 prolate spheroid exposed in HF stripline.

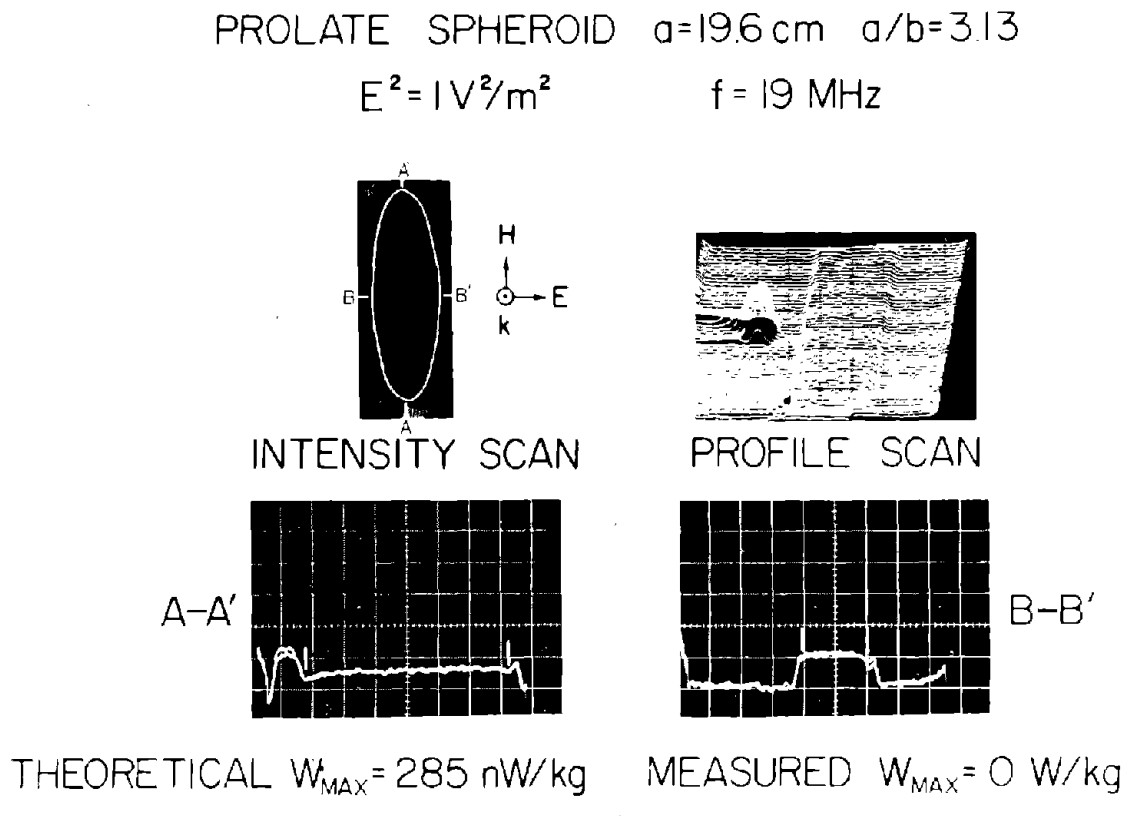

Figure 16. Thermograms obtained from 3.13:1 prolate spheroid exposed in HF stripline.

and size were scaled was a man. The remaining objects consisted of phantom models of synthetic tissue with proper electrical characteristics for 1600 MHz, or actual sacrificed animals. The results from actual exposure conditions are tabulated in Table X. The thermographic results are discussed below.

1. Spheroids

The 6-cm diameter sphere was exposed with two orientations, one with the sectioned plane aligned parallel to the applied electric field vector, and the other with the sectioned plane aligned perpendicular to the electric field vector. The thermographic line scan along the center line of the sphere was recorded for each case. Since the change in orientation is obtained by merely rotating the sphere about an axis which is the center line for the two exposures, the line scan heating patterns for the two cases should be identical. As seen from Fig. 18, the general shapes of the patterns are identical, but there is a slight variation (< 15%) in amplitude, probably due to imperfect surface contact between the two sections of the model. With the exception of being slightly lower, due to diffusion, the values of SAR seem to agree very well with the theoretical value tabulated at the top of the thermographic pictures.

The prolate spheroid was exposed such that the major axis was parallel to the electric field and perpendicular to the magnetic field. The section plane was an ellipse containing the major and minor axis of the ellipsoid. Thermograms illustrated in Fig. 19 show that the irradiated surface of the spheroid absorbed the maximum power. The power absorption dropped to a negligible value with about 2.5 cm penetration into the ellipsoid, comparing favorably with the theoretical penetration depth for 1600 MHz plane wave fields of 2.4 cm.

2. Exposure of Man Model

The same model man used for the 19 MHz exposures was exposed to the 1600 MHz in the chamber. It should be realized that the phantom material filling the model form was electrically equivalent to human muscle at 4.11 MHz. The observed results cannot be scaled according to the rules previously reported, since the dielectric content is not the proper value. When this variation is included in the scaling theory as reported by Sinclair (11), the exposure of the model man to 1600 MHz actually simulated a 23" high man weighing 5.8 pounds exposed to a 1200 MHz field having a field impedance of 437 Ω. Practically, the results would probably correspond reasonably well with those obtained for the exposure of a small, 5.8 pound infant to 1200 MHz plane wave field. The model was exposed in three different orientations, described in Table X. Thermographic results are illustrated in Figs. 20, 21, and 22, and tabulated in Table XI.

11. Sinclair, George, "Theory of models of electromagnetic systems," Proc. I.R.E., November 1948, pp. 1364-1369.

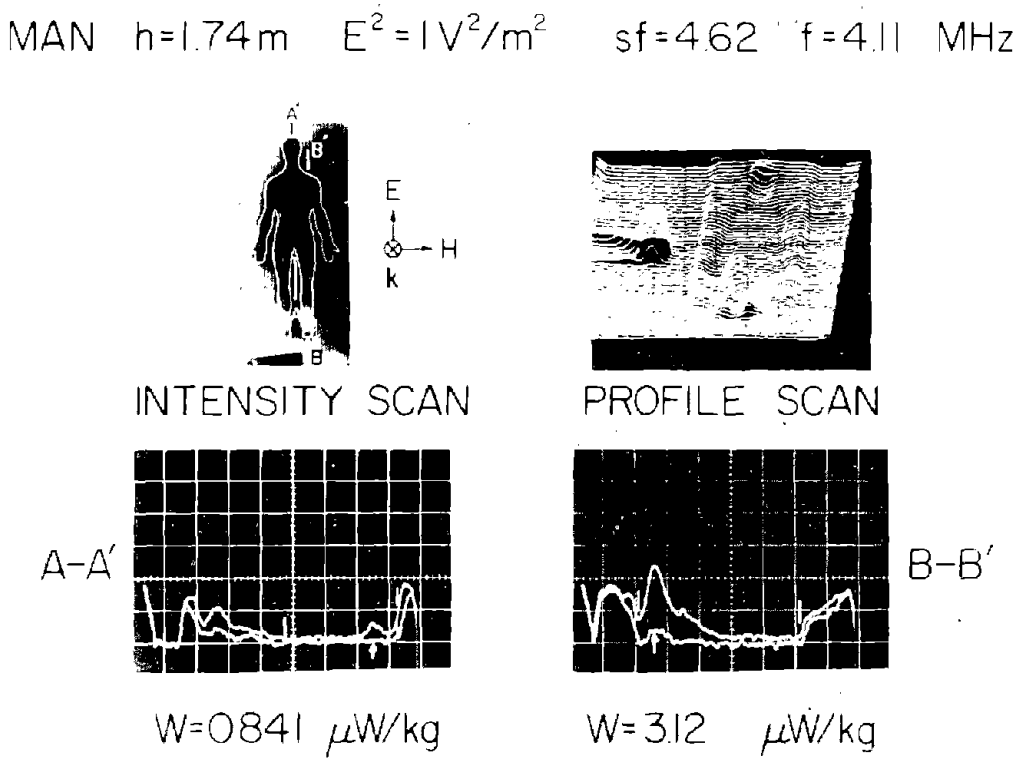

a

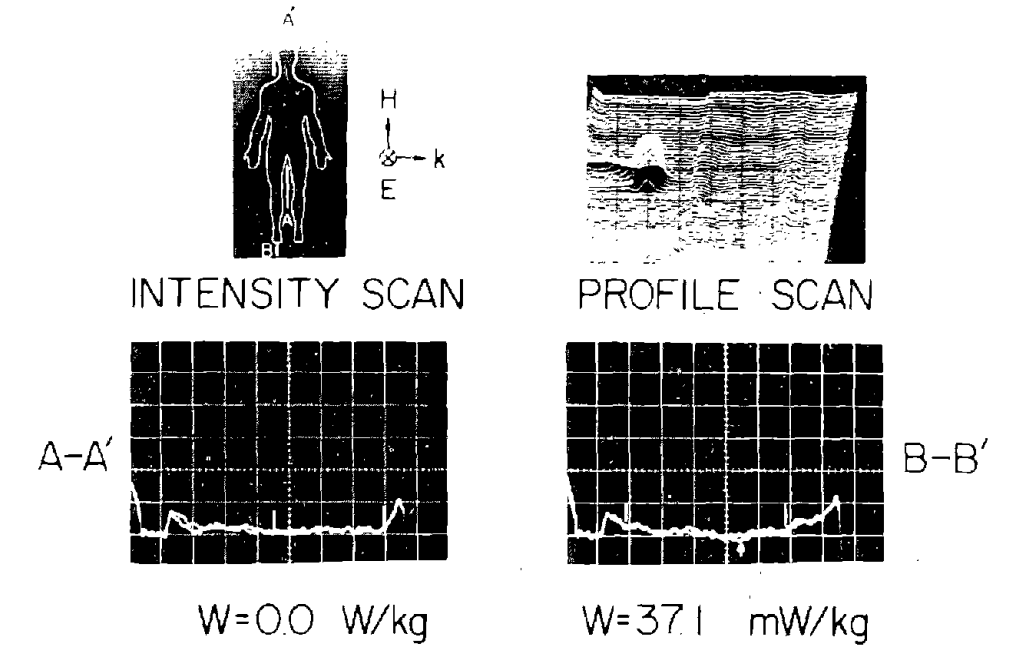

b

Figure 17. Thermograms and maximum values of SAR obtained for 1.74 m-high 70-kg man exposed in HF stripline. (All values pertain to full-scale exposure conditions.)

TABLE IX

COMPARISON OF MEASURED SAR FOR MAN EXPOSED
IN HF STRIPLINE AND VHF RESONANT CAVITY

USAFSAM HF STRIPLINE						UW BEMRL VHF RESONANT CAVITY		
Maximum SAR W/kg			Frequency Scaled Maximum SAR W/kg			Maximum SAR W/kg		
f = 4.11 MHz			f = 31.0 MHz			f = 31.0 MHz		
Major axis ∥ E and ⊥ H, Section plane ∥ to E, ∥ to H and ⊥ to k E^2=1 V^2/m^2 Silk Screen Interface						Major axis ∥ E and Section Plane Plastic Film Interface E^2=1 V^2/m^2		
Ankle	Knee	Neck	Ankle	Knee	Neck	Ankle	Knee	Neck
3.12×10^{-3}	1.62×10^{-6}	8.41×10^{-7}	178×10^{-6}	92×10^{-6}	47.8×10^{-6}	150×10^{-6}	54×10^{-6}	29.6×10^{-6}
Major axis ⊥ E and ∥ H, Section plane ⊥ to E, ∥ to H and ∥ to k H^2=1 A^2/m^2 Silk Screen Interface						Frontal Plane ⊥ to H Plastic Film Interface H^2=1 A^2/m^2		
Perineum			Perineum			Perineum		
37.1×10^{-3}			2.1			2.56		

TABLE X

MODEL EXPOSURE CONDITIONS IN USAFSAM ANECHOIC CHAMBER AT 1600 MHz

OBJECT	ORIENTATION	INPUT POWER (WATTS)	INCIDENT POWER DENSITY (mW/cm^2)	EXPOSURE TIME (SEC)	TEMPERATURE RISE (°C)	MAX SAR W· (W/kg)
6 cm Dia Sphere Scale Factor = 1.0	Cut ∥ E, ⊥ H	400	176	60	5.4	324
	Cut ⊥ E, ∥ H	400	176	60	4.7	282
3.13:1 Ellipsoid a = 19.6 cm Scale Factor = 1.0	Cut ∥ E, ⊥ H E ∥ long axis	400	176	150	2.7	0.35
1.74 cm Man Scale Factor = 4.62	Cut ∥ E and H E ⊥ long axis	400	176	120	5.7	173
	Cut ∥ E, ⊥ H E ∥ long axis	400	176	30	5.9	710
	Cut ∥ E and H E ∥ long axis	400	176	30	3.5	424
Phantom mouse	Cut ∥ E and H E ∥ long axis	400	176	60	8.3	479
Real mouse	Cut ∥ E and H E ∥ long axis	400	176	60	9.6	555
Rat	Cut ∥ E and H E ∥ long axis	400	176	60	5.4	315

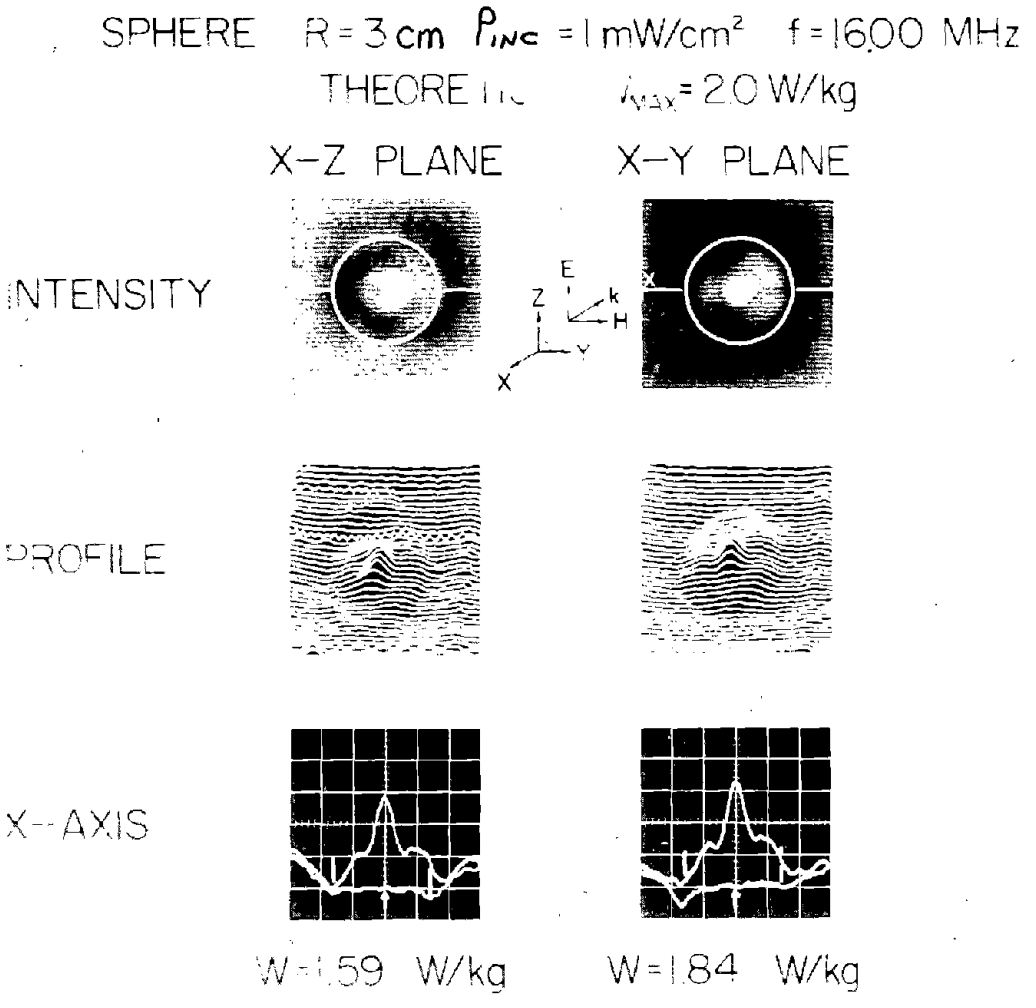

Figure 18. Thermograms and maximum values of SAR obtained for 3-cm radius sphere exposed to 1600 MHz plane wave EM fields.

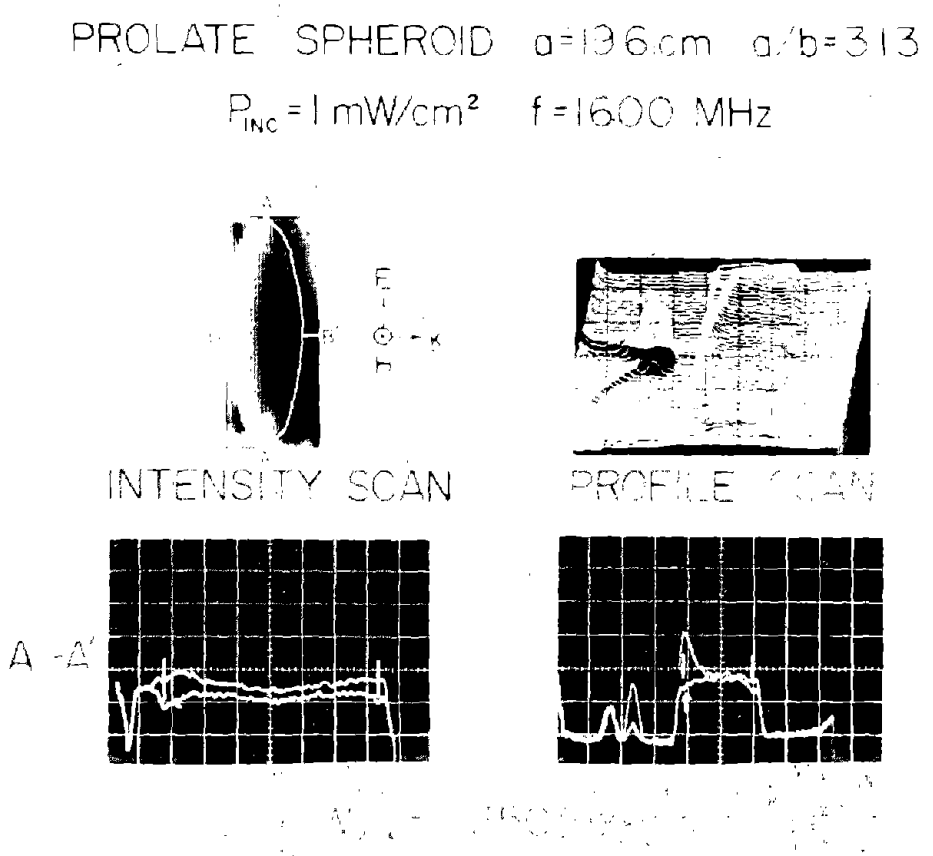

Figure 19. Thermograms and maximum values of SAR obtained for 3.13:1 prolate spheroid exposed to 1600 MHz plane wave EM fields.

3. Exposure of Animals and Animal Models

Both the 40 gm mouse and the 40 gm phantom mouse were exposed while contained in a polypropylene cylindrical holder which was actually the housing of a 30 cc hypodermic syringe. A 200 gm rat was exposed in a cylindrical container, consisting of the tip of a 30 cc hypodermic syringe housing and a 1½" diameter polyethylene tube. In each case, the medial plane along the long axis of the animal was oriented parallel to both the magnetic and electric fields such that the electric field was aligned with the long axis. Each model was exposed for a period of 1 min. The thermograms shown in Fig. 23 depict the SAR patterns and peak values obtained in terms of 1 mW/cm^2 incident power density. Note that the results between the phantom and real mouse are quite similar, and the peak SAR for the larger animal (rat) is less than that of the mouse.

D. Microwave Mouse and Rat Brain Deactivators

The 40 gm mouse and the 200 gm rat were also exposed to several types of microwave brain deactivators. Such devices are used to rapidly deactivate the brain tissue of test animals for neurological research purposes. Two of the units tested were located at the University of Texas Medical School, at San Antonio, and the other system is at the USAFSAM facilities. The devices are designed to apply a large amount of EM energy into the small head volume of the animal in order to sacrifice the animals as fast as possible while rapidly deactivating the brain. The main criteria is to do this quickly so that the animals' regulatory systems do not have time to react and attempt to counteract the intrusion. This will hopefully leave the animals' regulatory substances in their natural concentrations and at their natural locations. The exposure time is so small that the magnetron power sources do not have time to come up to full power, so that the SAR values cannot be normalized to some incident power density. The experimental results of the actual exposure conditions are tabulated in Tables XII and XIII. The details concerning the thermographic results are discussed below.

1. The University of Texas Systems

The University of Texas Medical School has two microwave brain deactivator systems. The 40 gm mouse and its phantom were exposed in both systems. One was constructed such that the animal could be inserted into a hole in the short sidewall of an S band waveguide, as shown in Fig. 4-a. The field configuration around the head of the animal is illustrated in Fig. 24-a. The S band waveguide system was fed by a magnetron which was controlled with a timing relay. Exposure times of 1/60 sec were used for the phantom mouse, and times of 1/720 sec were used for the 40-gm mouse. The mouse and its phantom were exposed in two orientations in this system, one with the medial plane parallel to the waveguide cross-sections, and the other with it perpendicular to the waveguide cross-section. Thermographic results are shown in Fig. 25 for both the mouse and the phantom. The results show that the SAR pattern for both the mouse and the phantom consisted of an annular ring in the region of the brain. This is due to the magnetic field producing circular eddy currents which are at maxima at the periphery of the mouse's brain. The peak values of SAR were 1.42 MW/kg for the phantom and 1.68 MW/kg for the

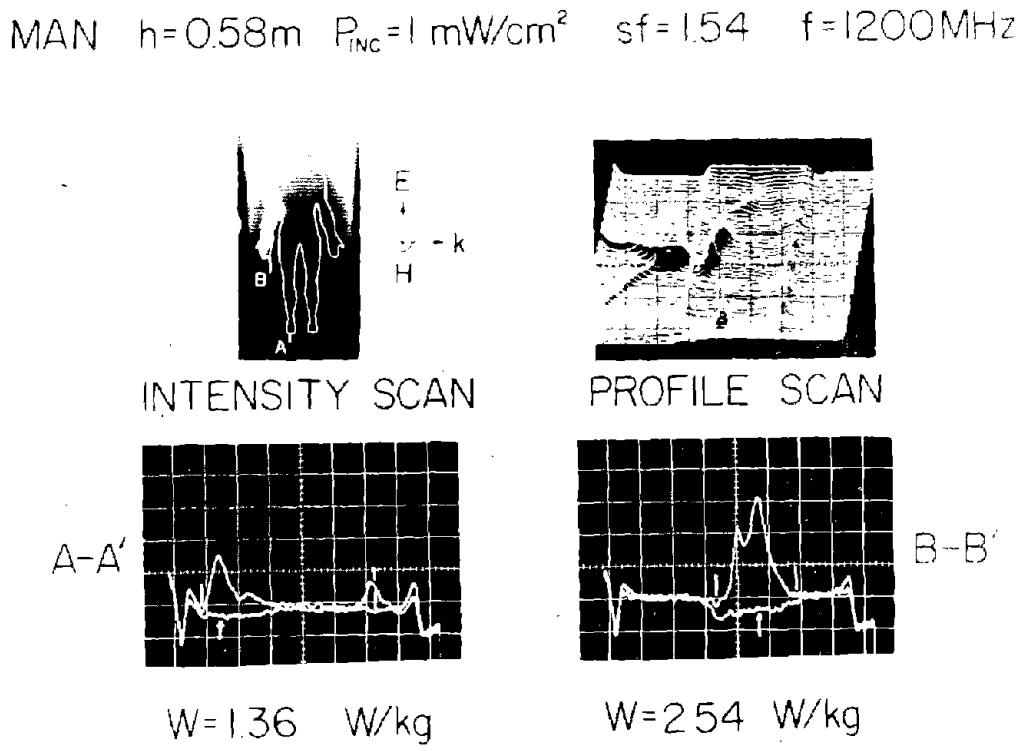

a

Figure 20. Thermograms and maximum values of SAR obtained for 58-cm high 2.6 kg man exposed to 1200 MHz plane wave EM fields. (All values pertain to full-scale exposure conditions).

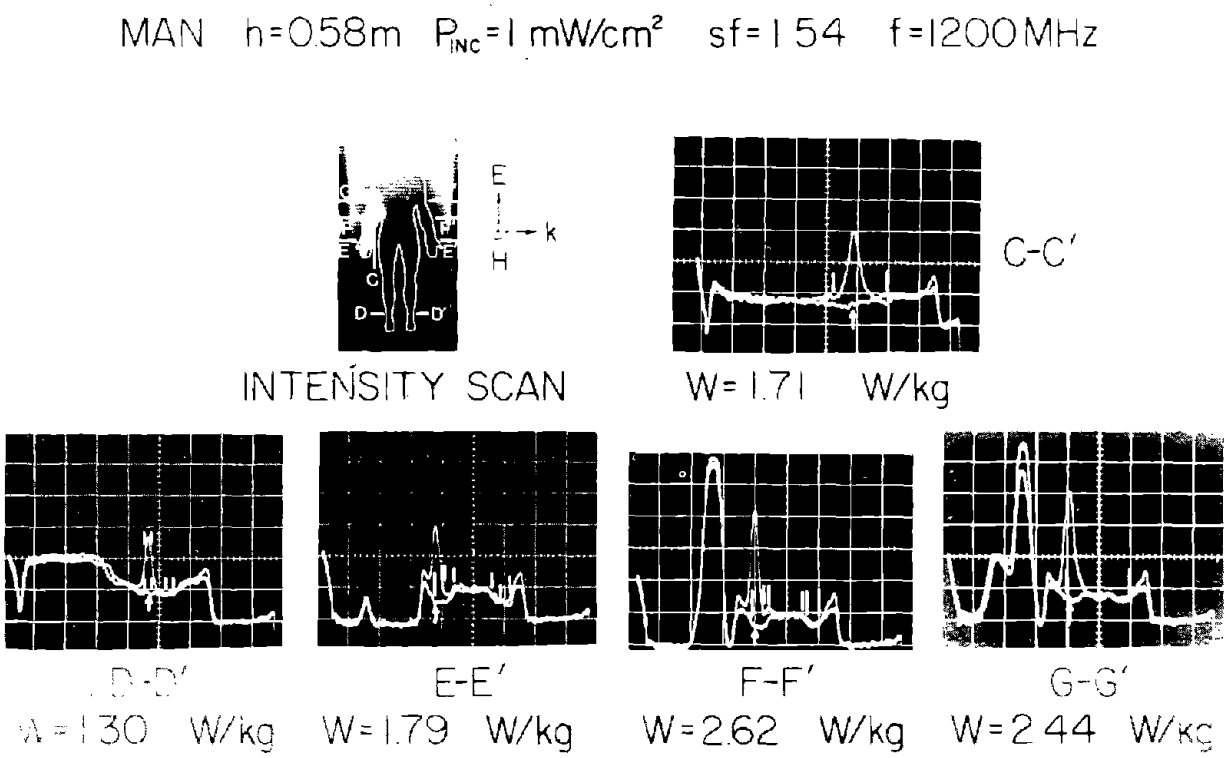

b

Figure 20. Thermograms and maximum values of SAR obtained for 58-cm high 2.6 kg man exposed to 1200 MHz plane wave EM fields. (All values pertain to full-scale exposure conditions.)

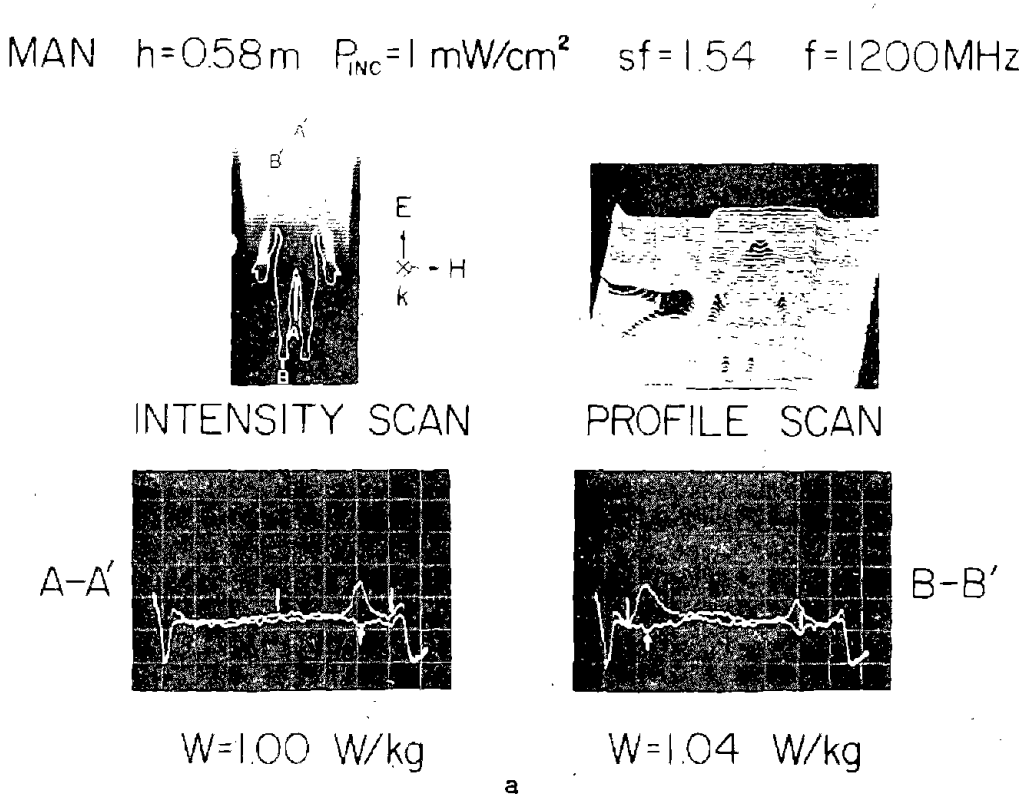

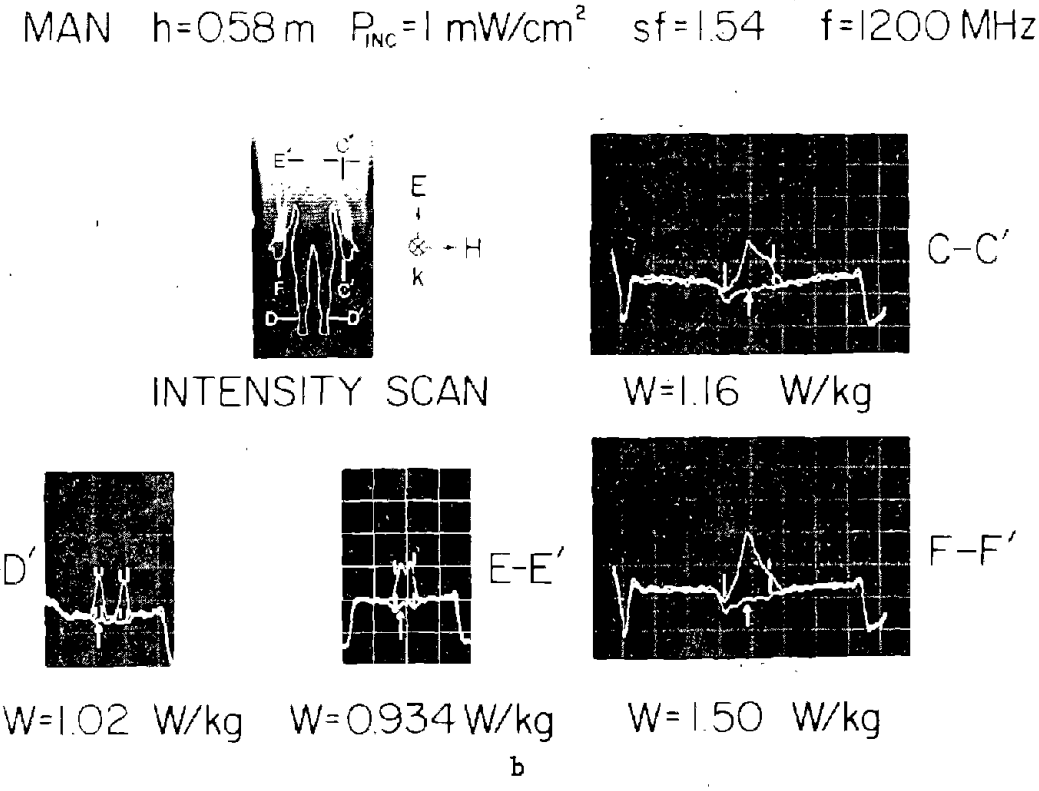

Figure 21. Thermograms and maximum values of SAR obtained for 58-cm high 2.6 kg man exposed to 1200 MHz plane wave EM fields. (All values pertain to full-scale exposure conditions.)

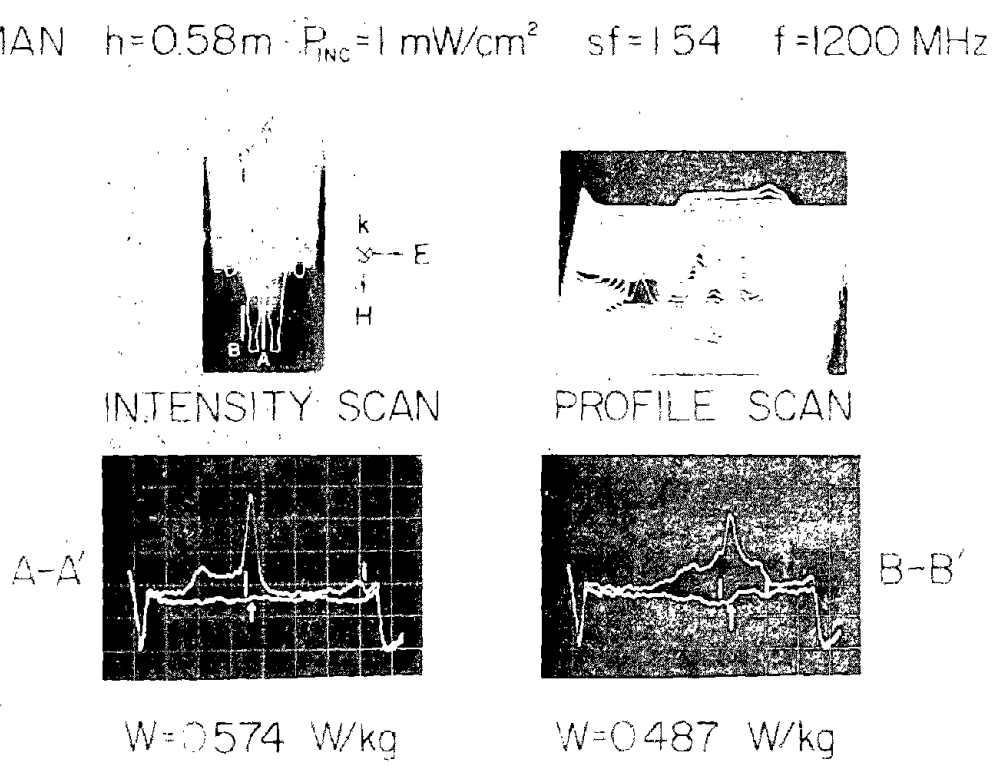

a

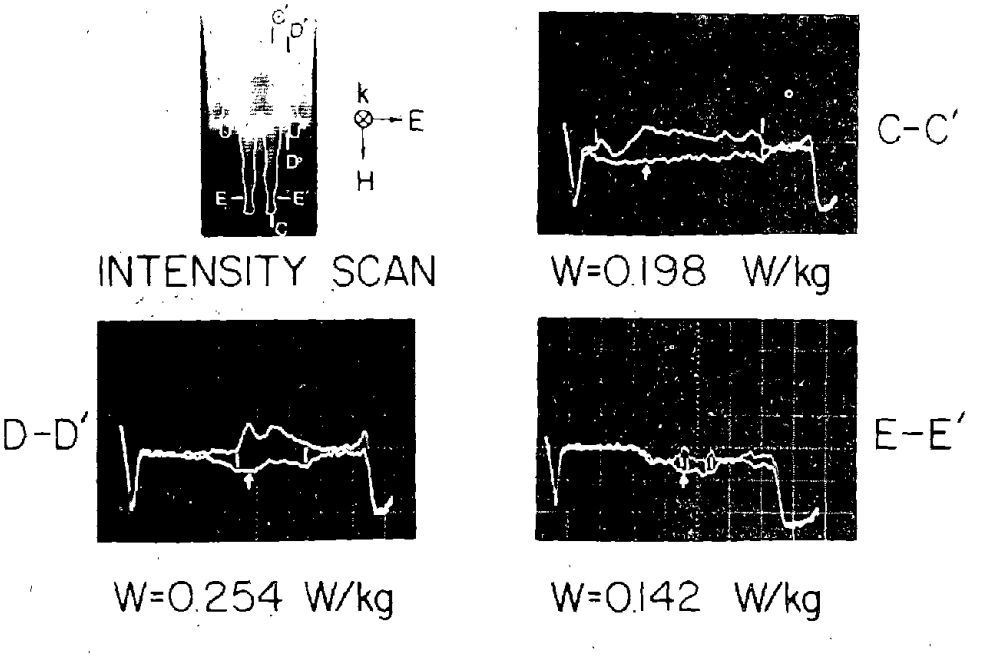

b

Figure 22. Thermograms and maximum values of SAR obtained for 58-cm high 2.6 kg man exposed to 1200 MHz plane wave EM fields. (All values pertain to full-scale exposure conditions.)

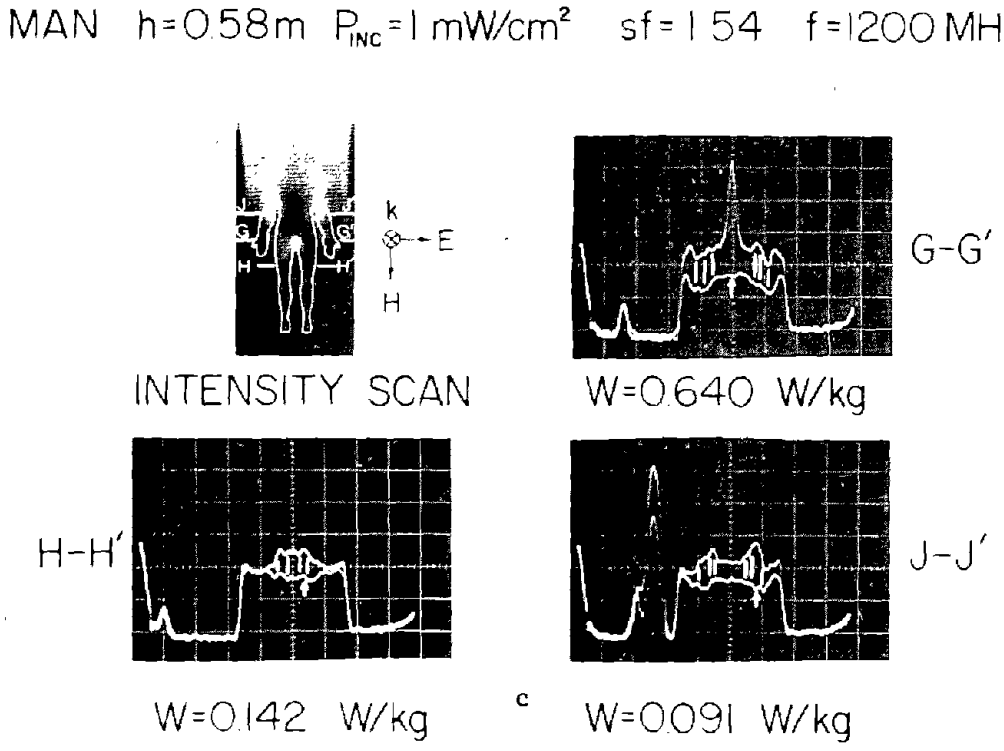

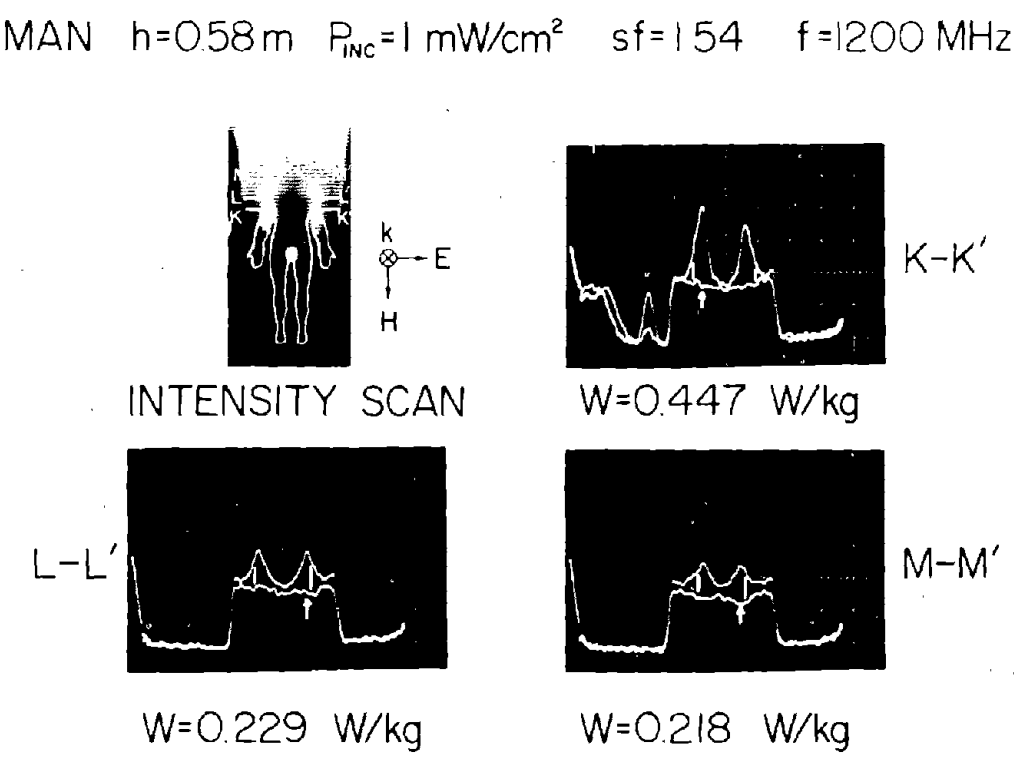

Figure 22. Thermograms and maximum values of SAR obtained for 58-cm high 2.6 kg man exposed to 1200 MHz plane wave EM fields. (All values pertain to full-scale exposure conditions.)

TABLE XI

MEASURED SAR FOR 0.58 m HIGH 2.6 kg
INFANT EXPOSED TO 1200 MHz PLANE WAVE EM FIELDS

MEASURED SAR W/kg for P_{inc} = 1 mW/cm^2			
LOCATION	Frontal plane $\parallel$ to E, $\parallel$ to H, and $\perp$ to k Transverse planes $\parallel$ to E and $\perp$ to H.	Frontal plane $\parallel$ to E, $\parallel$ to H, and $\perp$ to k Transverse planes $\perp$ to E and $\parallel$ to H	Frontal plane $\parallel$ to E, $\perp$ to H, and $\parallel$ to k Transverse planes $\perp$ to E and $\parallel$ to H.
Perineum	0.640		
Axilla	0.487		
Forearm	0.203	1.56	2.62
Arm	0.229	0.894	2.44
Ankle		1.02	1.36
Wrist			1.91
Neck	0.218	0.995	0.0
Hand	0.254		0.487
Calf	0.198		
Shoulder	0.183	0.711	0.731
Hip	0.173		
Thigh	0.162		
Foot	0.142		
Head	0.117		0.223
Abdomen	0.091		
Knee			1.47

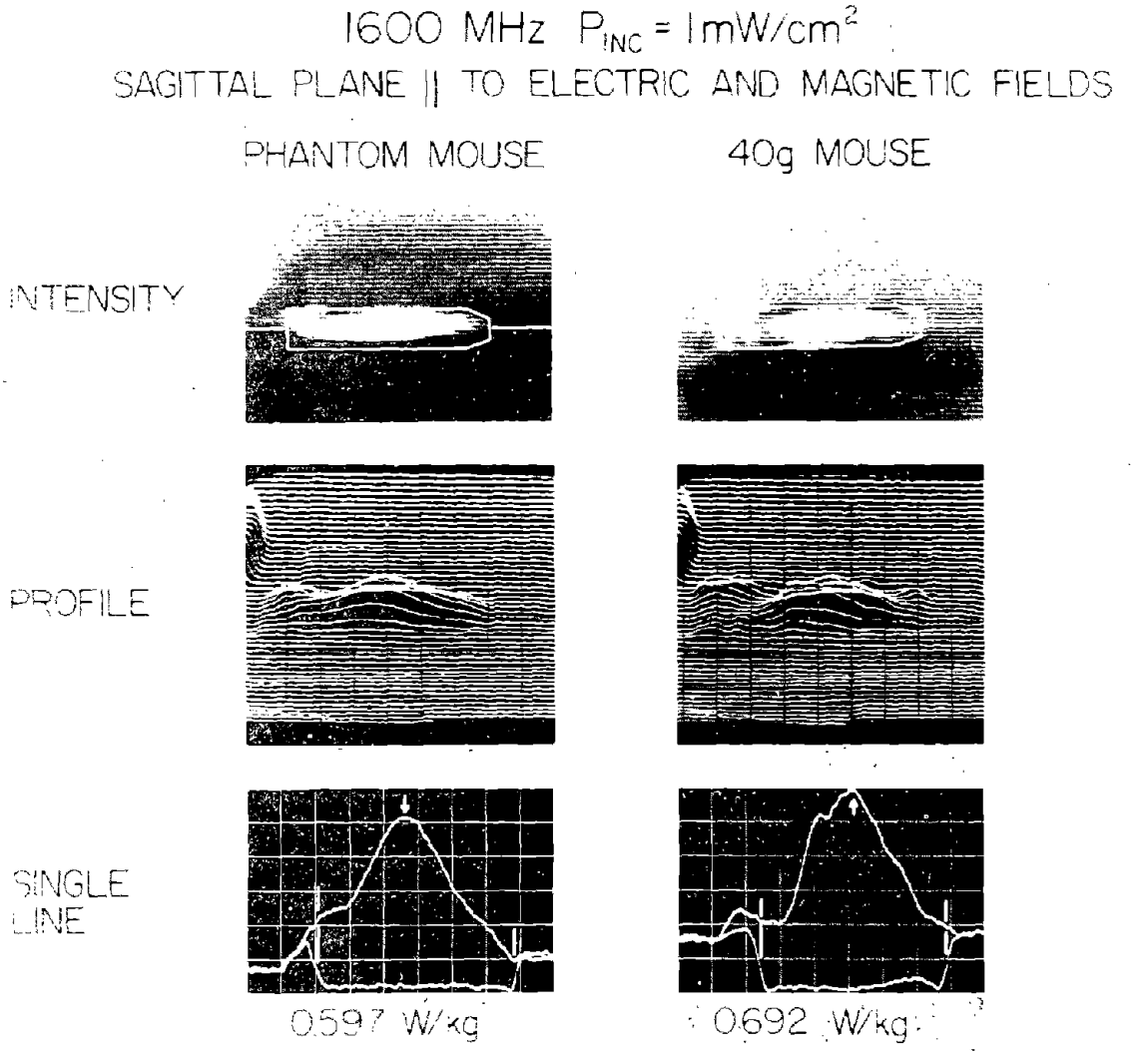

Figure 23. Thermograms and maximum SAR values obtained for 40 g mice and a phantom mouse exposed to 1600 MHz plane wave EM fields.

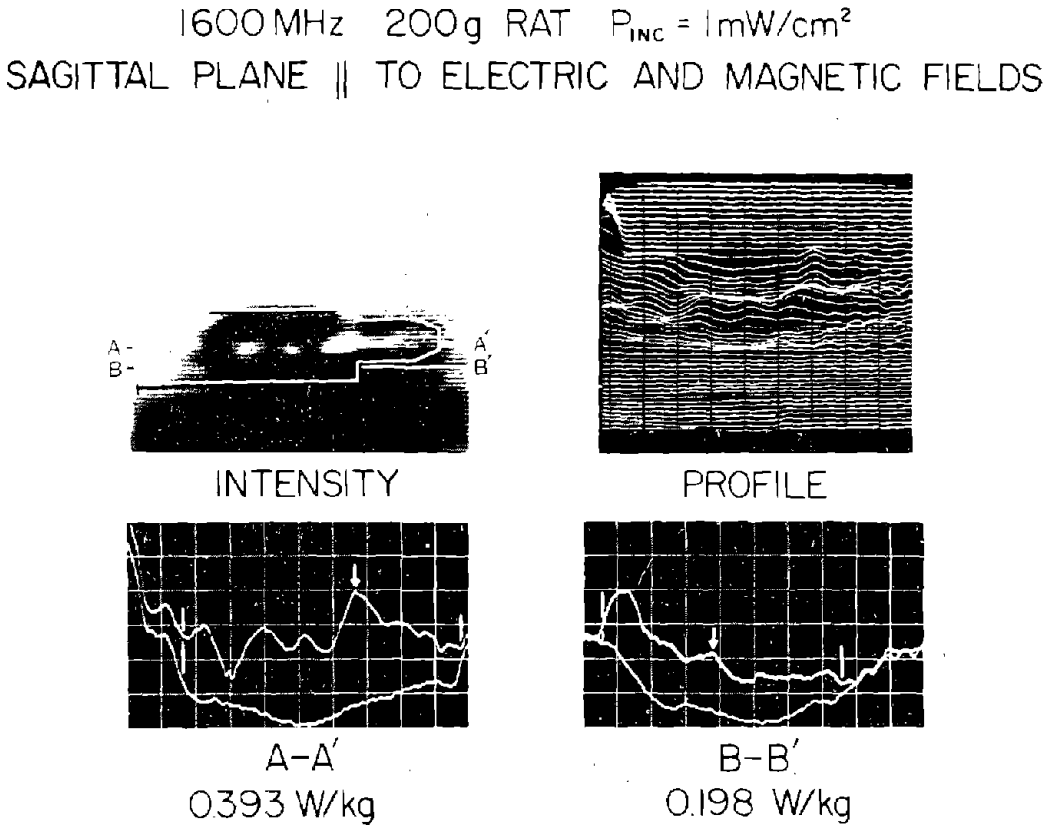

b

Figure 23. Thermograms and maximum SAR values obtained for 40 g mice and a phantom mouse exposed to 1600 MHz plane wave EM fields.

TABLE XII

EXPOSURE CONDITIONS IN UNIVERSITY
OF TEXAS MOUSE DEACTIVATORS AT 2450 MHz

	OBJECT	ORIENTATION	INPUT POWER (WATTS)	EXPOSURE TIME (SEC)	TEMPERATURE RISE (°C)	MAXIMUM SAR W (W/kg)
MOUSE DEACTIVATOR	PHANTOM MOUSE	Cut ∥ E	5 kW	1/60	6.8	1.42×10^{5}
		Cut ⊥ E	5 kW	1/60	8.6	1.79×10^{6}
	REAL MOUSE	Cut ∥ E	5 kW	1/720	4.0	1.68×10^{6}
		Cut ⊥ E	5 kW	1/720	4.5	1.88×10^{6}
IN MODIFIED OVEN	PHANTOM MOUSE	Cut ⊥ Waveguide Cross-Section	600	1.2	11.4	3.30×10^{4}
		Cut ∥ Waveguide Cross-Section	600	1.0	1.9	6.56×10^{3}
	REAL MOUSE	Cut ⊥ Waveguide Cross-Section	600	1.0	17.2	6.96×10^{4}

TABLE XIII

EXPOSURE CONDITIONS IN USAFSAM MOUSE
DEACTIVATOR AT 2450 MHz

OBJECT	ORIENTATION	INPUT POWER (WATTS)	EXPOSURE TIME (SEC)	TEMPERATURE RISE (°C)	MAX SAR W (W/kg)
MOUSE REAL	CUT ⊥ WAVEGUIDE CROSS-SECTION	2 kW	.25	8.8	1.22×10^5
PHANTOM	CUT ⊥ WAVEGUIDE CROSS-SECTION	2 kW	.25	10.8	1.50×10^5
RAT	CUT ⊥ WAVEGUIDE CROSS-SECTION	2 kW	.25	8.8	1.22×10^5

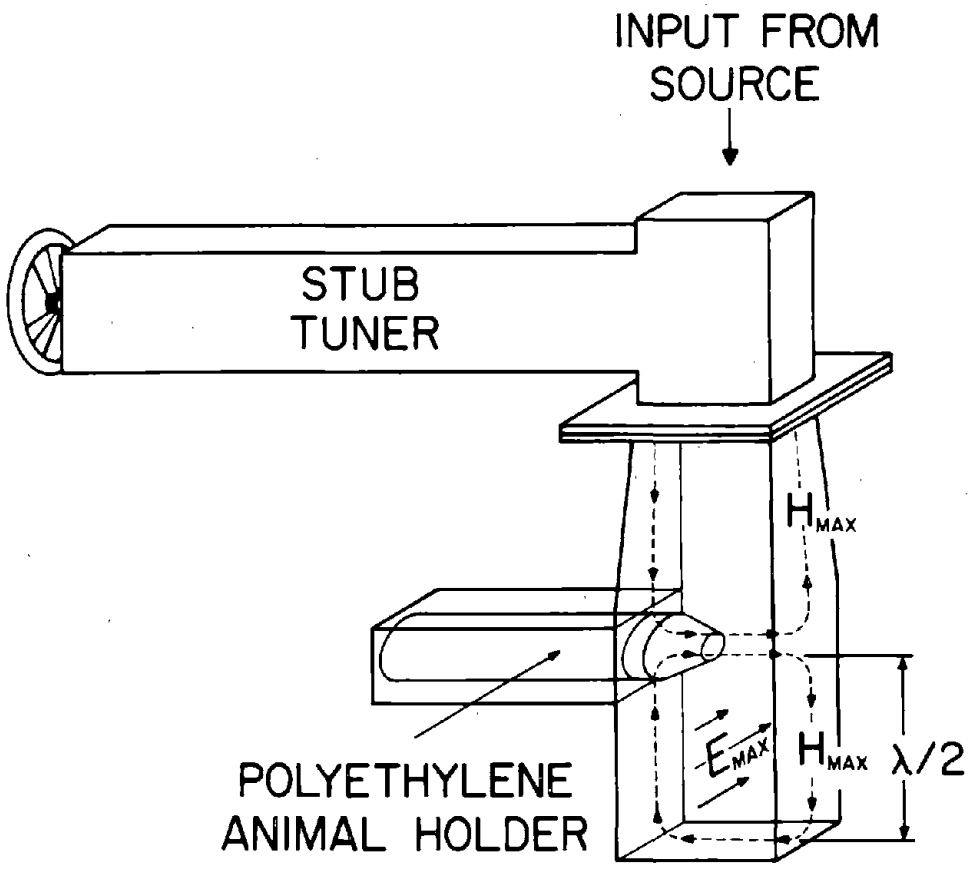

a

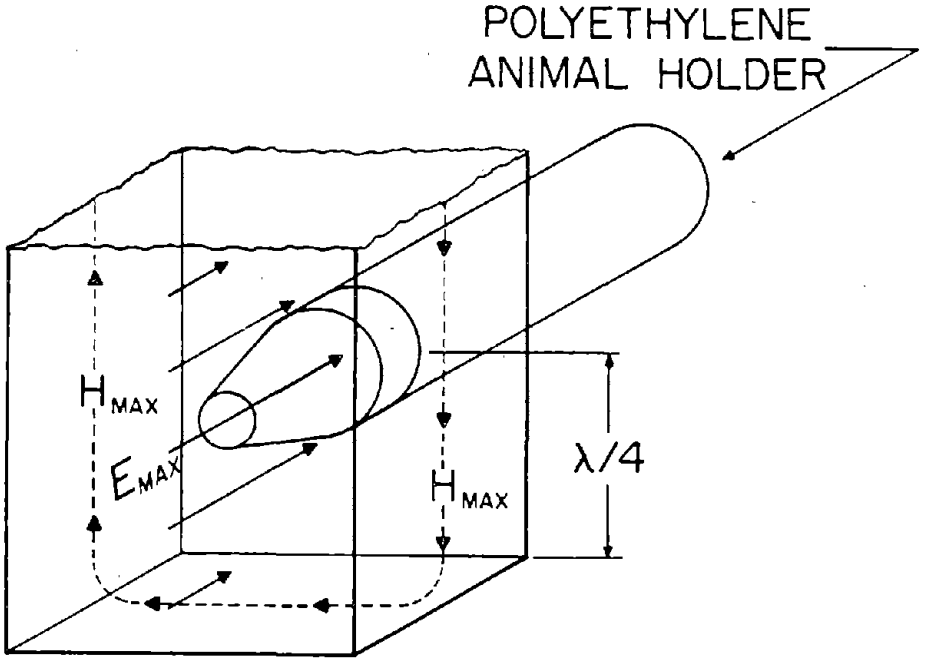

b

Figure 24. Animal orientation and field configuration of microwave brain deactivations at University of Texas Medical School

mouse. This illustrates that the sectioning technique used for the phantom models also worked well for the animals.

The other unit consisted of a system where the animal was inserted into a hole in the long wall of the waveguide feed system with power derived from an International microwave oven (as shown in the photograph in Fig. 4-b). The field configuration around the head of the animal is shown in Fig. 24-b. The phantom mouse and the real mouse were exposed in the microwave oven power device with the medial plane perpendicular to the waveguide cross-section. The phantom mouse was also exposed with the field plane parallel to the waveguide cross-section. The exposure times for these cases were 1-1.2 sec. Thermograms in Fig. 26 show that the power was absorbed along the animal midline for both exposure conditions. The power absorption was much larger for the perpendicular orientation than for the parallel orientation. Again, the absorption patterns for the real and phantom mouse were almost identical and on the same order of magnitude.

2. USAFSAM Microwave Brain Deactivator

The exposure facility at USAFSAM was a modified Raytheon Mark II microwave annealing oven. A 40-gm mouse, its phantom, and a 200-gm rat were exposed in this system. The animals were inserted in the waveguide exposure system with their medial plane perpendicular to the waveguide cross-section, as shown in Fig. 24-b. The exposure time was controlled with a timing relay which was set to give an exposure time of .25 sec. Longer exposure times resulted in temperature changes so large that the thermograph detector was saturated. Thermograms of the rat contained in Fig. 27-a show that the power absorption is concentrated in the nose and head region of the animal.

The power absorption patterns of the phantom mouse and the real mouse are illustrated in the thermograms in Fig. 27-b. The patterns are nearly identical and of the same order of magnitude. The SAR pattern in the mouse is more dispersed; however, the maxima is in the region of the brain for both the real and the phantom subjects.

IV. CONCLUSIONS

All objectives of the joint UW BEMRL and USAFSAM tests and comparisons were satisfied. The tests show that both the UW BEMRL VHF cavity near-field synthesizer and the USAFSAM near-field synthesizer will predict reasonably similar results for exposure of man or tissue models to HF frequencies by extrapolation from exposures of phantom scale models of man or tissue structures of various shapes to electric and magnetic fields at scaled frequencies. The results indicate that exposure times of less than 120 sec and temperature rises of more than 2° are required to obtain similar results between the exposure systems. The short exposure times and the minimum temperature rises are required to eliminate inadequacies due to thermal diffusion. Under these conditions, measurements made in the USAFSAM near-field synthesizer on tissue equivalent spheroids agree very well with theory and the values measured in the UW BEMRL resonant cavity near-field synthesizer.

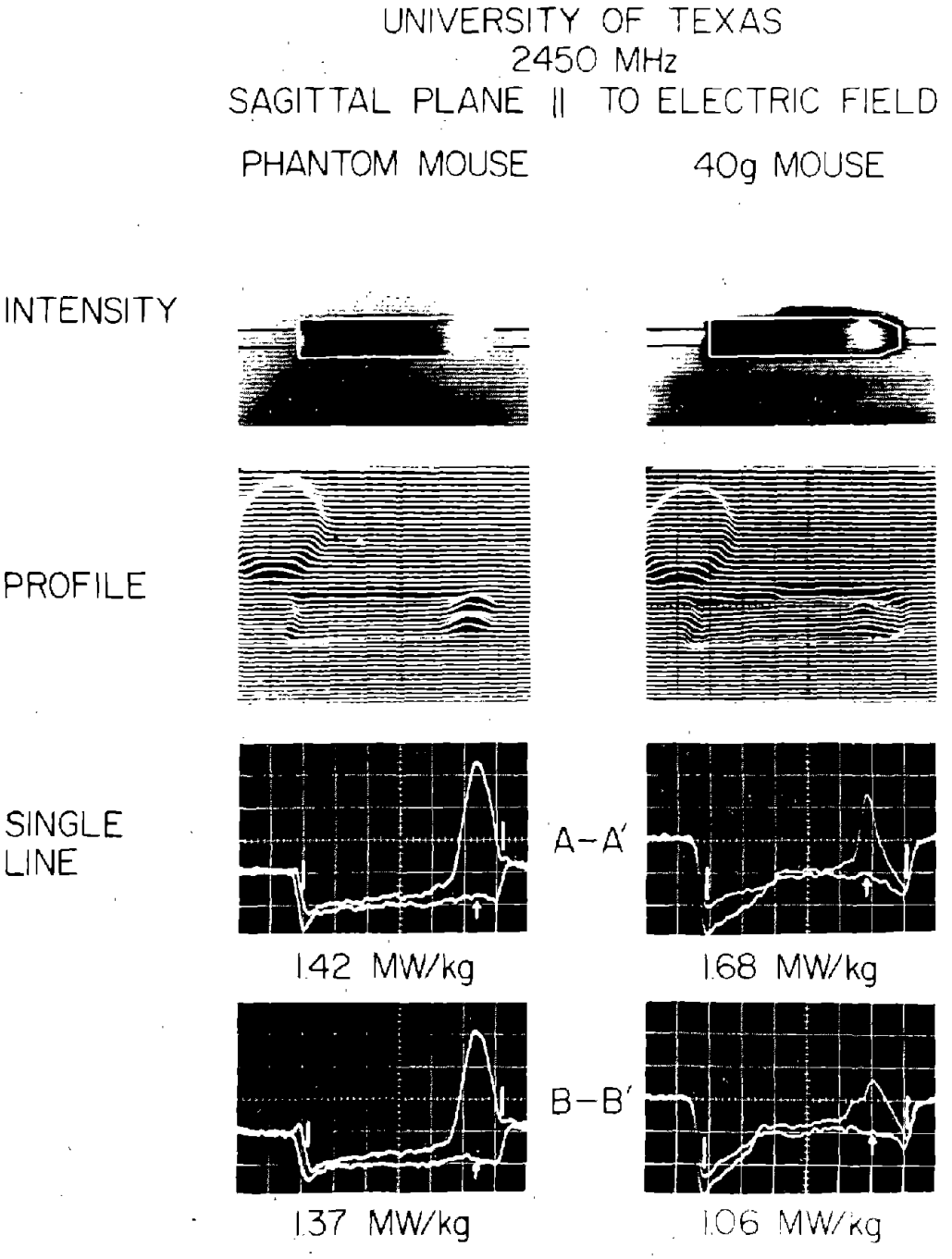

Figure 25. Thermograms and maximum values of SAR obtained for 40 g mice exposed in University of Texas microwave brain deactivator.

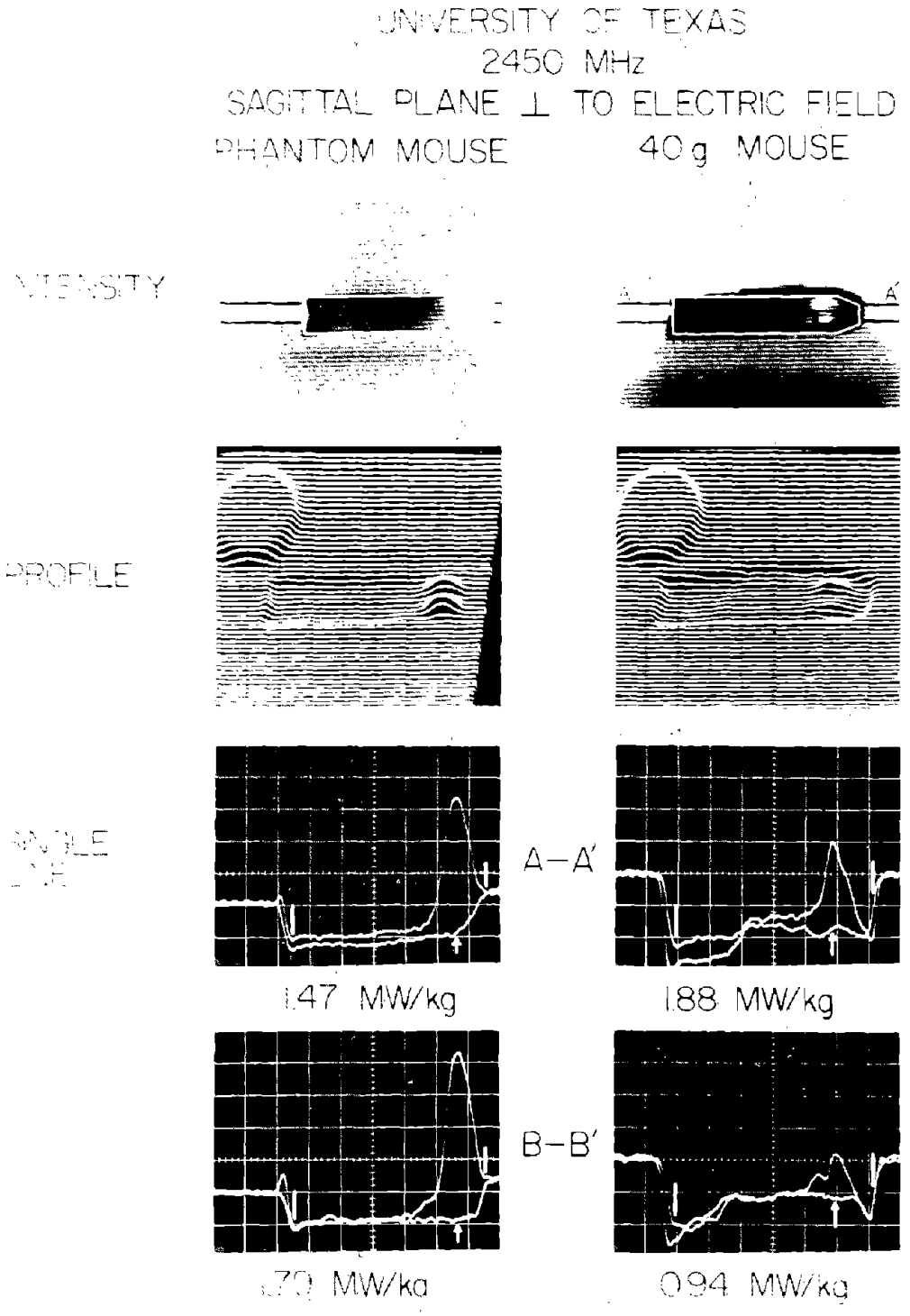

b

Figure 25. Thermograms and maximum values of SAR obtained for 40 g mice exposed in University of Texas microwave brain deactivator.

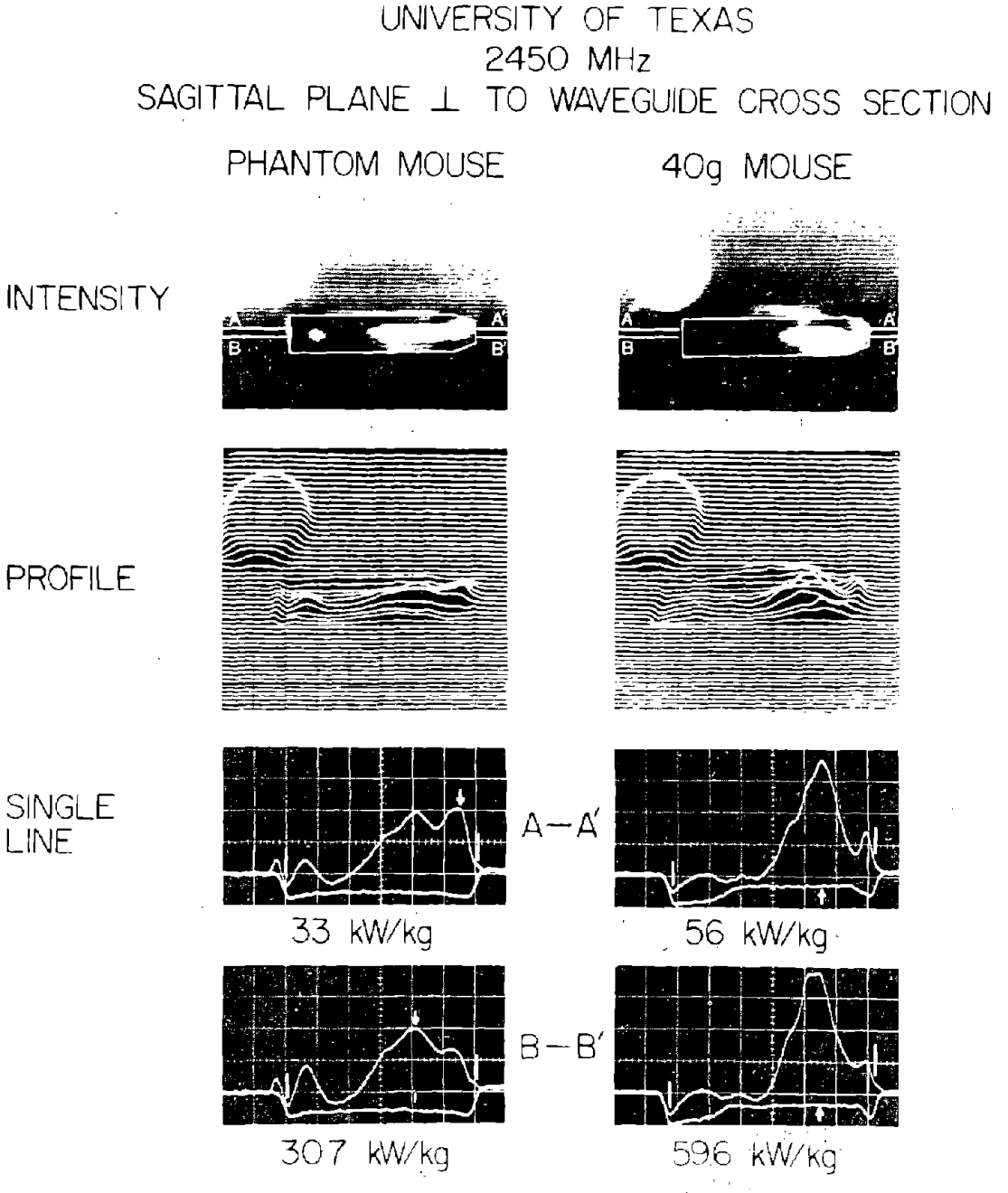

Figure 26. Thermograms and maximum values of SAR obtained for 40 g mice exposed in University of Texas microwave brain deactivator.

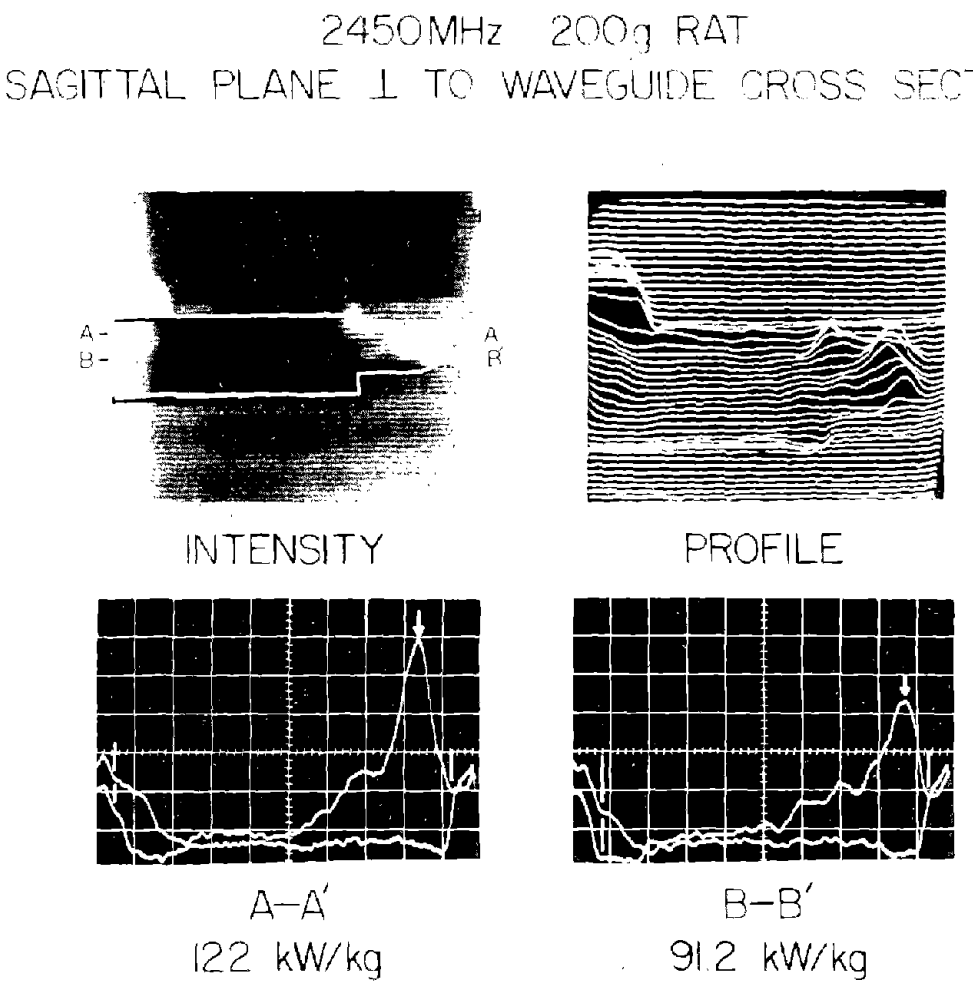

a

Figure 27. Thermograms and maximum values of SAR obtained for a 200 g rat exposed in USAFSAM microwave brain deactivator.

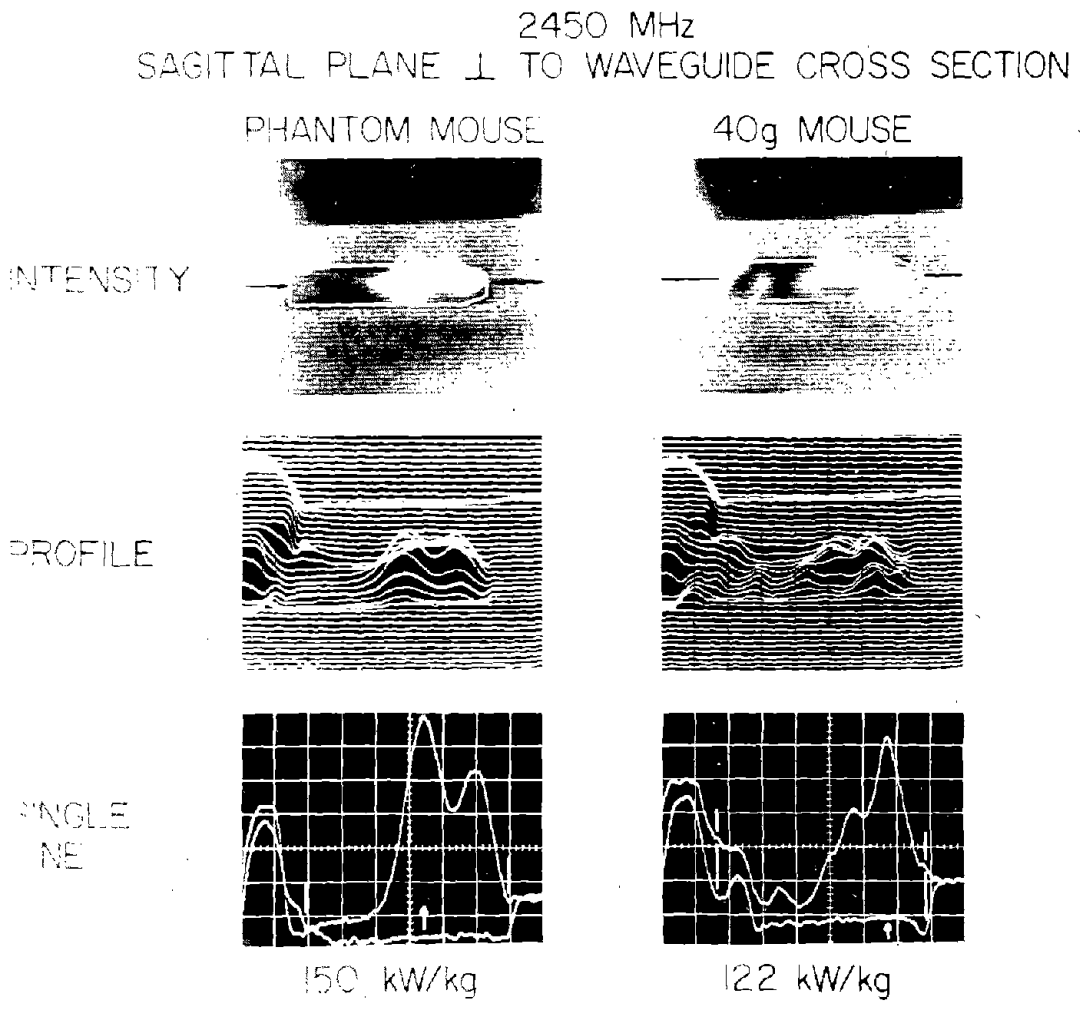

b

Figure 27. Thermograms and maximum values of SAR obtained for 40 g mice exposed in USAFSAM microwave brain deactivator.

The results support previous conclusions that the SAR in spheres of synthetic tissue exposed to magnetic fields is much greater than that produced by exposures to electric fields with the same stored energy. Furthermore, the results indicate that the SAR resulting from this coupling increases with the square of the frequency of the exposure fields.

The results also show that the electric field coupling will increase with the ratio of major to minor axis in prolate spheroids exposed to electric fields, with the electric field oriented parallel to the major axis of the ellipsoid. The measurements in the USAFSAM system obtained for a phantom model of man exposed to an electric field predict the same maximum SAR in the ankles as that predicted in the UW BEMRL system. The values measured in the knee and neck, however, predict only half the values as predicted in the UW BEMRL system. The USAFSAM measurements, taken for the model man exposed to the magnetic field, predict maximum SAR values of only 25% of those predicted by the UW BEMRL exposure system. The SAR patterns observed, however, are very similar to those observed in the UW BEMRL system. The lower values are attributable to the fact that the models are exposed for much longer times in the USAFSAM system than the UW BEMRL systems. The man models are much more susceptible to diffusion errors than the spheroids, since the volume of the various tissue appendices in the man are small compared to the total volume of the spheroids and ellipsoids tested. The measurements on phantom models of man exposed in the USAFSAM HF stripline exposure system predict values of SAR that are very close to those predicted by the UW BEMRL VHF cavity system. The values indicate that the SAR in man will vary with the frequency squared similar to that for the spheroid and the prolate spheroid exposures. The measured SAR in model spheres of tissue exposed to 16 MHz plane waves in the USAFSAM anechoic chamber agree very closely to that predicted by theory. SAR values were measured for a variety of phantom models of biological tissues, mice, rats, scale models of man exposed to 1600 MHz plane wave fields, and for mice and rats exposed to experimental microwave brain deactivators. The results for the brain deactivator show that maximum SAR values as high as 1.8 million W/kg can be produced in the head of the animals with a power source of 5 kW. This SAR is capable of producing temperature changes of 8.6° in an interval of time less than 1/60 sec. The results of the experiments clearly indicate phantom models and scaling techniques can be used to quantitatively determine SAR magnitudes and patterns in full-scale tissue structures and man exposed to electromagnetic fields, and the results are reasonably consistent when obtained from exposures made with different exposure systems in different laboratories.

APPENDIX: CALCULATOR PROGRAMS

Title Absorbed Power Long Wavelength Exposure of Spheroid Page 1 of 2

Programmer A.W. Guy HP-65 USER INSTRUCTIONS Date 1/10/76

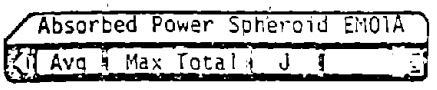

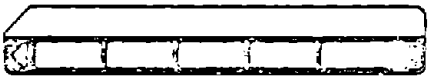

STEP	INSTRUCTIONS	INPUT DATA/UNITS	KEYS	OUTPUT DATA/UNITS
1.	Load Program I in reverse direction		RTN	
2.	Key in semi-major axis (a)	a(cm)	R↓	a(cm)
3.	Key in semi-minor axis (b)	b(cm)	R/S	b/2 (cm)
4.	Load Program II in forward direction			
5.	Key in conductivity	σ(S/m)	R↓	σ(S/m)
6.	Key in frequency	f(Hz)	R↓	f(Hz)
7.	Key in electric field strength E	E(V/m)		
8.	Choose any of the following three options to obtain max SAR			
	(a)exposure to electric polariz. (clear all flags)	if previously set	R/S	P_{PE}(W/kg)
	(b)exposure to magnetic polariz. (Clear flag 2)		fSF1 R/S	P_{PM}(W/kg)
	(c)exposure to cross polariz. (Clear flag 1)		fSF2 R/S	P_{PC}(W/kg)
9.	Calculate average SAR		A	P_{AT}(W/kg)
10.	Calculate total absorbed power		C	P_T(W)
11.	Calculate Maximum SAR (same result as in 8)		B	P_p(W/kg)
12.	Convert any SAR in x register to current density J		D	J(ma/cm^2)
13.	After any of steps 8-11 SAR			
	or power due to magnetic field component alone		R↓	P^H(W/kg)
	or due to electric field component alone		R↓ R↓	P^E(W/kg)
14.	With a new geometry begin step 2. With new			
	freq. conductivity or field strength begin			
	with step 5. With new exposure polarization			
	set appropriate flags and calculate as			
	described in steps 9-11 in any order followed			
	by steps 12 or 13 as desired.			

Title Absorbed Power Long Wavelength Exposure of Spheroid EM01A Page 2 of 2

Side II Max and Avg SAR

SWITCH TO W/PRGM PRESS f PRGM TO CLEAR MEMORY. HP-65 PROGRAM FORM

KEY ENTRY	CODE SHOWN	COMMENTS
g		σ in z, f in y, E in x
π		
x		πE
2		
x		2πE
$x_{\hat{y}}$		2πfE
f^{-1}		
$\sqrt{x}$		$(2\pi fE)^2$
x		$\sigma(2\pi fE)^2$
10 g		
EEx		
2		
3		9×10^{23}
÷		
STO 8		$(2\pi fE/c)^2\ \sigma \times 10^{-7}$
$x \rightleftarrows y$		
STO 6		σ
LBL		calculate average
A		spec.absorp.rate(SAR)
20 RCL 3		B_E, electric
RCL 1		A_E, polariz.
f		Test for polariz.
TF1		and select constants
RCL 7		B_H, magnetic
RCL 2		A_H, polariz.
f		Test for polariz.
TF2		
RCL 3		B_E, cross polariz
RCL 2		A_C
30 RCL 6		σ
÷		A/σ
f^{-1}		
$\sqrt{x}$		$(A/\sigma)^2$
RCL 7		b/2
.		
4		.4
x		b/5
RCL 8		k
x		Kb/2
40 $x \rightleftarrows y$		$(A/\sigma)^2$
1stx		K
x		P_{AE} avg SAR (E field)
R↓		kb/2
x		P_{AM} avg SAR (H field)
$x \rightleftarrows y$		B
R↓		P_{AM}
t		P_{AT} avg SAR (E & H)
1stx		P_{AM}
$x \rightleftarrows y$		P_{AT}
50 RTN		P_{AT} in x, P_{AM} in y, P_{AE} in z

KEY ENTRY	CODE SHOWN	COMMENTS
LBL		Calc. peak SAR
B		P_{AT} in x, P_{AM} in y, P_{AE}
A		in x and B in w
x		B in x and w
R↓		P_{AE}
Enter		
Enter		P_{AE} in x,y,z, B in w
RCL 8		$(2\pi f/c)^2\sigma x10^{-7} = K$
R↓		B
60 f^{-1}		
$\sqrt{x}$		B^2
x		kB^2
Enter		
R↓		$P_{AE} = K(A/\sigma)^2$
f		Polarization test
TF2		flag Off-E or H, on -C
t		
RTN		P_{PC} c pol.
f		
70 $\sqrt{x}$		$\sqrt{K}\ A/\sigma$
$x \rightleftarrows y$		KB^2
f		
$\sqrt{x}$		$\sqrt{K}$ B
t		$\sqrt{K}\ (A/\sigma + B)$
f^{-1}		
$\sqrt{x}$		
RTN		P_{PE} or P_{PM}
LBL		Calc Total
C		Absorbed Power
80 A		determine avg.SAR
RCL 5		V=total volume
R↓		P_{AE}
x		P_{TE} total absorbed P
RCL 5		electric field
R↓		P_{AM}
x		P_{TM} total absorbed P
RCL 5		magnetic field
R↓		P_{AT}
x		
90 RTN		P_T total absorbed pwr.
LBL		Calculate current
D		density
RCL 6		σ
x		σ^2E^2
1		
0		
x		σ^2E^2x10
f		
$\sqrt{x}$		
100 RTN		J current density

REGISTERS	
R_1	A_E
R_2	A_H, A_C
R_3	B_E
R_4	B_C
R_5	V
R_6	σ
R_7	B_H=b/2
R_8	K= $(2\pi fE/c)^2\sigma x10^-$
R_9	

LABELS	
A	Avg SAR
B	Max SAR
C	Total P
D	J
E	
0	
1	
2	
3	
4	
5	
6	
7	
8	
9	

FLAGS	
1	H Pol.
2	C Pol.

Title Absorbed Power Long Wavelength Exposure of Spheroid EM01A Page 1 of 2

Side 1 Geometric Constants

SWITCH TO W/PRGM. PRESS f PRGM TO CLEAR MEMORY. HP-65 PROGRAM FORM

KEY ENTRY	CODE SHOWN	COMMENTS
STO 7		a in y b in x
f-1		
$\sqrt{x}$		b^2
CHS		
x≠y		
STO 6		a
f-1		
$\sqrt{x}$		a^2
t		$a^2 - b^2$
43 dstx		a^2
x≠y		
÷		
STO 5		$u_0 2$
f		
$\sqrt{x}$		
STO 4		u_0
1		
t		$u_0 + 1$
RCL 4		
20 1		
-		$u_0 - 1$
÷		
f		
ln		$\ln(u_0+1/u_0-1)$
RCL 4		
x		
2		
÷		
STO 2		$u_0/2$ ln( )
30 1		
-		
RCL 5		$u_0 2$
1		
-		
STO 3		$u_0 2 - 1$
x		$[u_0 2-1][1- u_0/2 \ln( )]$
1		
.		
2		
40 9		
π		
x		
STO 4		1.2π
x		
g		
1/x		
STO 1		A_E
RCL 5		$u_0 2$
RCL 3		$u_0 2 - 1$
50 ÷		$u_0/(u_0 2 - 1)$

KEY ENTRY	CODE SHOWN	COMMENTS
RCL 2		$u_0/2$ ln[ ]
-		$u_0 2/(u_0 2 -1)-(u_0/2)\ln[ ]$
RCL 3		$u_0 2 - 1$
x		
RCL 4		1.2π
2		
÷		
x		
g		
43 d/x		
STO 2		$A_H=A_C$
RCL 3		$u_0 2 - 1$
RCL 3		
RCL 5		$u_0 2$
t		$2u_0 2 - 1$
÷		$(u_0 2-1)(2u_0 2-1)=b^2/(a^2+b^2)$
RCL 6		a
x		
STO 4		$B_C=ab^2/(a^2+b^2)$
73 1stx		a
÷		$b^2/(a^2+b^2)$
CHS		
1		
t		$a^2/(a^2+b^2)$
RCL 7		b
x		
STO 3		$B_E=a^2b/(a^2+b^2)$
4		
Enter		
80 3		
÷		
g		
π		
x		$4\pi/3$
RCL 7		b
f-1		
$\sqrt{x}$		b^2
x		
RCL 6		a
90 x		$[4\pi/2]\ ab^2$
EEx		
CHS		
3		
x		
STO 5		$V=[4\pi ab^2 x10^{-3}]/3$
RCL 7		b
2		
÷		
STO 7		B_H = b/2
100 R/S		

REGISTERS	
R1	A_E
R2	$u_0/2$ ln[ ] $A_H=A_C$
R3	$u_0 2 -1$ B_E
R4	u_0 1.2π B_C
R5	$u_0 2$
R6	a
R7	b B_H
R8	
R9	

LABELS	
A	
B	
C	
D	
E	
0	
1	
2	
3	
4	
5	
6	
7	
8	
9	

FLAGS	
1	
2	

☆ U.S. GOVERNMENT PRINTING OFFICE: 1977— 757-057/6725